Axial capacity of face-to-face built-up aluminium alloy columns: numerical simulation and design proposal

Nishantha Samarasinghe

A thesis submitted in fulfillment of the requirements

for the degree of Master of Engineering

Main supervisor: Dr Zhiyuan (Arthur) Fang

Co-supervisors: Prof James Lim and Dr Kris Roy

School of Engineering

The University of Waikato

New Zealand

THE UNIVERSITY OF
WAIKATO
Te Whare Wānanga o Waikato

2024

ABSTRACT

In recent years, aluminum alloy has seen increased use in construction due to its exceptional corrosion resistance and mechanical strength, especially in structural elements like channel sections, hollow pipes, and angles. Cold-formed aluminum alloy face-to-face (CAAFTF) built up channel sections with web holes or without web holes have emerged as a significant development in the construction industry, focusing on streamlining the installation of plumbing and electrical services as well as Glass walls in front of buildings. Previous research indicated that these aluminum alloy sections were studied on bending capacity with web holes and found the bending modified formula for plain webs as well as the web with perforated sections. However, no comprehensive study has been reported in the literature for such aluminum alloy built up face to face columns subjected to compression.

This study investigates the axial compression behaviour of aluminium alloy columns with perforated webs, focusing on the influence of screws and perforations on axial capacity. A numerical analysis was conducted on screw-fastened, perforated, face-to-face built-up aluminium alloy channel sections under axial compression. The finite element (FE) model developed using abaqus was validated against 29 experimental results from the literature. The validated nonlinear elasto-plastic FE model was then extended to analyse 495 parametric FE models to examine the effects of key parameters, including modified slenderness, screw number, number of web holes, hole diameter, and section thickness, on the axial strength.

The parametric analysis revealed a reduction in axial strength by approximately 8% for every 0.2 increment in the diameter-to-web width ratio (a/h). Axial strength results from experimental tests and FE analysis were compared with current design guidelines in the Australian/New Zealand Standards (AS/NZS 4600). The analysis showed that AS/NZS design strengths were overestimated by 15% for single perforated webs and underestimated strengths by 12% for

multiple perforated web sections but AS/NZS estimation for plain section is more closely match with experimental results.

A new strength reduction factor equation was developed for aluminium alloy face-to-face built-up channel sections with single and multiple perforated webs. Reliability analysis confirmed the accuracy of the proposed equation, which is applicable within specific limits of slenderness ratio, web width-to-length ratio, and web width-to-thickness ratio. The findings indicate that introducing perforations reduces the axial capacity of plain sections by 8% to 16% for single and multiple perforated webs, respectively. This study provides valuable insights for the design and optimization of aluminium alloy built-up sections with perforated webs.

Keywords: aluminium alloy, face-to-face channels, built-up columns, axial compression, screw fasteners, finite element analysis for strength reduction factor for perforated web section.

PREFACE

This thesis is submitted to the University of Waikato, New Zealand, in partial fulfilment of the requirements for a master's degree in civil engineering. The work presented here has not been submitted for any degree or diploma at any other institution. To the best of my knowledge, this thesis contains no material previously published or written by others, except where proper citation is provided.

ACKNOWLEDGEMENTS

Firstly, my sincere thanks to my main supervisor, Dr. Zhiyuan (Arthur) Fang, co-supervisors Professor James B.P. Lim and Dr. Krishanu Roy, for their unwavering support throughout my research, whose constant guidance and contributions were integral to the successful submission of my journal papers, making me an independent researcher.

Heartfelt gratitude goes to Shubam Tiwari, Dinesh Lakshmanan Chandramohan, Renzhe Ma, for their continuous support. I extend my sincere thanks to my well-wishers in New Zealand for shaping my thesis with invaluable encouragement.

I express my appreciation to my best friends in New Zealand, Vivekanandan Shivaji, Harsh Birwadkar and Gowrava Mohanswamy, Alexis Peyret for their year-round support. Special thanks to the University of Waikato, School of Engineering, for providing computing machines and research assistance.

Finally, I want to express my gratitude to my family, my father L P H Samarasinghe, my mother H I P Lilly, my Wife's father & mother A G Thilaka, S P Y Chandradasa. As well as my wife Kalani Senarath Parana Yapa, My Two Daughters of Nehansa D Samarasighe , and Sehansa S Samarasinghe for their unwavering support in pursuing my masters.

NOTATION

Cold-Formed Steel	CFS
Face-To-Face	FTF
Back-To-Back	BTB
American Iron and Steel Institute	AISI
Australian and New Zealand Standards	AS/NZS
Finite element	FE
Finite element analysis	FEA
Finite element modelling	FEM
Direct Strength Method	DSM
Effective Width Method	EWM
Hot Rolled Steel	HRS
Cross-section	C/S
Young's modulus	E
True stress	σ_t
True strain	ε_t
Engineering stress	σ_e
Engineering strain	ε_e
Megapascal	MPa
Kilo-Newton Metre	kN · m

Kilo-Newton	kN
Millimetres	mm
Metre	m
Thickness	t
Yield stress	f_y
Local buckling stress	f_{ol}
Distortional buckling stress	f_{od}
Imperfection magnitude for local buckling	S_{ol}
Imperfection magnitude for distortional buckling	S_{od}
Reference point	RP
Radius	R
Length	l
Screw spacing	s
Elastic flexural buckling stress	f_{oc}
Elastic distortional buckling stress	f_{od}
Critical stress	f_n
Elastic local buckling stress	f_{ol}
Elastic buckling stress about x-axis	f_{ox}
Non-dimensional slenderness used to determine	λ_l
Elastic buckling stress about y-axis	f_{oy}

Non-dimensional slenderness used to determine	λ_d
Elastic buckling stress about z-axis	f_{oz}
Nominal member capacity of a member in compression	N_C
Elastic buckling load	N_e

TABLE OF CONTENTS

ABSTRACT i

PREFACE iii

ACKNOWLEDGEMENTS iv

NOTATION v

TABLE OF CONTENTS 0

LIST OF FIGURES 3

LIST OF TABLES 6

Chapter 1 – Introduction 8

Chapter 2 – Literature Review 13

2.1 Research on Aluminium alloy single channel section under axial compression 13
2.2 Research on Aluminium Alloy built up section under compression 13
2.3 Research on Stainless-Steel Built-up section under axial Compression 15
2.4 Research on cold form aluminium Alloy (CAA) channel sections 16
2.5 Research Gap 17
2.6 Aim and Objective of the research 17
2.7 Outline of the thesis 18

Chapter 3 – Summary of previous experimental study 20

3.1 Test specimens and test procedure 20
3.2 Material testing 21
3.3 Analysis of Experimental results 26

Chapter 4 – Description of finite element modelling and Validation 31

4.1 General 31
4.2 Modelling of geometry and material properties 31
4.3 FE meshing 32
4.4 Boundary conditions and loading procedure 34

4.5 Geometrical imperfections 35
4.6 Geometrical imperfections Application for many holes web section 37
4.7 Contact modelling 40
4.8 Analysis procedure 40
4.9 Validation of the FE model 41
4.9.1 Validation of plain Aluminium Alloy Face to Face Column 41
4.9.2 Validation of Aluminium Alloy Face to Face Column with one web hole and many holes 48
Chapter 5 – Parametric study 60
5.1 General 60
5.2 Parametric Range 61
5.3 Influence of parameters to the axial capacity in Aluminium Alloy FTF plain section. 67
5.3.1 Influence of different grades of Aluminium FTF channel sections vs Axial Force 67
5.3.2 Influence of Screw Spacing vs Axial Force for aluminium FTF plain channel sections 70
5.3.3 Influence of Column Length (L) on Axial Capacity 73
5.3.4 Effect of section thickness aluminium Alloy FTF channel sections 74
5.4 Influence of parameters to the axial capacity in aluminium alloy FTF with one web hole and many web holes section 75
5.4.1 Influence of Screw spacing vs axial Force for aluminium FTF with one web hole section and many holes section 76
5.4.2 Influence of column length vs axial force for FTF section with one web hole and many web holes 77
5.5 Parametric study on the strength reduction factor (R) 80
5.5.2 Effect of a/h ratio on the strength reduction factor (R) 81
5.5.3 Effect of no of screws on the strength reduction factor (R) 82
5.5.4 Effect of column length (L) and modified slenderness ((KL/r)m) on the strength reduction factor (R) for one web hole section 83
Chapter 6 – Current design guidelines 86
6.1 EWM for CFSS channel sections with plain webs 86
6.2 DSM for CFSS channel sections with plain webs 87
6.3 DSM for CFSS channel sections with single or multiple web holes 88

6.3.1 Comparison of design strength with the FEA results for plain web sections, single web hole sections and multiple web holes sections. 90
6.4 Proposed design reduction factor for one or more web hole FTF channel section.. 93
Chapter 7 – Conclusion and Future studies 99
7.1 Key finding 99
7.1.2 The experimental results and FEA results in terms of failure mode 100
7.2 Limitations and future study 101
References 102
Appendix "A" – Coupon testing for material properties 110
Appendix "B" – Python Programme used to build multiple holes model in parameter study. 112
Appendix "C" – All Parametric result 139

LIST OF FIGURES

Figure 2-1: The application of aluminium alloy face to face columns used to build glass wall frame for commercial building 14

Figure 3-1: Visual depiction of the test setup 21

Figure 3-2: Tensile coupon test sample..... 22

Figure 3-3: Instron testing machine with a load cell of 100KN and set up coupon sample 23

Figure 3-4: Tensile testing machine generated displacement vs force graph 23

Figure 3-5: Tensile testing machine generated displacement vs force graph 24

Figure 3-6: Stress-strain curves of the specimens..... 25

Figure 3-7: Number of screws vs axial capacity (kN) as experimental results 27

Figure 3-8: Displacement (mm) vs axial capacity (KN) of the specimens..... 28

Figure 3-9: Displacemnt (mm) vs axial capacity (KN) of the specimens..... 28

Figure 3-10: Localized deformation near the column..... 29

Figure 4-1: Mesh detail, boundary condition and loading point for (a) L=500 without hole, (b) L =500 with single hole , (c) L =1500 with multiple hole 33

Figure 4-2: Sensitivity analysis for selecting the optimum mesh size..... 34

Figure 4-3 General imperfection shape in buckling analysis for plain, single hole and multiple holes with web section 37

Figure 4-4: Displacement(mm) vs axial capacity(KN) for various imperfection scales for three-hole 1500mm length FTF in 100mm screw spacing..... 38

Figure 4-5; Various imperfection scales for three-hole with 1500mm length FTF channel section in 100mm screw spacing 38

Figure 4-6: Imperfection scale vs axial capacity(KN) and compression of percentage change base to experimental result for three holes 1500mm length FTF in 100mm screw spacing ... 39

Figure 4-7: Deformed shapes at failure from experimental and FEA for Plain section with FTF channel 47

Figure 4-8: Axial displacement vs axial capacity from experimental and FEA Plain section for FTF built-up channel..... 48

Figure 4-9 :Deformed shapes at failure from experiments and FEA for one hole at web with FTF Channel 54

Figure 4-10: Axial capacity (KN) versus lateral displacement (mm) curves versus loading for one hole in web 55

Figure 4-11: Deformed shapes at failure from experiments and FEA for many holes at web with FTF Channel 57

Figure 4-12: Axial capacity (KN) versus lateral displacement (mm) curves versus loading for many holes in web 59

Figure 5-1: Cross-sectional details of channel for plain and web hole at centre (All dimensions are in mm) 61

Figure 5-2: Different grade of aluminium alloy with axial capacity for different column length 68

Figure 5-3: Different grade of aluminium alloy compressive force with different column length 69

Figure 5-4: Different grade of aluminium alloy vs increment of axial capacity with optimum column length..... 70

Figure 5-5: axial force changes against screw spacing in short column L -500mm varied thickness for grade 5052-HS32..... 71

Figure 5-6: Influence of screw numbers(s) vs axial force for plain web section with varied thickness and different length for-5052 - HS 32 71

Figure 5-7: Influence of screw numbers(s) vs axial force for plain web section with varied thickness and length-5052 - HS 34 72

Figure 5-8: Influence of screw numbers(s) vs axial force for plain web section with varied thickness and length-5052 - HS 36 73

Figure 5-9: Influence of length(s) vs axial force for plain web section with varied thickness and grades 74

Figure 5-10: Influence of section thickness (t) vs axial force for plain web section with varied screws spacing 74

Figure 5-11: Influence of section screw spacing vs axial force for one web hole section..... 76

Figure 5-12: Influence of screw spacing vs axial force for many web hole section..... 76

Figure 5-13: Length to axial capacity variation for one web holes section with various thickness 78

Figure 5-14: Length (mm) to axial capacity(KN) variation for multiple web holes section with various thickness and grades (H -hole spacing, L-length, S-screws no's).....79

Figure 5-15: Influence of hole diameter vs axial capacity for one web hole column with various column length, thickness,& grades 79

Figure 5-16 a/h ratio vs axial strength for all channel sections. 80

Figure 5-17: Modified slenderness ratio vs strength reduction factor (R) for all channel sections 81

Figure 5-18: The a/h ratio vs reduction factor (R) for all channel length.....82

Figure 5-19: The number of screws vs axial capacity reduction factor (R) for all channel length. 83

Figure 6-1: Comparing the outcomes of the P_{Exp}/P_{DSM} and P_{Exp}/P_{FEA} results for FTF channel sections with plain web 90

Figure 6-2: Comparing the results of the DSM, FEA results, and experimental results for single and multiple hole in the web.....91

Figure 6-3: Comparing the outcomes of the P_{Exp}/P_{DSM} and P_{Exp}/P_{FEA} results for FTF channel sections for one web holes. 92

Figure 6-4: Comparing the outcomes of the P_{Exp}/P_{DSM} and P_{Exp}/P_{FEA} results for FTF channel sections for many web holes. 92

Figure 6-5: Finite Element Analysis (FEA) axial capacity(KN) Vs P_{FEA} / P_{DSM} for 5032 –HS32 grade aluminium with 2 mm thickness for one web hole 93

Figure A-0-1: Instron testing machine 110

Figure A-0-2: Deformed shape of the coupons.....111

Figure A-0-3: Stress-strain curve from the coupon testing.....111

LIST OF TABLES

Table 3-1: The dimensions of the test specimens 20

Table 3-2: Dimension of tensile coupon sample.....22

Table 3-3: Detail of material properties generated from Machine.....24

Table 3-4 Braking value of force of each Sample.....25

Table 3-5: Material properties obtained from tensile coupon tests.....26

Table 3-6: Past experimental result.....26

Table 4-1 Material used for modelling.....32

Table 4-2: Mesh sensitivity analysis for selecting the optimum mesh size 33

Table 4-3: Axial strength of face-to-face built-up aluminium alloy plain section.....42

Table 4-4 compression of experimental, finite element and DSM result for FTF section with plain web. 44

Table 4-5: Axial capacity of FTF channel sections with one web holes.....50

Table 4-6: Compression of experimental, finite element and DSM results for FTF section with single web hole 51

Table 4-7: Compression of experimental, finite element and DSM results for FTF section with multiple holes in the web 52

Table 5-1: The Parametric study parameters and details of variation.....61

Table 5-2: The Parametric study parameters used to plain channel section with grade 5052 HS -32 62

Table 5-3: The Parametric study parameters used to plain channel section with grade 5052 HS-34.....63

Table 5-4: The Parametric study parameters used to plain channel section with grade 5052 HS-36.....63

Table 5-5 The Parametric study parameters used to with one web hole section with grade 5052 HS-32 64

Table 5-6: The Parametric study parameters used to channel with one web hole section with grade 5052 HS-34 65

Table 5-7: The Parametric study parameters used to channel with one web hole section with grade 5052 HS-36. 65

Table 5-8: The Parametric study parameters used to channel with multiple holes in web section with grade 5052 HS-32 66

Table 5-9: The Parametric study parameters used to channel with many holes in web section with grade 5052 HS-34 66

Table 5-10: Different grade of aluminium alloy compressive force with different column Length 67

Table 5-11: Upgrade in grade of aluminium alloy and % increment in axial capacity 68

Table 5-12: Upgrade in grade of aluminium alloy and % increment in axial capacity 69

Table 5-13: The strength reduction factor changing with length, slenderness ratio for many web hole section 84

Table 5-14: the strength reduction factor changing with length, slenderness ratio for one web hole section 84

Table 6-1 Average axial capacity reduction factor based on proposed equation for one hole section 94

Table 6-2: Axial capacity reduction factor based on proposed equation for one web hole section and reliability 95

Table 6-3: Axial capacity reduction factor based on proposed equation for many web holes section and reliability 97

Chapter 1 – Introduction

Aluminium alloy members are widely chosen for structural engineering applications due to their advantageous properties (Miller et al., 2000; Fang et al.,). Because of its high strength-to-weight ratio, superior corrosion resistance, and efficient manufacturing process through extrusion, aluminium alloy members are increasingly used in structural applications (Siwowski, 2006). Their lightweight nature, high resistance to corrosion, high toughness, and excellent fabricability—including ease of production of complex hollow shapes optimized for structural design and assembly—make them particularly valuable for bridge construction (Das & Kaufman, 2007). Additionally, the aesthetic appeal and structural efficiency of aluminium alloy channel sections contribute to their growing use in modern bridge designs (Das & Kaufman, 2007). Aluminium is also prominently employed in residential bridges, particularly footbridges, where prefabricated channel sections are widely used (Siwowski, 2006).

The use of face-to-face built-up aluminium alloy channel sections as compression members is becoming increasingly common. This study aims to develop a design method for face-to-face compression members and evaluate their suitability for bridge construction. Figure 5-1 illustrates the general arrangement and cross-sectional details of the built-up columns investigated in this study. Current design standards, including the *Aluminium Design Manual (ADM)* (The Aluminium Association, 2015), Australian/New Zealand Standards (Standards Australia/Standards New Zealand, 2010), and *Eurocode 9 (EC9)* (CEN, 2007), provide guidelines for calculating the axial strength of aluminium alloy single channel section columns. However, these standards do not specifically address the design considerations for face-to-face built-up aluminium alloy channel sections under compression.

The American Iron and Steel Institute (AISI, 2016) and Australian/New Zealand Standards (Standards Australia/Standards New Zealand, 2010) advocate for a modified

slenderness approach that accounts for the spacing of screws in built-up columns. Although initially developed for carbon steel members, research by Jacob et al. (2012) has demonstrated the efficacy of applying *AISI* and *AS/NZS* design calculations to accurately assess the axial strength of aluminium built-up plain channels. Consequently, this study explores the suitability of these design calculations for aluminium face-to-face (FTF) channels in bridge construction.

Jacob et al. (2012) investigated the axial capacity of cold-formed aluminium alloy back-to-back built-up columns connected with screws, while Zhu et al. (2013) examined the ultimate strength of members using the Direct Strength Method (DSM). Furthermore, Zhu et al. (2013) studied aluminium tubular members used in curtain walls, space structures, and other structural applications, highlighting that these members can be joined by welding. Despite extensive research on aluminium alloy channel sections, there remains a noticeable gap concerning the axial strength of face-to-face built-up aluminium alloy channel sections under axial compression and their application in the bridge construction industry. While limited studies have investigated face-to-face built-up cold-formed steel (CFS) channel columns (Roy et al., 2014), empirical research in this area remains scarce. Roy et al. (2015, 2016) have recently conducted further tests, contributing valuable insights into the behaviour of these structures.

Ananthi and Ashvini (2017) explored the impacts of web and flange stiffeners on the axial capacity of face-to-face CFS channel sections, highlighting that web stiffeners provide more significant enhancement than flange stiffeners. Gardner (2018) conducted research to determine cross-sectional capacity using the Continuous Strength Method (CSM) for aluminium plate and channel sections, offering alternative capacity formulas for existing design guidelines. Roy et al. (2019) recently conducted both experimental and numerical investigations on face-to-face steel column sections, finding a 15% strength gain using the DSM in combination with conventional design guides. Dabon et al. (2020) analysed the

behaviour and design of CFS battened built-up columns, while Roy et al. (2021) investigated the influence of thickness on axial strength. Zhang and Hancock (2022) studied the application of cold-formed steel channel columns in North America, contributing to the development of the Direct Strength Method within the *AISI Specification*. Furthermore, Roy et al. (2021) explored the effect of screw spacing on the axial strength of back-to-back built-up CFS un-lipped channel sections, revealing potential inaccuracies in current design standards.

Research on CFS structures has significantly advanced in recent years, with various studies examining the axial strength of built-up CFS columns. Roy et al. (2019) investigated the beneficial effects of gaps on the axial strength of back-to-back gapped built-up CFS channels, while Crisan et al. (2014) developed numerical models for back-to-back built-up CFS columns with battens and stitches. Experimental studies by Rondal and Niazi (1990) examined the axial strength of back-to-back gapped built-up CFS columns connected with spacers and stitches. Further contributions by Dabon et al. (2015) focused on the behaviour and design of CFS battened built-up columns. More recently, Roy et al. (2018) examined the effect of thickness on the axial strength of back-to-back built-up CFS channels, and Frat Amico et al. (2012) analysed the buckling and collapse behaviour of back-to-back built-up CFS lipped channel section columns.

For un-lipped channels, Roy et al. (2019) investigated the impact of screw spacing on the axial strength of back-to-back built-up CFS un-lipped channel sections, revealing potential unconservatism in the *AISI (2016)* and *AS/NZS (2010)* standards for stub and short columns. Kesawan et al. (2017) provided a detailed experimental analysis of the structural performance and behaviour of built-up CFS hollow flange I-section columns.

Stainless steel back-to-back columns have gained popularity due to their aesthetic appeal, high corrosion resistance, ease of maintenance, and construction convenience (Kesawan et al.,

2017). Current standards for stainless steel built-up columns include AS/NZS (2010), AISI (2016), and ASCE (2025), although these design rules are not specific to different grades of stainless steel. Yuan et al. (2014) conducted experimental tests on stainless steel back-to-back built-up sections under axial compression. Subsequent studies by Roy et al. (2018) and Dobric et al. (2018, 2018) examined the mechanical behaviour of various cross-sectional geometries of built-up cold-formed stainless-steel channels under axial compression. Additionally, Kechidi et al. (2017, 2020) investigated the effects of screws on the axial strength of stainless-steel back-to-back channels.

Research on aluminium alloy single-channel section columns is limited. Feng et al. (2015, 2016, 2017) studied the structural behaviour of perforated aluminium alloy single-channel section columns, including square and circular hollow section members, concluding that most current design rules (The Aluminium Association, 2015; CEN, 2007; Standards Australia/Standards New Zealand, 2010) are generally inappropriate for calculating axial strength. Huynh et al. (2018, 2019) conducted experiments on the buckling behaviour of aluminium alloy channel sections. Mazzolani et al. (2000) examined the relationship between width-to-thickness ratio and local buckling under axial compression in aluminium alloy angle sections. Su et al. (2014) developed the Continuous Strength Method (CSM) to study the compression resistance of aluminium alloy column members.

This paper presents the results of nine new experimental tests on the axial strength of face-to-face built-up aluminium alloy channel sections conducted by Dr. Arthur Fang. Prior to the compression tests, initial geometric imperfections were measured using a laser scanner. Tensile coupon tests were conducted to determine the material properties of the aluminium alloy channel sections. A nonlinear elastic-plastic finite element (FE) model was then developed and validated against experimental results in terms of failure loads and deflected

shapes. Using the validated FE model, a parametric study involving 495 simulations was conducted to investigate the effects of modified slenderness, screw number, and section thickness on axial strength. The axial strengths obtained from tests and finite element analysis (FEA) were used to assess the performance of current design standards, including AISI (2016) and AS/NZS (2010).

Chapter 2 – Literature Review

2.1 Research on aluminium alloy single channel section under axial compression

This chapter provides a comprehensive review of the literature on the behaviour of aluminium-alloy Face-to-Face (AAFTF) sections, particularly examining the effects of screw spacing, unstiffened holes, and plain webs under compression loading conditions. Notably, there is currently no research available on the axial capacity of AAFTF channel sections with unstiffened holes and plain sections.

Zhu et al. (2019) conducted a study on the behaviour of aluminium alloy structural members through both experimental and numerical approaches. Their experiments included tests on aluminium alloy columns, beams, and beam-columns with square, rectangular, and circular hollow sections.

Similarly, Fang (2020) conducted a numerical investigation on fixed-ended aluminium alloy tubular columns, both with and without transverse welds at their ends. This research focused on examining the effects of transverse welds on the structural behaviour of the columns. Additionally, the study applied the Direct Strength Method (DSM), originally developed for cold-formed carbon steel members, to the design of aluminium alloy columns. Based on the findings, modified design rules using DSM were proposed specifically for aluminium alloy columns, improving the accuracy and applicability of the method.

2.2 Research on aluminium alloy built up section under compression

The literature review on the structural behaviour of AAFTF channel sections indicates that as these sections become more popular in the construction industry (Miller et al., 2000; Roy et al., 2021), the use of back-to-back built-up sections as primary load-bearing column members is increasing (Roy et al., 2021).

Figure 2-1: The application of aluminium alloy face to face columns used to build glass wall frame for commercial building

The literature review on the structural behaviour of AAFTF channel sections did not identify a comprehensive summary of significant studies conducted by various researchers. Roy et al. (2021) conducted an experimental investigation involving 12 screw-fastened back-to-back built-up aluminium alloy slender columns under axial compression, complemented by a numerical finite element study producing 246 results. The numerical study examined the effects of modified slenderness, the number of screws, and section thickness. The axial strengths obtained from both the tests and finite element analysis were used to evaluate the guidance provided in the *Aluminium Design Manual* (ADM, 2020), *Eurocode 9* (CEN, 2007), *Australian/New Zealand Standards* (AS/NZS, 2018), and *American Iron and Steel Institute* (AISI, 2016) standards. It was found that ADM (2020) and CEN (2007) were conservative by 30%.

The study by Roy et al. (2018) explored the use of back-to-back built-up aluminium alloy channel sections as compression members to achieve higher strengths and longer spanning capabilities. The research included results from 15 axial compression tests and a comprehensive parametric study conducted using a validated finite element (FE) model. This study examined the effects of modified slenderness, the number of screws, and section thickness on the axial strength of back-to-back built-up aluminium alloy channel sections. The

findings were compared against guidelines provided by the *Aluminium Design Manual* (ADM), *Australian/New Zealand Standards* (AS/NZS), *Eurocode 9* (EC9), *Eurocode 3* (EC3), and *American Iron and Steel Institute* (AISI) standards. It was found that these design standards were generally conservative by up to 20%, except for the allowable stress design method in AS/NZS (1664.2:1997). However, the ADM (2020) and AISI & AS/NZS (4600:2018) standards offered highly accurate predictions.

2.3 Research on stainless-steel built-up section under axial compression

However, Cold-formed stainless steel is becoming increasingly popular as a structural material due to its excellent corrosion resistance and longer lifespan compared to carbon steel. Jacob et al. (2018) specifically investigated the buckling behaviour of face-to-face built-up cold-formed stainless steel (CFSS) channel sections under axial compression. Although AAFTF channel sections under compression have not been extensively investigated, the use of face-to-face built-up CFSS channel sections as compression members is gaining more attention, as revealed by literature surveys. Three different grades of stainless steel—duplex EN1.4462, ferritic EN1.4003, and austenitic EN1.4404—were examined, with a total of 160 finite element models analysed. The results of the parametric study indicated that the AISI and AS/NZS standards tended to provide a conservative estimate, by about 15%, for all stainless steel face-to-face built-up columns that failed due to global buckling. In contrast, these standards showed an unconservative tendency, by around 5%, for face-to-face built-up stainless-steel columns that failed due to local buckling. Additionally, another study by Roy et al. (2021) focused on back-to-back cold-formed stainless steel lipped channel sections under axial compression.

2.4 Research on cold form aluminium alloy (CAA) channel sections

Cold-formed Cold-formed aluminium alloy (CAA) channel sections are becoming increasingly popular as load-bearing elements in glass walls in building structures, particularly when they include web openings that allow for the installation of various services. A new generation of cold-formed steel (CFS) channel sections with edge-stiffened web openings has been developed, providing enhanced strength compared to sections with unstiffened openings. These sections are widely utilized in New Zealand.

Chen et al. (2022) conducted an extensive study that included 75 results, comprising 26 axial compression tests and 49 finite element analysis (FEA) simulations, to evaluate the compression resistance of CFS channel sections with edge-stiffened web openings, unstiffened web openings, and plain webs. The study employed a validated finite element model to perform a parametric investigation, examining the effects of variables such as column length, hole diameter, stiffener length, number of holes, and fillet radius. The findings revealed that for channel sections with seven edge-stiffened web openings, compression resistance increased by up to 22% compared to plain channel sections. In contrast, sections with unstiffened web openings exhibited a 20% reduction in compression resistance relative to plain sections.

Additionally, the study compared the compression resistance derived from FEA with design strengths calculated using the Direct Strength Method (DSM). The results showed that DSM tends to be conservative, overestimating the strength by approximately 34.5% for plain channel sections with plain webs, particularly those failing due to global buckling or a combination of local and global buckling. However, no studies have investigated CAA channel sections in the context of these research findings.

2.5 Research gap

Aluminium alloy channel sections are increasingly favoured as load-bearing elements in building structures, particularly those designed with web openings to facilitate the installation of various services. The original idea of this study was developed based on the previous work (Fang et al., 2021, 2022 a,b,c,d, 2023, and 2024; Paul et al., 2024), and the analysis methods were similar to these studies. A new generation of aluminium alloy channel sections with web openings has been developed, offering enhanced strength compared to sections with unstiffened holes. These sections are widely used in New Zealand, as highlighted by Zhu et al. (2019).

Despite advancements in this field, a review of the existing literature reveals a significant gap: no research has yet been conducted on the structural behaviour of cold-formed aluminium alloy face-to-face columns under axial compression. This thesis aims to address this gap by exploring the structural behaviour of these channel sections and developing new predictive rules.

2.6 Aim and objective of the research

The primary objective of this study is to investigate the axial compression capacity of cold-formed Aluminium Alloy Face-to-Face (AAFTF) channel sections, both with and without central web holes, using finite element analysis. Additionally, the study will explore the application of these channel sections in the design and construction of prefabricated superstructure frames for bridge construction. The specific objectives of the research are as follows:

1. To develop nonlinear finite element (FE) models that simulate the structural behaviour of AAFTF channel sections under axial compression. These models will incorporate the measured cross-sectional dimensions, material properties obtained from the

literature, and geometric imperfections. The FE models will be validated by comparing the experimental results, including deformed shapes, stress-strain curves, and axial capacity.

2. The validated FE models will be used in a parametric study, involving 660 finite element models, to explore the effects of various parameters on the load-bearing capacity of AAFTF channel sections with web holes subjected to axial compression.
3. To evaluate the accuracy of current design guidelines in predicting the load-bearing capacity of AAFTF channel sections with web holes, the results from finite element analysis (FEA) will be compared with the design strengths predicted by existing guidelines, such as AISI (2016) and AS/NZS (2018).
4. Based on the findings from the parametric study, appropriate equations for design reduction factors will be proposed to determine the load-bearing capacity of AAFTF channel sections with web holes. Furthermore, analysis will be performed to evaluate the accuracy this proposed reduction factor equations.

2.7 Outline of the thesis

Your thesis focuses on the capacity of AAFTF channel sections with web holes under compression and is structured into six chapters:

Chapter 1: Introduces the background, problem statement, and provides an outline of the thesis.

Chapter 2: Reviews the literature on the behaviour and design of AAFTF and AAFTF channel sections, including those with web holes, unstiffened web holes, and plain webs under compression.

Chapter 3: Experimental study of the tensile coupon test and result.

Chapter 4: Details the finite element modelling and validation process.

Chapter 5: Explains the parametric analysis performed to assess the axial capacity of AAFTF channel sections with web holes, and plain webs.

Chapter 6: Offers design recommendations based on the Australia/New Zealand Standards (AS/NZS). Presents the proposed design reduction factor equation and evaluates its reliability for AAFTF channel sections with experimental results.

Chapter 7: Concludes with the study's findings, limitations, and recommendations for future research and engineering practice

Chapter 3 – Summary of previous experimental study

3.1 Test specimens and test procedure

This study used the result of experiment of axial compression tests on a total of nine face-to-face aluminium alloy built-up channel sections was conducted by Dr Arthur Fang at University of Auckland the test data was under review by the journal. A universal testing machine with a capacity of 500 kN was employed to subject the aluminium alloy built-up columns to axial loading. The load was applied through the specimens' centre of gravity under pin-ended boundary conditions. The dimensions of the test specimens are summarized in Table 3-1. These specimens were categorized into three groups based on their column lengths: short (500 mm), intermediate (1000 mm), and slender (1500 mm). Figure 3-1 provides a visual depiction of the test setup utilized for slender column tests, during the column tests, a displacement control method was implemented, maintaining a constant loading rate of 0.02 mm/s. This setup ensured accurate measurement and monitoring of the behaviour and deformation of the aluminium alloy built-up columns under axial compression.

Table 3-1: The dimensions of the test specimens

Specimen	**Web A' mm**	**Flang B' mm**	**Length L mm**	**Thickness t mm**	**Screw Spacing S Mm**
Short					
FTF240-t1.98-L500-S100	240	45	500	1.98	100
FTF240-t1.98-L500-S200	240	45	500	1.98	200
FTF240-t1.98-L500-S400	240	45	500	1.98	400
Intermediate					
FTF240-t1.98-L1000-S225	240	45	1000	1.98	225
FTF240-t1.98-L1000-S450	240	45	1000	1.98	450
FTF240-t1.98-L1000-S900	240	45	1000	1.98	900
Slender					
FTF240-t1.98-L1500-S350	240	45	1500	1.98	350
FTF240-t1.98-L1500-S700	240	45	1500	1.98	700
FTF240-t1.98-L1500-S1400	240	45	1500	1.98	1400

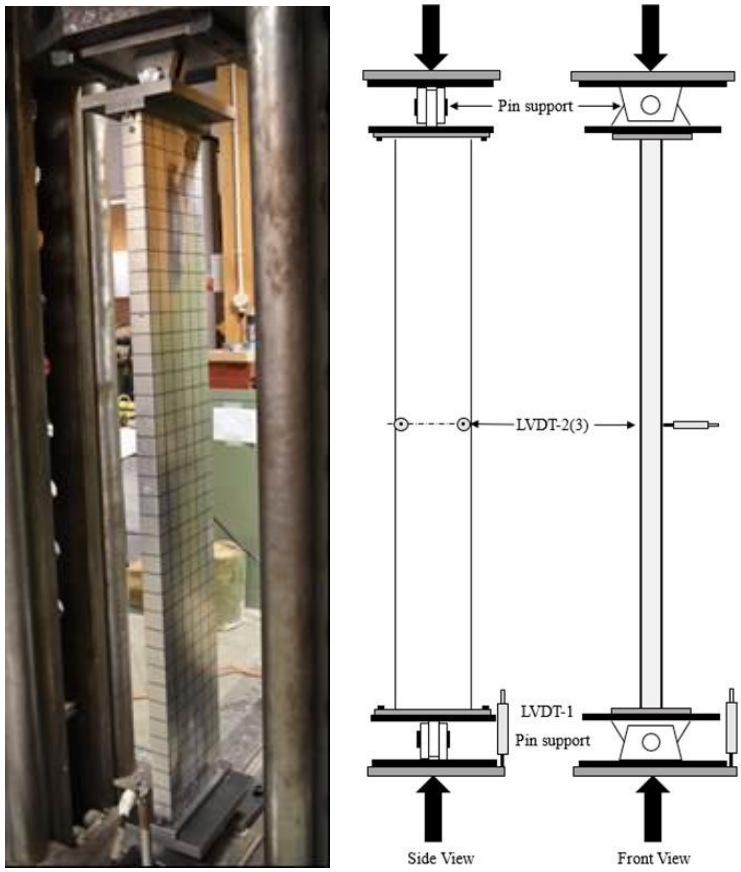

(a) Photograph (b) Schematic drawing

Figure 3-1: Visual depiction of the test setup

3.2 Material testing

The material properties of the specimens were determined through tensile coupon tests. These coupons were extracted from the centre of the web plate along the longitudinal direction of the untested specimens, which were fabricated from the same material as those used in the study by Roy et al. (2020). Following the specifications outlined in *AS 1391:2020* for metallic materials—tensile testing (Standards Australia, 2020), the dimensions of the tensile coupons were meticulously prepared and are presented in Table 3-2 and test sample drawing is in Figure 3-2.

Table 3-2: Dimension of tensile coupon sample

Sample no.	1	2	3	4
	12.55	12.51	12.64	12.72
Width (mm)	12.52	12.57	12.65	12.0
	12.53	12.48	12.85	12.64
Average(mm)	12.54	12.52	12.71	12.69
	1.83	1.9	2.09	2.1
Thickness (mm)	183	1.91	2.01	2.00
	1.85	1.94	1.9	1.98
Average (mm)	1.84	1.92	2.02	2.03
	63.07	63.92	64.3	64.2
Length(mm)	62.9	64.03	63.75	64.2
	64.01	63.83	64.65	64.11
Average(mm)	63.15	63.93	64.23	64.14

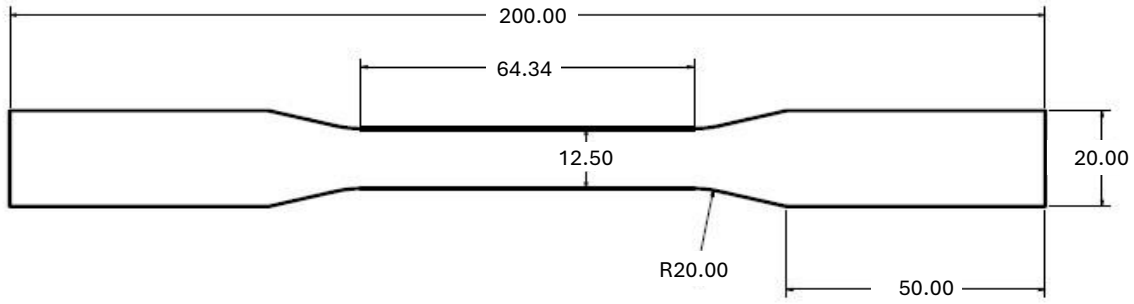

Figure 3-2: Tensile coupon test sample

The tensile coupons were tested using an Instron testing machine with a capacity of 100 kN, as shown in Figure 3-3. In accordance with the AS 1391-2020 standard for Metallic Materials - Tensile Testing, to obtain the ultimate yield strength, the rate of load applied to the specimen must be less than 10 MPa per minute, or the displacement rate of the crosshead must be 0.0007 mm per second or 0.27 mm per minute. Consequently, the machine's operating crosshead separation speed was set to 0.27 mm per minute to ensure a consistent load application across all four sets of samples.

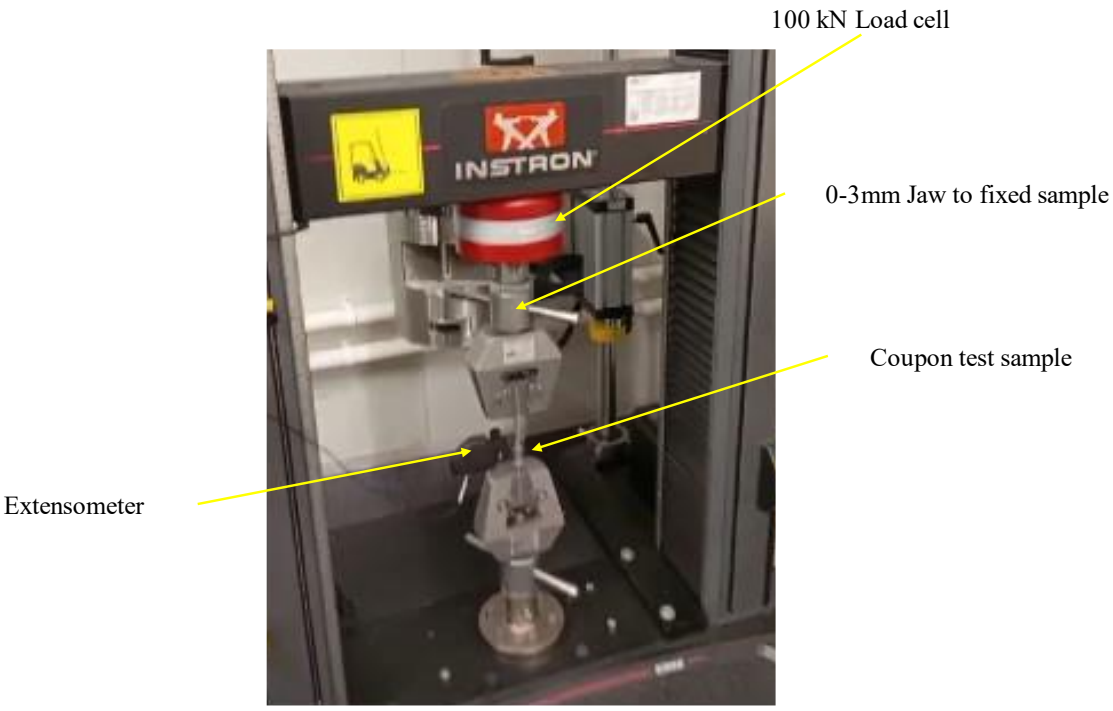

Figure 3-3: Instron testing machine with a load cell of 100KN and set up coupon sample

The tensile strain of the coupons was recorded using a calibrated extensometer. The tensile testing machine generated data used to draw displacement vs force graph in Figure 3-4 and it generated detail of material properties are in Table 3-3: Detail of material properties generated from Machine 3.3.

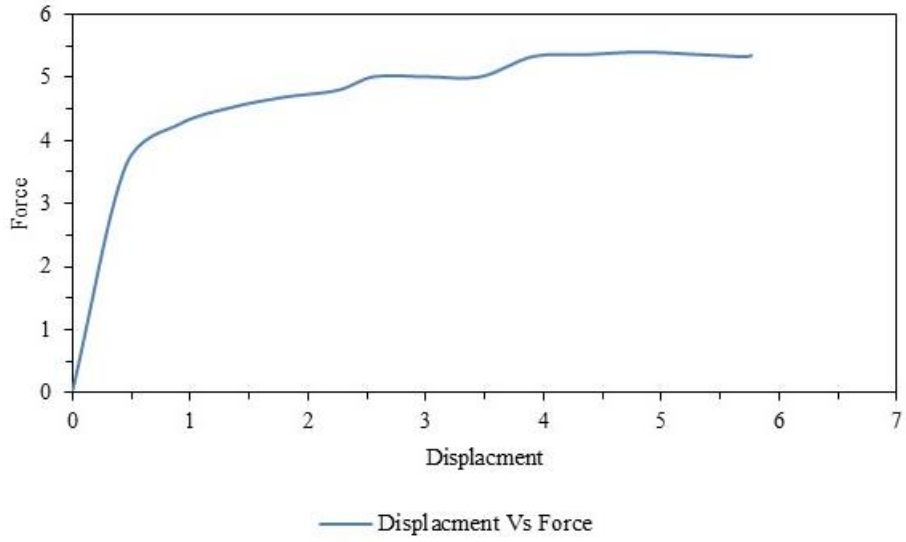

Figure 3-4: Tensile testing machine generated displacement(mm) vs force (KN) graph

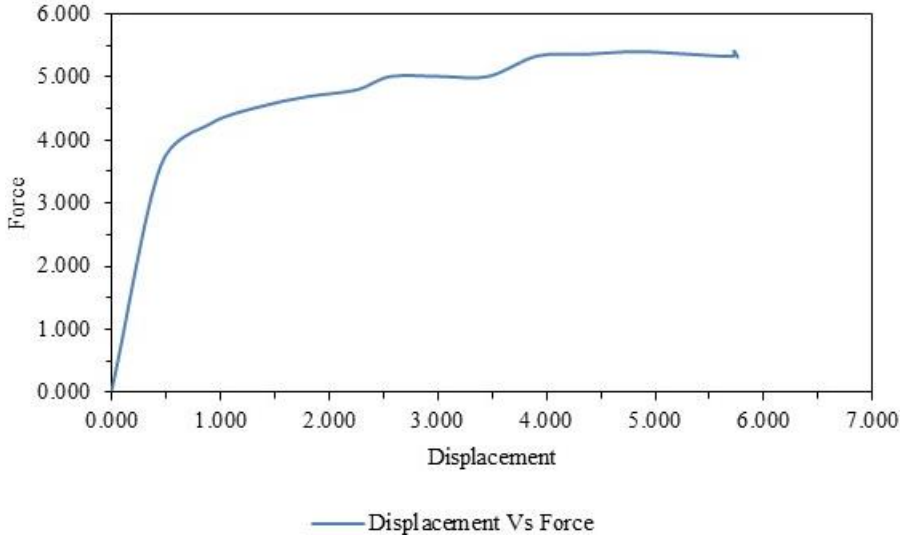

Figure 3-5: Tensile testing machine generated displacement (mm)vs force (KN) graph

Table 3-3: Detail of material properties generated from Machine

Sample no	Rate(mm/min)	Modulus of Elastic	Tensile stress at Yield (Mpa)	Strain at Yield (Zero Slopes (%))
Sample -2	.27	71572.9	229.94	2.75
Sample-3	.27	68995.52	207.89	2.75

Based on the above test result, specimen four had been subjected to initial slip due to not tightening in the upper and lower jaw at the required level, it depends on the experience of the test conductor. The other three specimens reached their upper level of tensile stress, but it gained some difference due to the specimen's cross-section area. The displacement vs force curve has shown the oscillation of load change with displacement, due to the rapture of the Material, so it is used to average Force divided by area in each displacement value to calculate the stress at each loading point. Sample 1 was broken with less time of displacement due to some notch at the surface of the coupon sample, so it is noticeable that the sample of coupon must be free of notch, or any surface shape changes will impact the results. Therefore, the result of test sample 2 and test sample- 3 used to calculate stress and strain at each loading stage .The Figure 3-6: Stress-strain curves of the specimens base on above calculated data ,and that graph

used to calculate the material property of Yield stress and stain for the aluminium alloy. The braking value of the force of each sample is given in Table 3-4, and it's column -4 represent strain 2 which represent the strain values obtained from the extensometer reading and it's column – 3 ,represent the tensile displacement which provide the displacement got from initial preload force at jaw were tighten but it was kept less than 500 N.

Table 3-4 Braking value of force of each Sample

Sample no	Tensile stress at Break (Standard)(MPa)	Tensile Displacement at Break (Standard)(mm)	Tensile Strain (Strain 2) at Break (Standard)(%)
1	53.63	2.4	9.36
2	46.18	3.05	12.19
3	42.96	3.13	12.53
4	72.04	2.53	10.12

The complete stress-strain curve of the specimens is illustrated in Figure 3-6: Stress-strain curves of the specimens Table 3 6 provides a detailed overview of the material properties derived from the tested coupons. Notably, the suggested yield strength value for the specimens is reported as 152.45 MPa and proof Strength is 168.MPa.

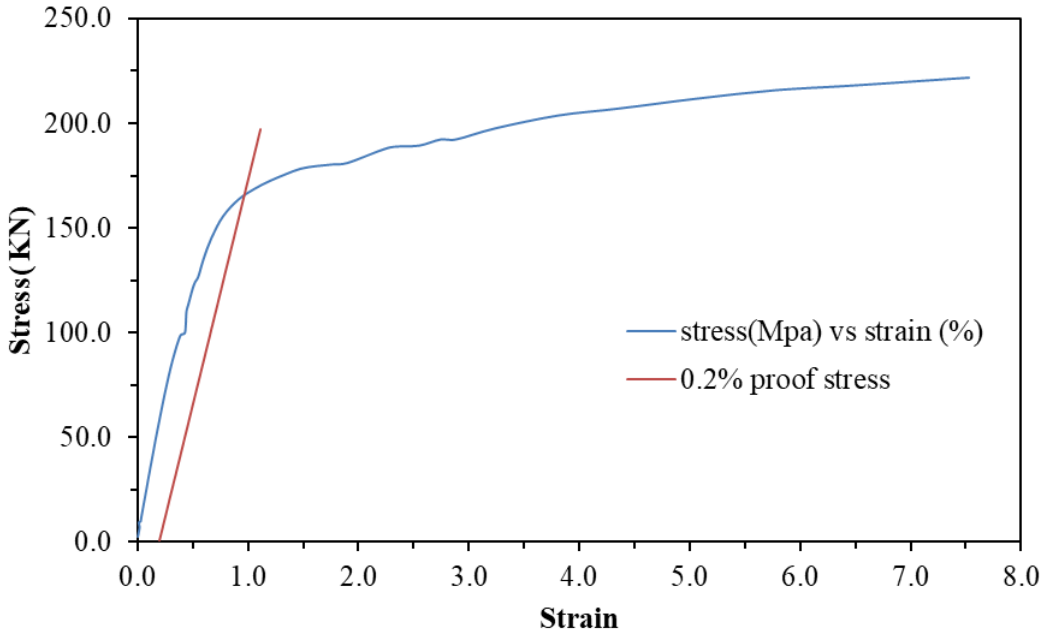

Figure 3-6: Stress-strain curves of the specimens

Table 3-5: Material properties obtained from tensile coupon tests

Coupon ID	Thickness t (mm)	Ultimate stress fu (MPa)	Yield stress fy (MPa)
FTF240-2	1.92	170.2	152.45
FTF240-3	2.02	168.4	152.50
Mean	1.97	169.3	152.45

3.3 Analysis of experimental results

Table 3-6 presents a concise overview of the column dimensions alongside the experimental failure loads (PEXP) for all nine test specimens. It was determined that local and distortional buckling were the predominant failure modes across all tested short and intermediate columns, and global buckling with local buckling occurs in failure load in slender columns as concluded in Table 4-5. Visual representations of these failure modes are provided in Figure 8, showcasing the typical shapes of columns upon failure. The length and no of screws used in the column change with it axial compressive strength as provided in Figure 3-7. The axial capacity is reduced with column section length increased from 500mm to 1500mm.

Figure 3-7Table 3-6: Past experimental result

Specimen	Web A' mm	Flange B' mm	Length L mm	Thickness T mm	Spacing S mm	Experimental Results P_{EXP} KN
Short						
FTF240-t1.98-L500-S100	240	45	500	1.98	100	83.21
FTF240-t1.98-L500-S200	240	45	500	1.98	200	78.8
FTF240-t1.98-L500-S400	240	45	500	1.98	400	72.66
Intermediate						
FTF240-t1.98-L1000-S225	240	45	1000	1.98	225	80.26
FTF240-t1.98-L1000-S450	240	45	1000	1.98	450	74.85
FTF240-t1.98-L1000-S900	240	45	1000	1.98	900	72.42
Slender						
FTF240-t1.98-L1500-S350	240	45	1500	1.98	350	69.21
FTF240-t1.98-L1500-S700	240	45	1500	1.98	700	61.91
FTF240-t1.98-L1500-S1400	240	45	1500	1.98	1400	61.03

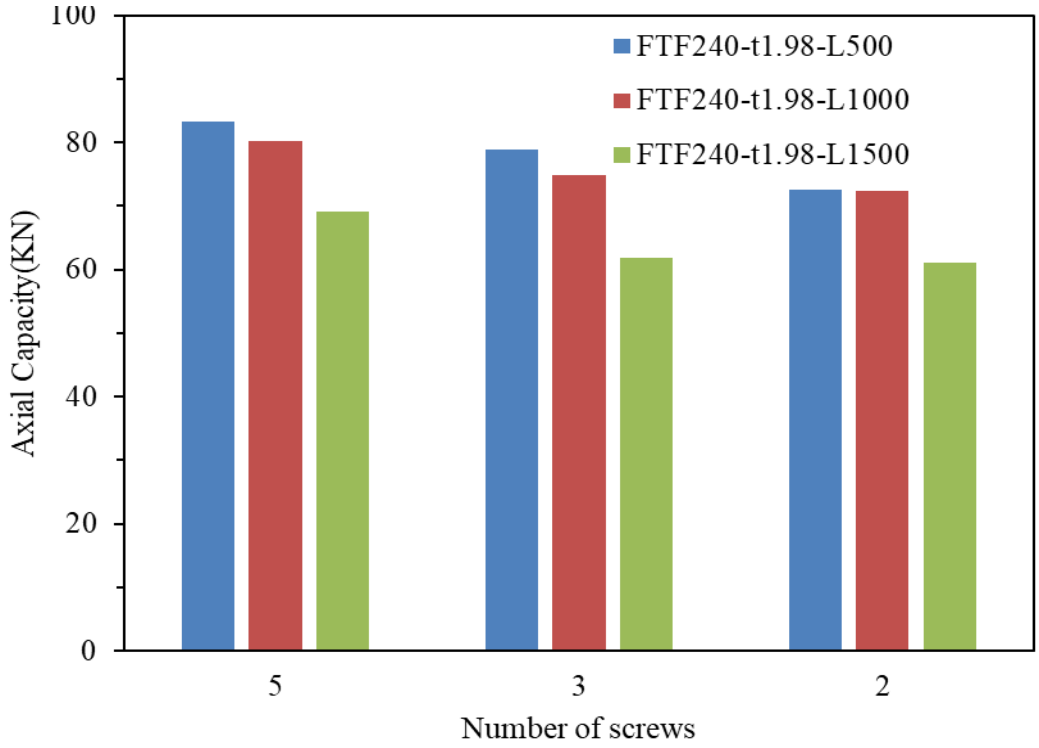

Figure 3-7: Number of screws vs axial capacity (kN) as experimental results

Additionally Figure 3-8, Figure 3-9 illustrates the axial load versus mid-height lateral displacement graphs for select channels, namely FTF240-t1.98-L500-S100, FTF240-t1.98-L500-S200, and FTF240-t1.98-L1000-S225.. The experiment experienced initial slip due to inconsistencies in the loading increments throughout the loading process. This caused the experimental curve to exhibit a lower gradient, indicating higher stiffness. However, this does not affect the critical axial capacity of the column. Therefore, the experimental results are still suitable for validating the finite element model for the perforated web with FTF built-up column.

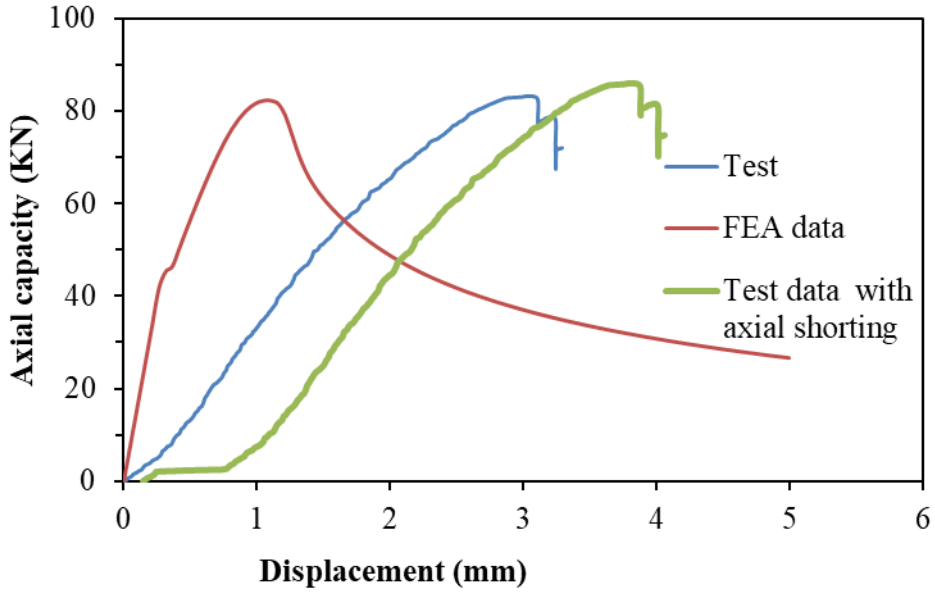

Figure 3-8: Displacement (mm) vs axial capacity (KN) of the specimens

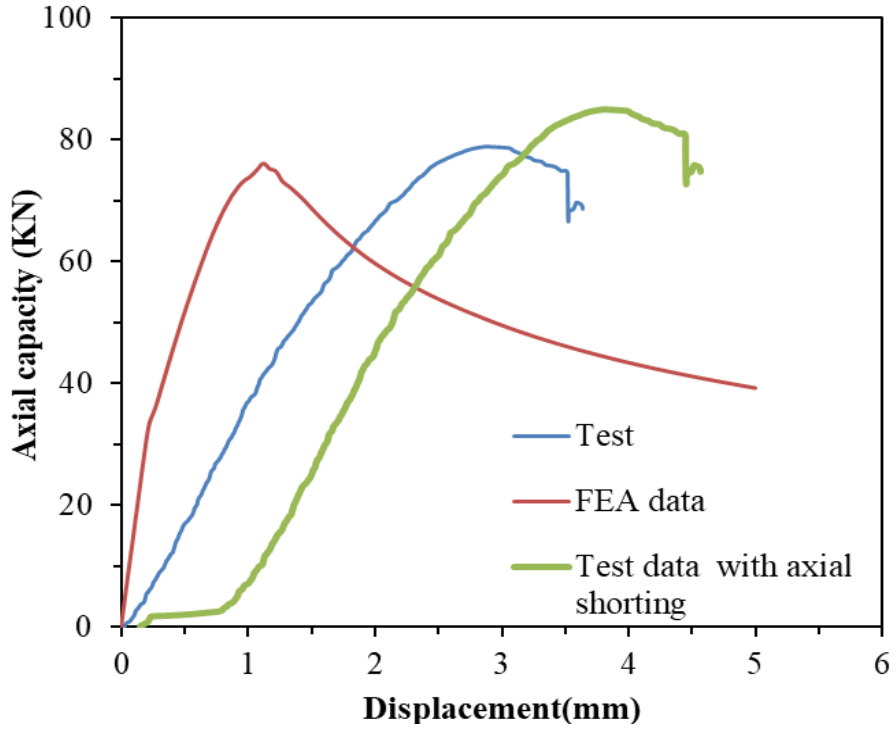

Figure 3-9: Displacement (mm) vs axial capacity (KN) of the specimens

The behaviour of axial shortening versus loading is depicted in Figure 3-9. Prior to reaching the plastic stage, the relationship between load and axial shortening exhibited near-linearity until approximately 78.81 KN, representing approximately 92.82% of the ultimate

failure load (85.01 KN) for specimen FTF240-t1.98-L500-S200. Subsequently, as the specimen entered the plastic stage, nonlinear behaviour became evident. Similar observations were noted across other tested specimens.

For specimen FTF240-t1.98-L500-S100, characterized by two single channels connected by five fasteners with 100 mm spacing, both local and distortional buckling were observed in the failure mode. Notably, the aluminium FTF built-up channels remained structurally intact at failure, with localized deformation near the column ends becoming apparent upon reaching the ultimate load, as illustrated in Figure 3-10 c.

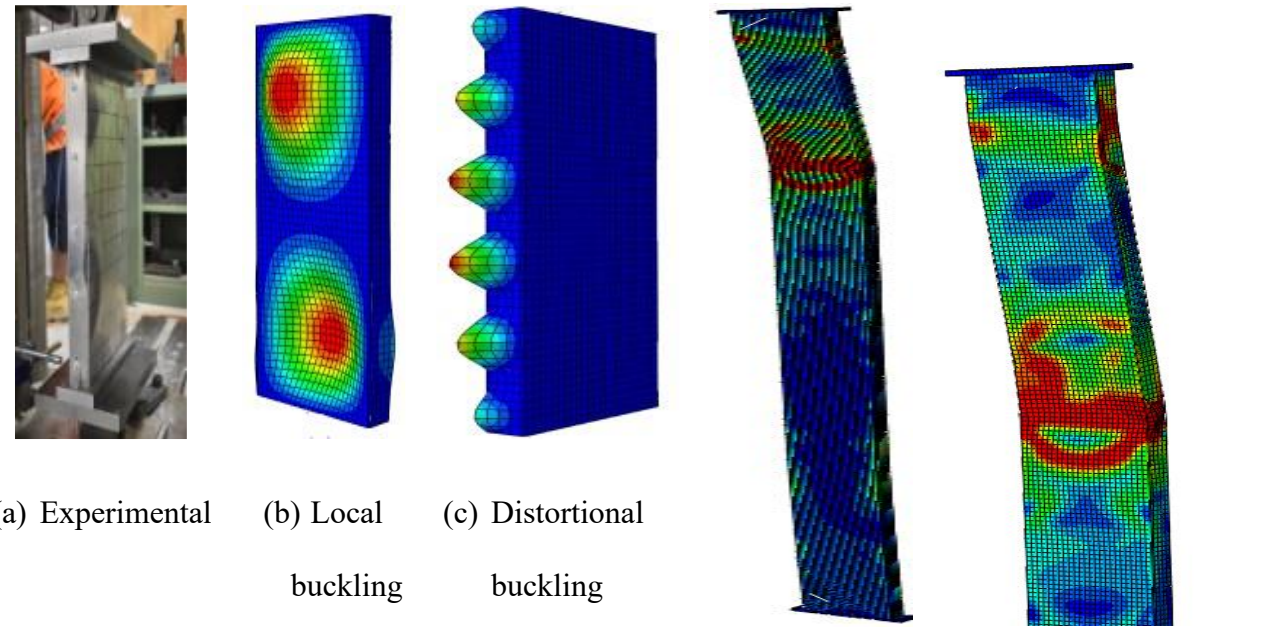

(a) Experimental (b) Local buckling (c) Distortional buckling (d) Global buckling full view & detail view at one end

Figure 3-10: Localized deformation near the column

This detailed analysis highlights the importance of understanding the failure modes and deformation behaviours of aluminium alloy built-up channel sections under axial compression, contributing valuable insights to the field of structural engineering.

Chapter 4 – Description of finite element modelling and Validation

4.1 General

Abaqus software was used to develop a nonlinear elasto-plastic FE model to simulate the face-to-face built-up aluminium alloy channel sections subject to axial compression as given in Figure 4-1. The FE model used the measured cross-section dimensions and material properties obtained from the tensile coupon tests. The detailed modelling techniques are discussed below. The key parameters considered in this study were material properties, screw spacing, and the thickness of the channel sections. For example, the label "FTF240-S100-T1.98-L500-0.2D" is elaborated below. FTF240- Web width, S100- Spacing of Screws, T1.98 -Thickness of plate,L500-length of channel,0.2D – Diameter of hole, H -number of holes

4.2 Modelling of geometry and material properties

An elastic-plastic model was used to model the overall geometry of the built-up columns. The von Mises yield surface was used in the classical metal plasticity model to define the isotropic yielding and plastic hardening of the steel. The material properties were taken from the results of tensile coupon tests and included in the FE models. As per the abaqus manual, the engineering material curve was converted into a true material curve by using the equations given next.

$$\sigma_t = \sigma_e(1 + \varepsilon_e) \text{----------} \quad (1)$$

$$\varepsilon_t = ln(1 + \varepsilon_e) - \frac{\sigma_t}{E} \text{----------} (2)$$

where E is Young's modulus; σ_t refers to true stress; ε_t is true strain; σ_e indicates engineering stress; and indicates engineering strain.

The material properties used in the parametric study analysis were extracted from the *Atlas Quality Management Manuals* for the aluminium alloy 5052 datasheet (Atlas, 2020). is given below Table 4-1.

Table 4-1 Material used for modelling

Alloy and Temper	Elastic Modules (GPa)	Yield strength (MPa)	Poison ratio
5052-HS32	70	160	0.3
5052-HS34	70	180	0.3
5052-HS36	70	200	0.3

4.3 FE meshing

The face-to-face built-up aluminium alloy channel sections were modelled using the S4R shell elements available in abaqus. The S4R elements are 4-noded linear quadrilateral thick shell elements that have six degrees of freedom per node. The C3D8 solid elements were used to model the upper and lower endplates. As the Table 4-2 and Table 4-2, the results of a mesh sensitivity analysis, and the capacity of the computer to time consuming for analysis of the model, the mesh size of 10 mm × 10 mm was used for modelling the face-to-face built-up aluminium alloy channel sections and the endplates. However, finer mesh sizes were employed in specific regions such as the corner area between the flange and web of the section. The aspect ratio of the elements was close to one. A typical FE mesh is shown in Figure 4-1 for two models of FTF240-t1.98-L500 S100 & FTF 240 -t 1.98-L 500 S100- D0.2D.

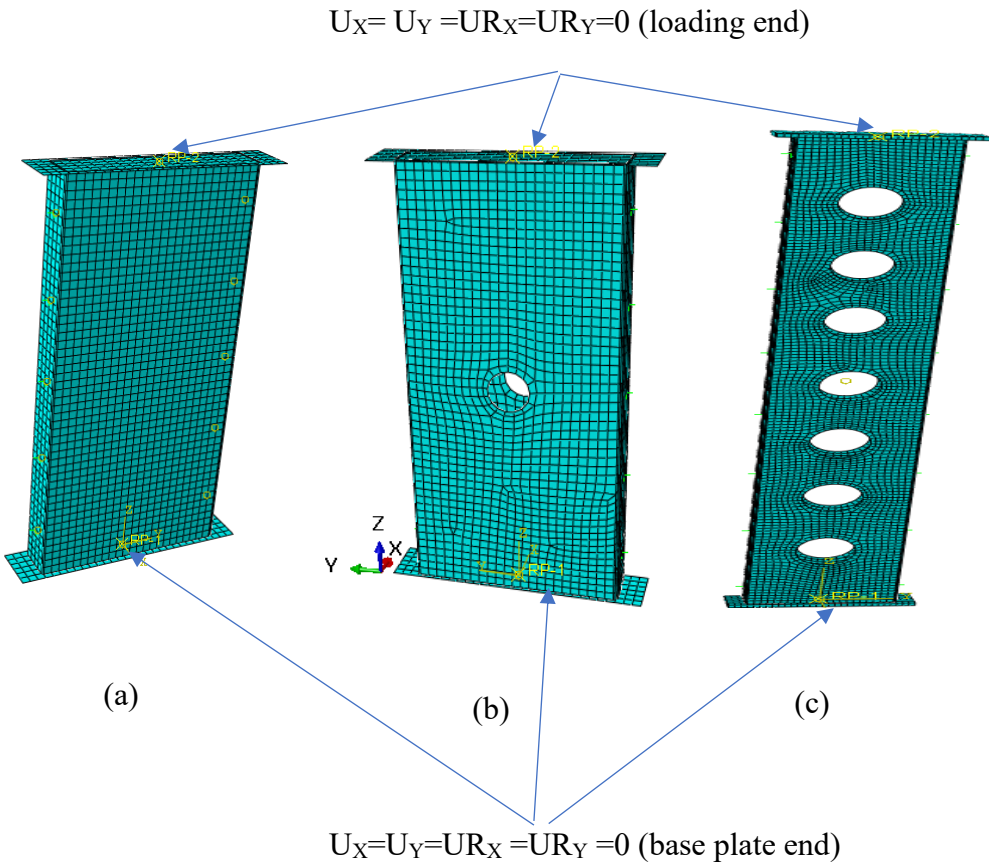

Figure 4-1: Mesh detail, boundary condition and loading point for (a) L=500 without hole, (b) L =500 with single hole , (c) L =1500 with multiple hole

Table 4-2: Mesh sensitivity analysis for selecting the optimum mesh size

Mesh size (mm)	**Axial capacity (KN)**	**% change in axial capacity**
25	284.23	
15	280.91	1.12
10	277.75	1.16
5	276.86	0.33

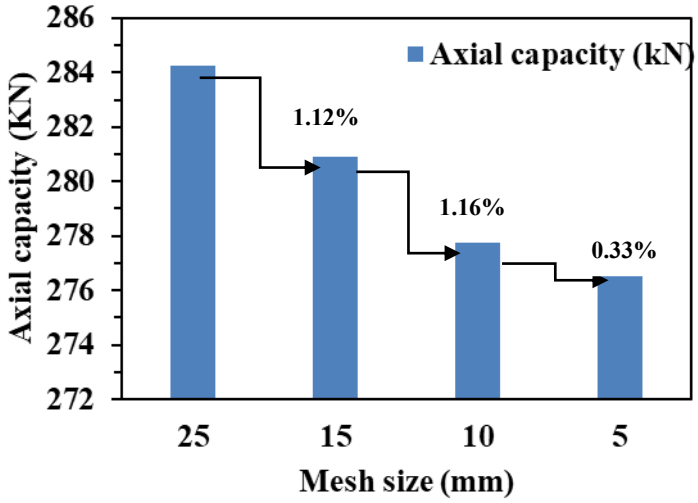

Figure 4-2: Sensitivity analysis for selecting the optimum mesh size

4.4 Boundary conditions and loading procedure

The face-to-face built-up aluminium alloy channel sections considered in this study were pin-ended columns. The displacements and rotations (boundary conditions) were assigned to the upper and lower end plates through reference points to simulate the upper and lower pin-end supports. The reference points were considered the centre of gravity of the cross-section at the top and bottom portions of the columns. The applied boundary conditions in the FE model are shown in Figure 4-1 for FTF240-t1.98-L500-S100. To simulate the experimental boundary conditions, the translation in the x and y were restrained, while the vertical translation in the z direction was not restrained at the top reference point (loading point). For the bottom reference point (reaction point), the translation in the x, y, and z were restrained. It should be noted that two ends were free to rotate along the minor axis. A beam connector with MPC rigid element available in the abaqus library was used to model the stiffness of the intermediate fasteners. Experimental setups might involve boundary conditions that cannot be directly modelled using standard constraints available in FEA software. MPCs provide a way to represent such conditions by specifying relationships between different points or degrees of freedom. The use of MPCs fastener connector screw type ensures that the simulated model closely matches the experimental setup, allowing for good comparison and accurate predictions of system

behaviour. The load was applied in increments using the Static General step and Displacement method available in the abaqus library, through the reference point of the top base plate as in Figure 4-1.

4.5 Geometrical imperfections

When accounting for imperfections in the finite element (FE) modelling process, the following factors were considered. For aluminium alloy channels with a thickness (t) less than 3 mm, the magnitude of the buckled shape was scaled to 0.34t for local buckling and 0.94t for distortional buckling, as outlined in *EN 1999-1-1:1999* (CEN, 1999). For samples with a thickness exceeding 3 mm, the imperfection magnitude was calculated using the equation proposed by Walker (2001).

$$\omega_d = 0.3t\sqrt{(\sigma_{0.2\%} / \sigma_{cr})} = 0.3t\,\lambda_s \text{ ----------(3)}$$

Where $\sigma_{0.2\%}$ and σ_{cr} is 0.2% proof stress of the material and elastic critical local/distortional buckling stress of the cross-section, and λ_s is the cross-sectional slenderness, given by

$$\lambda_s = \sqrt{(f_y / \sigma_{cr})} \text{ ----------(4)}$$

The The overall magnitude of buckling imperfections also accounted for the member's length. In the finite element (FE) models of short elements, either a local or distortional imperfection was incorporated, depending on which mode exhibited the lower critical buckling stress. For medium- and long-length sections, however, a combination of three buckling modes—local, distortional, and global—was introduced. This method was used to effectively integrate the imperfection magnitudes into the model, as described by Chen et al. (2022). The finite element models for the behaviour of plain sections, single-web-hole sections, and

multiple-web-hole sections under local, distortional, and global buckling patterns are presented in Figure 4-3. These models were generated using the output file from a buckling analysis. A static general analysis procedure was employed, and a scale factor of 1.5 was applied in the edit keyword to enhance the clarity of the deformed shapes, illustrating the different local, distortional, and global imperfection modes. But those shape consist with combination of local, distortional or global buckling mode, pure buckling mode obtain this section is very rare as given Figure 4-3

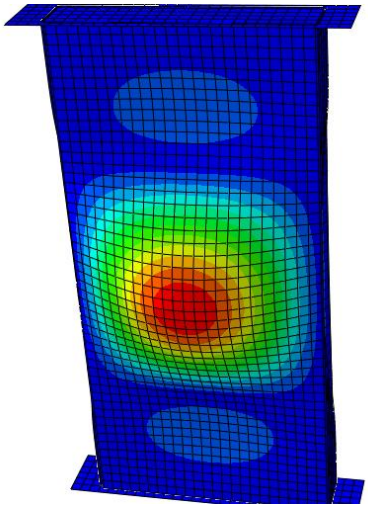

local buckling of plain

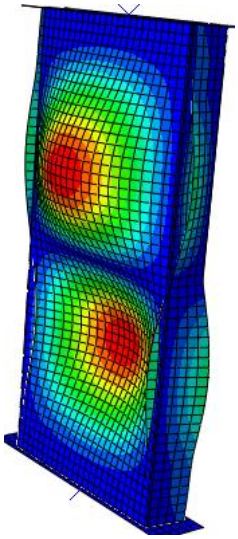

distortional buckling of plain

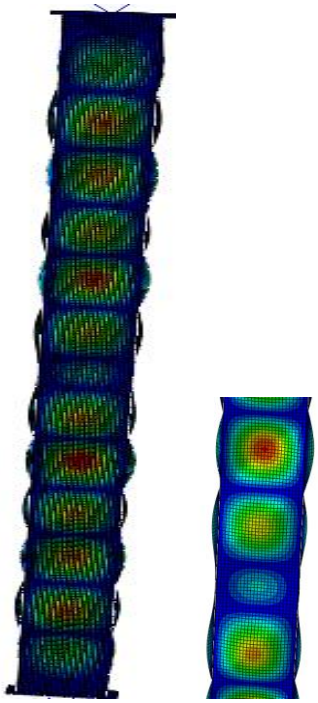

combined effect of Global and distortional buckling of plain section

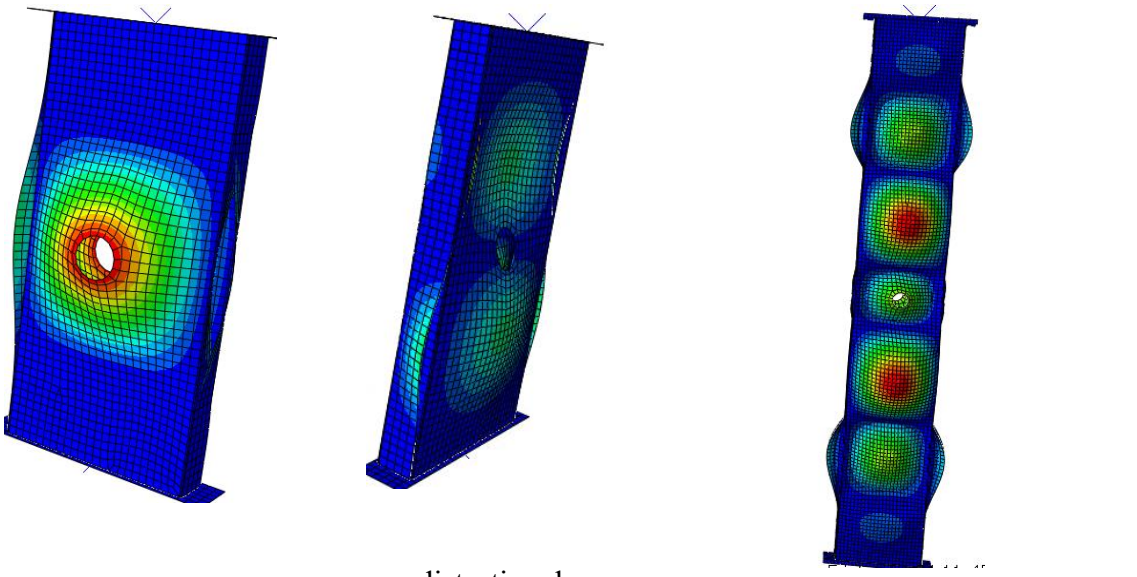

local buckling of one web hole

distortional buckling one web hole section

combined effect of global and distortional buckling of one web hole section

Figure 4-3 General imperfection shape in buckling analysis for plain, single hole and multiple holes with web section

4.6 Geometrical imperfections application for many holes web section

The buckling model and compression model for a 500 mm length of column with three holes in the web were built to apply the imperfection by changing the value of scale from 0 to 3.3. The model results are as below in Figure 4-4, Figure 4-6. As per the model analysis result was obtained with the imperfection value was changed to 0,0.5, 1,1.5,3.3 and the displacement vs force for each imperfection scale value then drawn in the graph as in Figure 4-4.

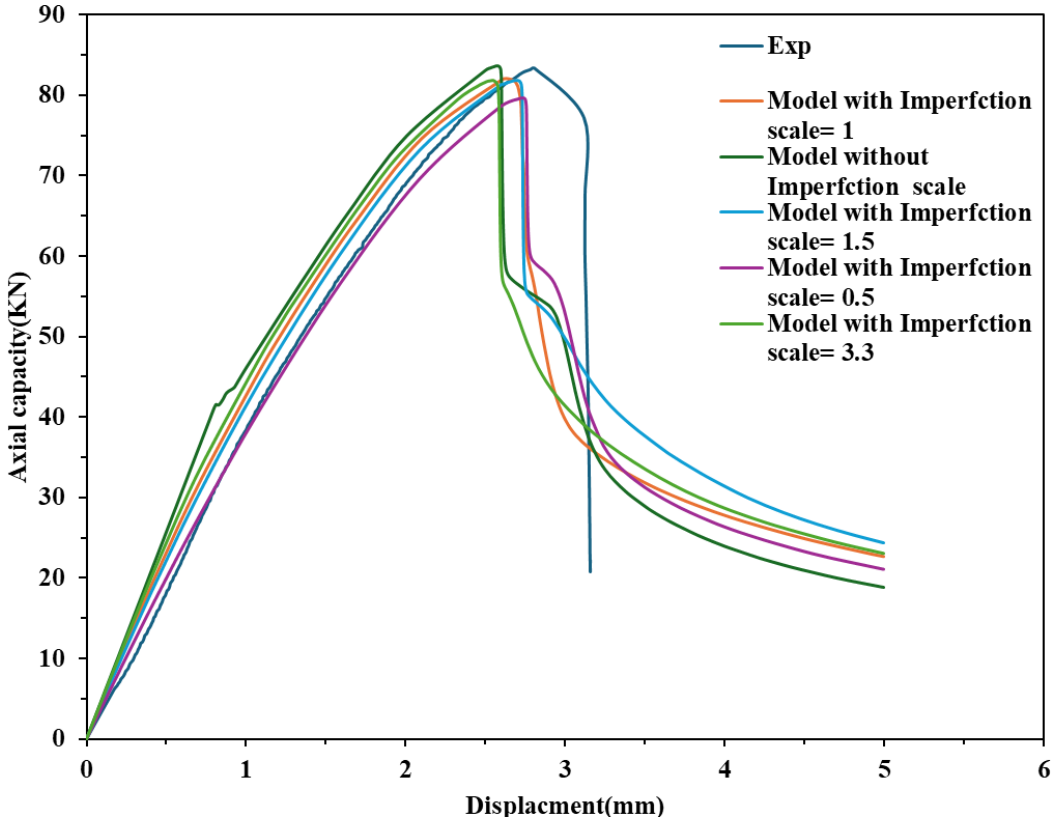

Figure 4-4: Displacement(mm) vs axial capacity(KN) for various imperfection scales for three-hole 1500mm length FTF in 100mm screw spacing

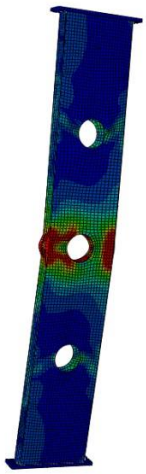	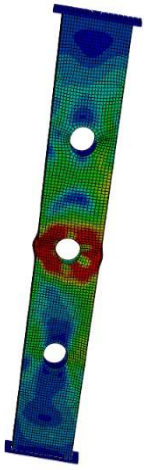	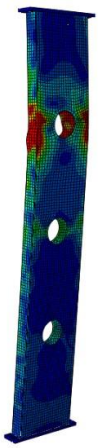	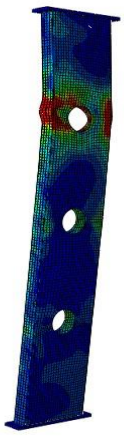	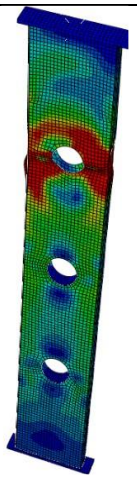
Model Without imperfection Consider, P_{FEA}= 83.7	Model with imperfection scale = 0.5, P_{FEA} = 81.86	Model With imperfection scale = 1, P_{FEA} = 81.88	Model With imperfection scale = 1.5, P_{FEA} = 79.69	Model With imperfection scale = 3.3, P_{FEA} = 81.75

Figure 4-5; Various imperfection scales for three-hole with 1500mm length FTF channel section in 100mm screw spacing

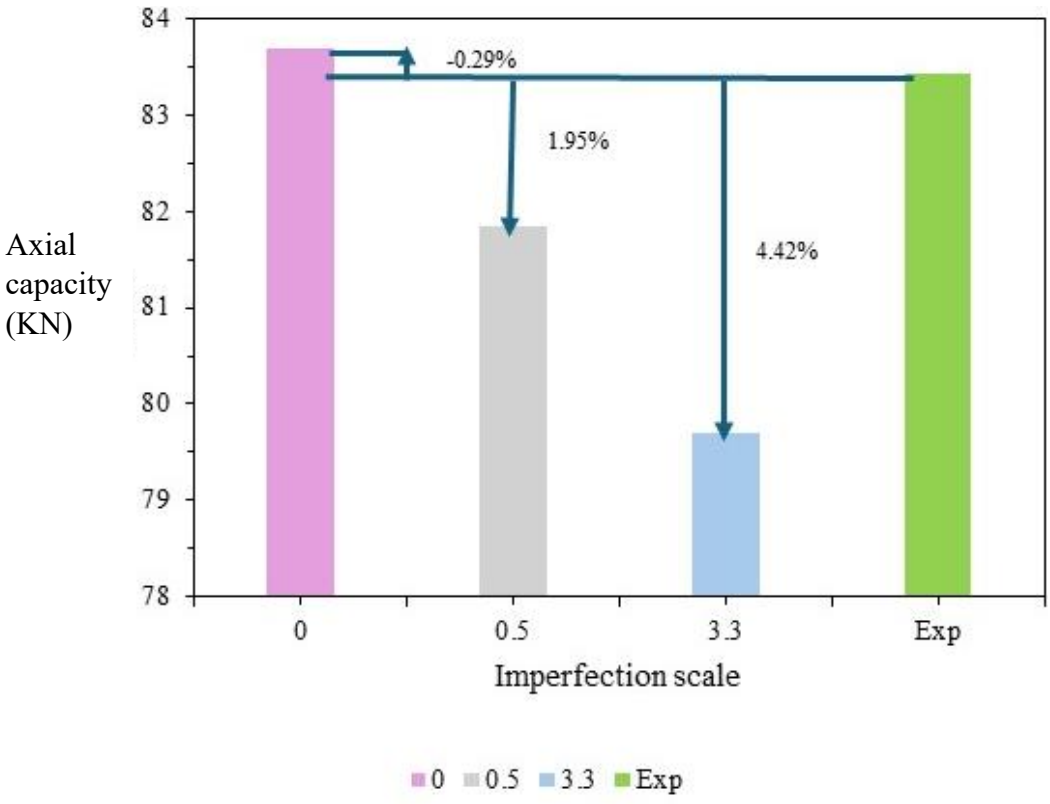

Figure 4-6: Imperfection scale vs axial capacity (KN) and compression of percentage change base to experimental result for three holes 1500mm length FTF in 100mm screw spacing

According to Figure 5-2 and Figure 4-4, the scale factor used in the model impacts the critical load differently compared to the model without a scale factor. This indicates that imperfections affect the critical force value in numerical modelling. However, the percentage difference between results obtained with and without imperfections is more realistic when compared to experimental results, as shown in Figure 4-6. For the remaining model simulations, the effect of imperfections becomes negligible, contributing less than 1% difference when compared to results from models without imperfections.

Therefore, imperfections are not considered in the parametric study due to their minimal impact on the final critical force derivation process. However, when graphically representing the displacement versus force graph, the experimental results align more closely with the model

using a scale factor of 1.5 (L/1000). This value lies between the EN 1993-1-3:2006 limits of 0.94t (1.86 mm) for distortion buckling and 0.34t (0.675 mm) for local buckling.

Hence, it can be concluded that the section is subjected to both distortion and local buckling in the same simulation. Based on these results, the modelling approach without imperfections is applied for the parametric study in this thesis.

4.7 Contact modelling

"Surface to surface" contact was used for modelling the interaction between the webs of two channel sections. Surface-to-surface interaction was used to model the intersection of the edges of channel sections and the top surfaces of the base plates. It should be noted that the web surface of one channel was considered as a master surface. The other was considered as a slave surface. The edges of the channel section were modelled as the slave surface, while the top surfaces of the end plates were considered as the master surface. The normal behaviour of the surface was defined as "Hard Contact", indicating that no penetration of the surfaces into

4.8 Analysis procedure

Two different methods of analysis were used to analyse the face-to-face built-up aluminium alloy channel sections: elastic buckling analysis and nonlinear static general analysis. Elastic buckling analysis was conducted to obtain the eigenvectors for the initial geometric imperfections. The magnitudes of the initial geometric imperfections were determined based on the *Australian/New Zealand Standard (AS/NZS 4600:2018)* (Standards Australia/New Zealand, 2018. Nonlinear static general analysis was used to apply the axial load on the face-to-face built-up aluminium alloy channel sections. The Buckling analysis method is used to predict the buckling behaviour of the built-up columns and find the most achievable geometric imperfection for each length and the most common imperfection result

used to apply in general static analysis for determining the direct compressive strength of the section.

4.9 Validation of the FE model

4.9.1 Validation of plain aluminium alloy face to face column

The comparison of axial strengths from both experimental tests and Finite Element Analysis (FEA) for FTF240 sections is presented in

Table 4-33. The results show that the FEA predictions are closely aligned with the test outcomes in terms of both axial strength and failure modes of the face-to-face built-up aluminium alloy channel sections. Additionally,

Table 4-34 compares the test results with those obtained using the Direct Strength Method (DSM) from AS/NZS 4600 for cold-formed steel design. The ratios of P_{EXP}/P_{FEA} and P_{EXP}/P_{DSM}, representing the experimental-to-FEA and experimental-to-DSM axial strength comparisons, are consistently close across all screw spacing. This indicates that the DSM, traditionally used for cold-formed steel, provides an accurate prediction of axial capacity for the aluminium alloy sections tested. This highlights the effectiveness of the DSM in evaluating the strength of these sections. Figure 4-7 shows the deflected shapes of short, intermediate, and slender columns obtained from the FE analysis, which agrees well with the experimental failure modes. Displacement vs axial capacity behaviour for both the FEA and experiments is plotted in Figure 4-88, for short, intermediate, and slender columns. Comparison results showed that the differences between the FE model prediction and the test results are very small. The mean value of the ratio between the experimental and numerical results (P_{EXP}/P_{FEA}) is 1.04, with a COV of 0.0002.

Table 4-3 shows how the FEA strengths are close to experimental strengths. FEA results are slightly conservative for all columns compared to experimental results. This might be a

consequence of the friction between the base plates and the edges of face-to-face built-up aluminium alloy channel sections. The lateral displacement versus axial capacity curves is plotted in Figure 4-8, for FTF240-S100-L500, FTF240-S200-L500, and FTF240-S225-L1000 sections and demonstrate good comparisons between the FEA and test results. As shown in Figure 4-8, there was reasonably good agreement between the FEA and experimentally measured axial capacity at mid-height of the built-up columns. Overall, the FE model showed very good correlations against the experimental results. It is important to note that the experimental results, as depicted in the displacement versus axial capacity graph in Figure 4-8, do not closely align with the finite element (FE) analysis results in terms of the initial stiffness of the axial capacity-displacement curves, while this does not affect the ultimate load results obtained from the FE models. This discrepancy is primarily attributed to the higher loading speed used in the experimental tests, which altered the stiffness of the specimens compared to the FE results.

Table 4-3: Axial strength of face-to-face built-up aluminium alloy plain section

Specimen	Web	Flange	Length	Thickness	Spacing	Modified Slenderness	Exp Results	FEA result		
	A'	B'	L	t	S	(KL/t) m	PEXP	PFEA	PEXP/ PFEA	Failure Mode
	mm	mm	mm	mm	mm		KN	KN		
Short										
FTF240-t1.98-L500-S100	240	45	500	1.98	100	24.73	83.21	82.27	1.01	LB-DB
FTF240-t1.98-L500-S200	240	45	500	1.98	200	28.71	78.8	76.52	1.03	LB-DB
FTF240-t1.98-L500-S400	240	45	500	1.98	400	40.93	72.66	71.41	1.02	LB-DB
Mean						31.46			1.02	
COV						71.28			8.8E-05	
Intermediate										
FTF240-t1.98-L1000-S225	240	45	1000	1.98	225	50.22	80.26	79.46	1.01	LB-DB
FTF240-t1.98-L1000-S450	240	45	1000	1.98	450	60.00	74.85	75.92	0.99	LB-DB
FTF240-t1.98-L1000-S900	240	45	1000	1.98	900	88.93	72.42	71.61	1.01	LB-DB
Mean						66.38			1.00	
COV						405.13			0.00021	

Slender										
FTF240-t1.98-L1500-S350	240	45	1500	1.98	350	75.74	69.21	67.21	1.03	LB-DB-GB
FTF240-t1.98-L1500-S700	240	45	1500	1.98	700	91.34	61.91	59.21	1.05	LB-DB-GB
FTF240-t1.98-L1500-S1400	240	45	1500	1.98	1400	137.00	61.03	58.12	1.05	LB-DB-GB
Mean						101.36			1.04	
COV						1013.57			0.00011	

Table 4-4 compression of experimental, finite element and DSM result for FTF section with plain web.

Specimen	Web	flange	Length	Thickness	Spacing	Modified Slenderness	Experimental Results	FEA result	P_{EXP}/P_{FEA}	Failure Mode	AS/NZ result (DSM)	Comparison	
	A'	B'	L	t	S	(KL/t)m	P_{EXP}	P_{FEA}					
	Mm	mm	mm	mm	mm		KN	KN			KN	P_{EXP}/P_{FEA}	P_{EXP}/P_{DSM}
Short													
FTF240-t1.98-L500-S100	240	45	500	1.98	100	6.27	83.21	82.27	1.01	LB-DB	85.61	1.01	0.97
FTF240-t1.98-L500-S200	240	45	500	1.98	200	8.31	78.8	76.52	1.03	LB-DB	83.42	1.03	0.94
FTF240-t1.98-L500-S400	240	45	500	1.98	400	13.69	72.66	71.41	1.02	LB-DB	82.72	1.02	0.88
Mean									1.02				
COV									8.8E-05				
Intermediate													
FTF240-t1.98-L1000-S225	240	45	1000	1.98	225	12.96	80.26	79.46	1.01	LB-DB	75.61	1.01	1.06
FTF240-t1.98-L1000-S450	240	45	1000	1.98	450	17.83	74.85	75.92	0.99	LB-DB	72.84	0.99	1.03
FTF240-t1.98-L1000-S900	240	45	1000	1.98	900	30.30	72.42	71.61	1.01	LB-DB	70.72	1.01	1.02
Mean									1.00				
COV									0.00021				
Slender													
FTF240-t1.98-L1500-S350	240	45	1500	1.98	350	19.65	69.21	67.21	1.03	LB-DB-GB	64.63	1.03	1.07
FTF240-t1.98-L1500-S700	240	45	1500	1.98	700	27.37	61.91	59.21	1.05	LB-DB-GB	62.27	1.05	0.99
FTF240-t1.98-L1500-S1400	240	45	1500	1.98	1400	46.92	61.03	58.12	1.05	LB-DB-GB	57.31	1.05	1.06
Mean									1.04				
COV									0.00011				

	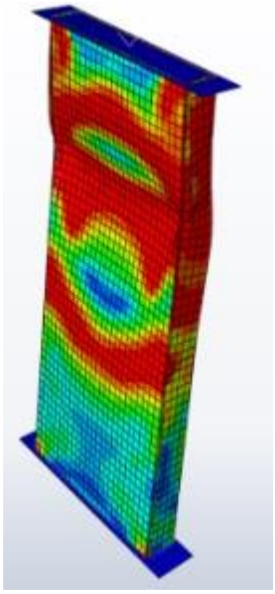	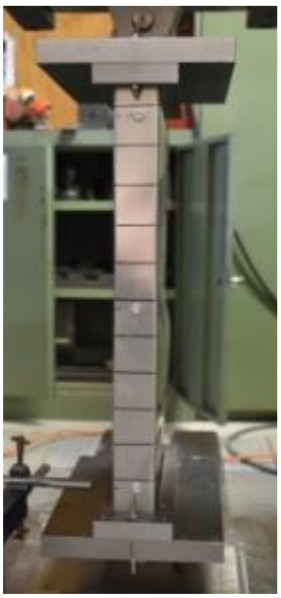	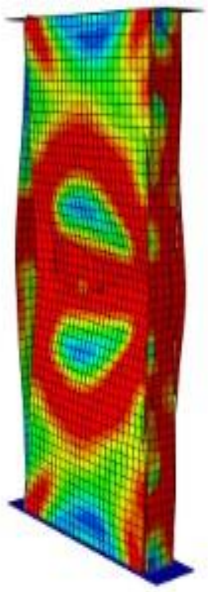
TEST	FEA	TEST	FEA
FTF240-t1.98-L500-S100		FTF240-t1.98-L500-S200	
	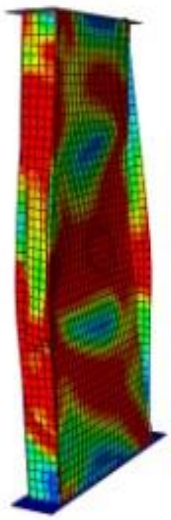		
TEST	FEA	TEST	FEA
FTF240-t1.98-L500-S400		FTF240-t1.98-L1000-S225	

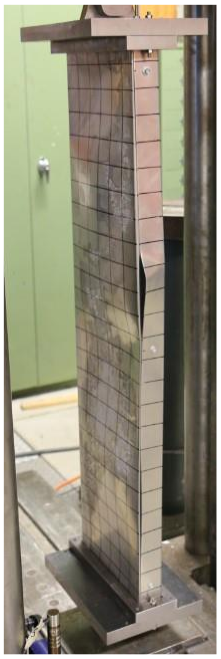	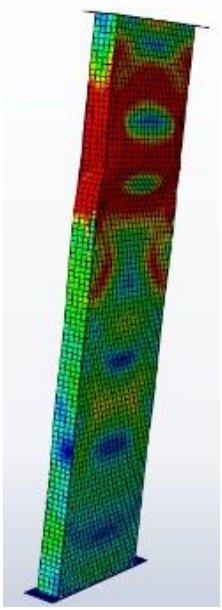	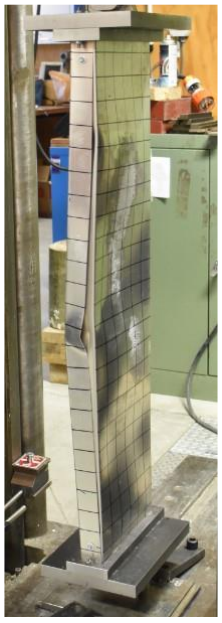	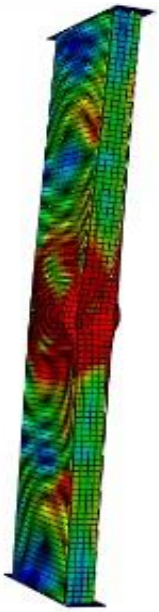
TEST	FEA	TEST	FEA
FTF240-t1.98-L1000-S450		FTF240-t1.98-L1000-S900	
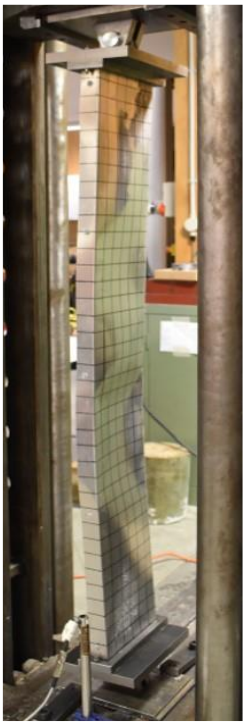	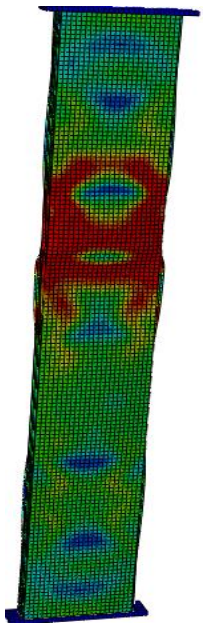		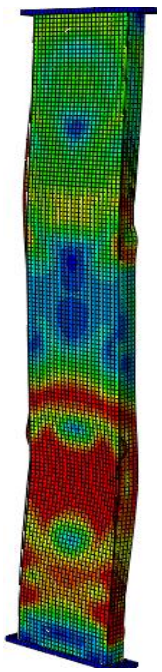
TEST	FEA	TEST	FEA
FTF240-t1.98-L1500-S350		FTF240-t1.98-L1500-S700	

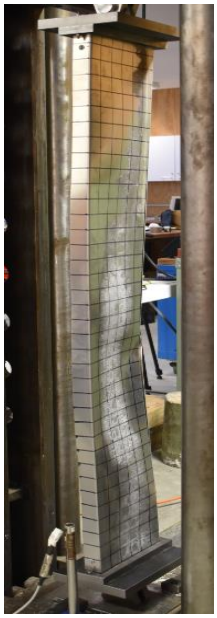

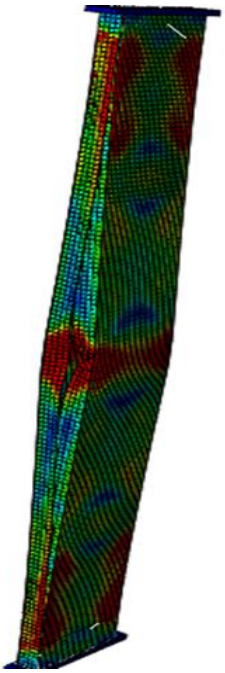

TEST	FEA
FTF240-t1.98-L1500-S1400	

Figure 4-7: Deformed shapes at failure from experimental and FEA for Plain section with FTF channel

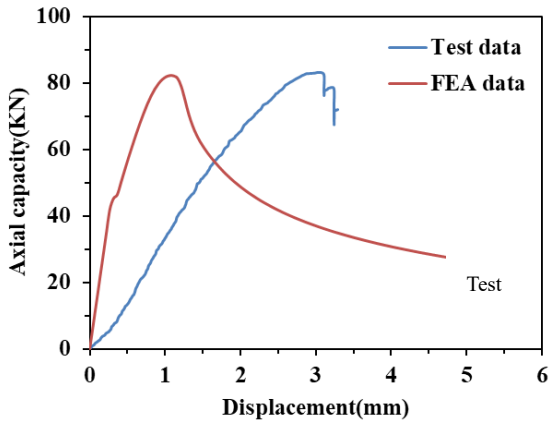

FTF240-t1.98-L500-S100

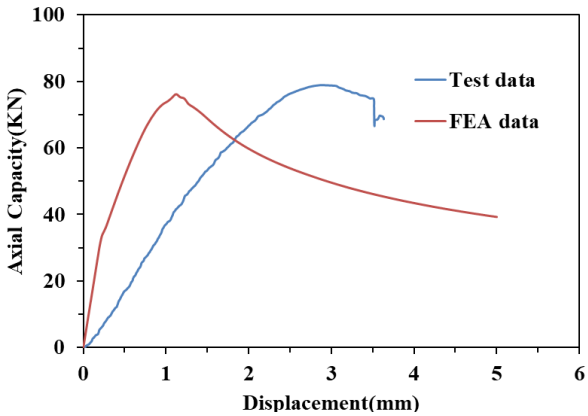

FTF240-t1.98-L500-S200

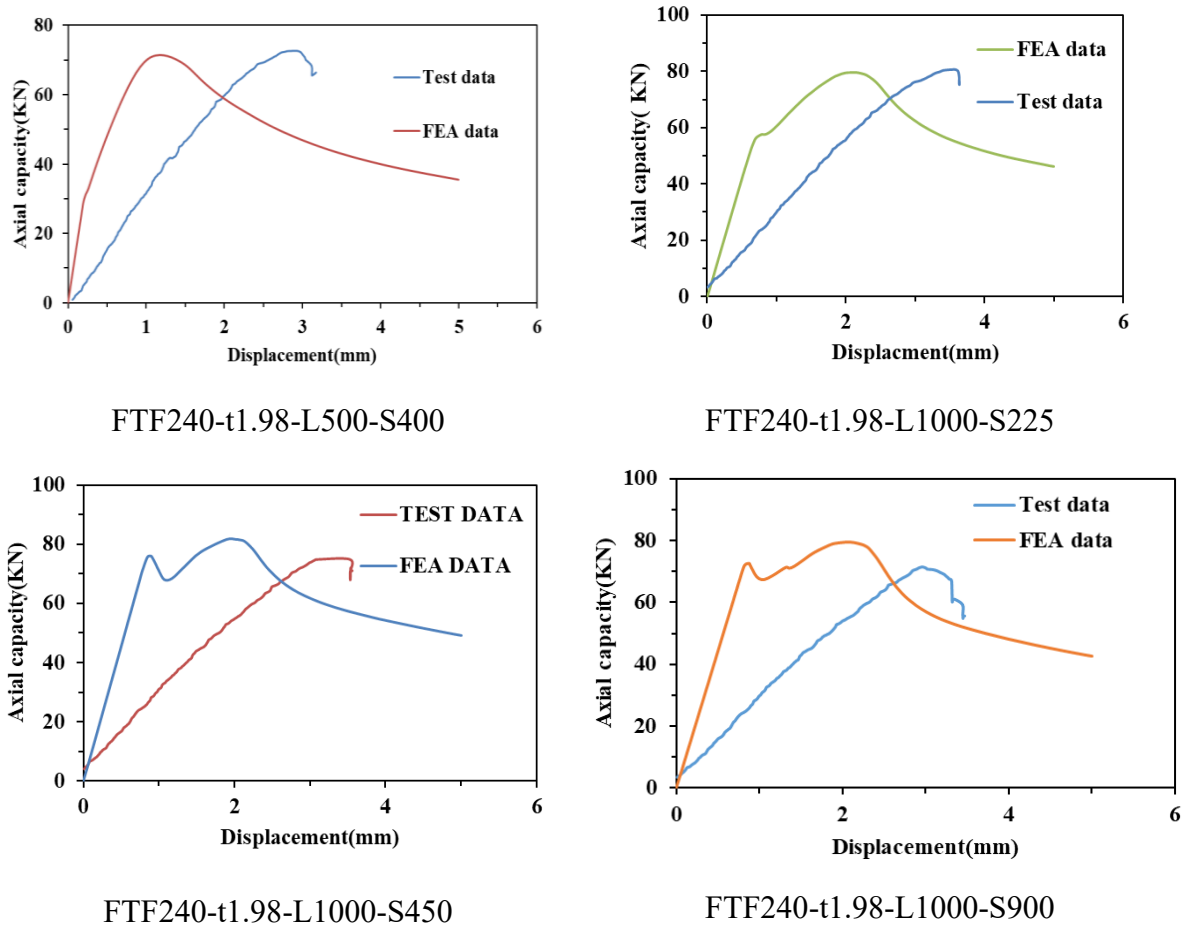

Figure 4-8: Axial displacement vs axial capacity from experimental and FEA Plain section for FTF built-up channel

4.9.2 Validation of aluminium alloy face to face column with single web hole and multiple holes.

The comparison of axial capacity from the tests and FEA are shown in Table 4-5, Table 4-6 , Table 4-7 for above FTF section. When compared to the test results, FE results were close in terms of axial capacity and failure modes of face-to-face built-up aluminium alloy channel sections with single web hole and multiple web hole. Figure 4-7, Figure 4-9 shows the deflected shapes of short, intermediate and slender columns obtained from the FE analysis for single hole and multiple holes, which presents good agreement with the experimental failure modes. Displacement-axial capacity shortening behaviour from both the FEA and experiments is plotted in Figure 4-8, Figure 4-10 for short, intermediate and slender columns for all one hole and many holes in the web. Comparison results showed that the differences between the FE model prediction and the test results are very small. The mean value of the ratio between the

experimental and numerical results (P_{EXP}/P_{FEA}) are 0.975, with a COV of 0. 00079 for one hole channel experimental and numerical results (P_{EXP}/P_{FEA}) for many holes in web are 0.98, with 0.0025. The Table 4- 6, Table 4-7, shows how the FEA strengths are close to experimental strengths but direct strength Method (DSM) Calculation as AS/NZ4600 is not close match with experimental result. The finite element analysis (FEA) results are slightly conservative compared to all columns' experimental and DSM results. This discrepancy may be attributed to several factors, including the friction between the base plates and the edges of the face-to-face built-up aluminium alloy channel sections. Additionally, experimental errors, such as inconsistencies in applying the compressive load and using a higher displacement increment rate during load application, may have contributed to the differences observed. The load versus lateral displacement curves is plotted in Figure 4-8 for FTF240-S100-L500-0.2D, FTF240-S200-L500-0.4D, and FTF240-S225-L1000-0.2D sections and demonstrate good comparisons between the FEA and test results for one hole in web channel section. The load versus lateral displacement curves is plotted in Figure 4-10 for FTF240-S100-L500-0.4D-3H, FTF240-S100-L1500-0.4D-5H, FTF240-S100-L1500-0.4D-7H, FTF240-S100-L1500-0.4D-9H,FTF240-S200-L1500-0.4D-3H and FTF240-S200-L1500-0.4D-7H sections and demonstrate good comparisons between the FEA and test results for many holes in web channel section. As shown in Figure 4-8, Figure 4-10, Overall, the FE model showed very good correlations against the experimental results.

Table 4-5: Axial capacity of FTF channel sections with one web holes

Specimen	Web	Flange	Length	Thickness	Spacing	Modified Slenderness	Exp. Results	FEA Results	P_{EXP}/P_{FEA}	Failure mode
	A' (mm)	B' (mm)	L (mm)	t (mm)	S (mm)	(KL/t)m	P_{EXP} (kN)	P_{FEA} (kN)		
Short										
FTF240-t1.98-L500-S100-0.2D	240	45	500	1.98	100	24.7	80.18	78.14	1.03	LB-DB
FTF240-t1.98-L500-S100-0.4D	240	45	500	1.98	100	24.7	76.79	75.11	1.02	LB-DB
FTF240-t1.98-L500-S100-0.6D	240	45	500	1.98	100	24.7	73.01	72.16	1.01	LB-DB
FTF240-t1.98-L500-S200-0.4D	240	45	500	1.98	200	28.7		77.41	0.00	LB-DB
FTF240-t1.98-L500-S200-0.2D	240	45	500	1.98	200	28.7		73.91	0.00	LB-DB
FTF240-t1.98-L500-S200-0.6D	240	45	500	1.98	200	28.7		72.68	0.00	LB-DB
FTF240-t1.98-L500-S400-0.2D	240	45	500	1.98	400	40.9	72.66	71.41	1.02	LB-DB
FTF240-t1.98-L500-S400-0.4D	240	45	500	1.98	400	40.9		72.38	0.00	LB-DB
FTF240-t1.98-L500-S400-0.4D	240	45	500	1.98	400	40.9		72.38	0.00	LB-DB
FTF240-t1.98-L500-S400-0.6D	240	45	500	1.98	400	40.9		72.029	0.00	LB-DB
Mean									0.45	
COV									2.9E-01	
Intermediate										
FTF240-t1.98-L1000-S225-0.2D	240	45	1000	1.98	225	50.2	78.36	77.029	1.02	LB-DB
FTF240-t1.98-L1000-S225-0.4D	240	45	1000	1.98	225	50.2		73.61	0.00	LB-DB
FTF240-t1.98-L1000-S225-0.6D	240	45	1000	1.98	225	50.2	69.6	71.12	0.98	LB-DB
FTF240-t1.98-L1000-S450-0.2D	240	45	1000	1.98	450	60.0		76.86	0.00	LB-DB
FTF240-t1.98-L1000-S450-0.4D	240	45	1000	1.98	450	60.0		72.63	0.00	LB-DB
FTF240-t1.98-L1000-S450-0.6D	240	45	1000	1.98	450	60.0		70.56	0.00	LB-DB
FTF240-t1.98-L1000-S900-0.2D	240	45	1000	1.98	900	88.9	66.28	72.11	0.92	LB-DB-GB
FTF240-t1.98-L1000-S900-0.4D	240	45	1000	1.98	900	88.9	68.59	71.51	0.96	LB-DB-GB
FTF240-t1.98-L1000-S900-0.6D	240	45	1000	1.98	900	88.9	66.41	70.31	0.94	LB-DB-GB
Mean									0.54	
COV									0.25869	
Slender										
FTF240-t1.98-L1500-S350-0.2D	240	45	1500	1.98	350	75.7		73.25	0.00	LB-DB-GB
FTF240-t1.98-L1500-S350-0.4D	240	45	1500	1.98	350	75.7	69.96	71.45	0.98	LB-DB-GB
FTF240-t1.98-L1500-S350-0.6D	240	45	1500	1.98	350	75.7		70.66	0.00	LB-DB-GB
FTF240-t1.98-L1500-S700-0.2D	240	45	1500	1.98	700	91.3		72.25	0.00	LB-DB-GB
FTF240-t1.98-L1500-S700-0.4D	240	45	1500	1.98	700	91.3		70.87	0.00	LB-DB-GB
FTF240-t1.98-L1500-S700-0.6D	240	45	1500	1.98	700	91.3		69.69	0.00	LB-DB-GB
FTF240-t1.98-L1500-S1400-0.2D	240	45	1500	1.98	1400	137.0	65.27	71.34	0.91	LB-DB-GB
FTF240-t1.98-L1500-S1400-0.4D	240	45	1500	1.98	1400	137.0	66.42	70.43	0.94	LB-DB-GB
FTF240-t1.98-L1500-S1400-0.6D	240	45	1500	1.98	1400	137.0	63.4	67.15	0.94	LB-DB-GB
Mean									0.42	
COV									0.24849	

Note: LB=Local buckling; DB=Distortional buckling; GB=Global buckling

Table 4-6: Compression of experimental, finite element and DSM results for FTF section with single web hole

Specimen	Web A' (mm)	Flange B ' (mm)	Length L (mm)	Thickness t (mm)	Spacing S (mm)	Modified Slenderness (KL/t)m	Exp. Results P_{EXP} (KN)	FEA Results P_{FEA} (KN)	Failure mode	DSM (KN)	Comparison P_{EXP}/P_{FEA}	Comparison P_{EXP}/P_{DSM}
Short												
FTF240-t1.98-L500-S100-0.2D	240	45	500	1.98	100	6.12	80.18	78.14	LB-DB	89.6	1.03	0.89
FTF240-t1.98-L500-S100-0.4D	240	45	500	1.98	100	6.09	76.79	75.11	LB-DB	88.16	1.02	0.87
FTF240-t1.98-L500-S100-0.6D	240	45	500	1.98	100	6.06	73.01	72.76	LB-DB	87.2	1.00	0.84
Mean											1.02	
COV											0.0001	
FTF240-t1.98-L500-S400-0.2D	240	45	500	1.98	400	13.9	77.44	76.29	LB-DB	84.5	1.02	0.92
FTF240-t1.98-L500-S400-0.4D	240	45	500	1.98	400	13.61	75.19	72.328	LB-DB	83.2	1.04	0.90
Mean											1.03	
COV											0.0003	
Intermediate												
FTF240-t1.98-L1000-S225-0.2*D	240	45	1000	1.98	225	8.82	78.36	77.029	LB-DB	77.98	1.02	1.00
FTF240-t1.98-L1000-S225-0.6*D	240	45	1000	1.98	225	8.54	69.6	71.12	LB-DB	76.66	0.98	0.91
Mean											1.00	0.96
COV												
FTF240-t1.98-L1000-S450-0.2D	240	45	1000	1.98	450	15.09	74.85	75.92	LB-DB	76.01	0.99	0.98
Mean											0.99	0.98
COV								0				
FTF240-t1.98-L1000-S900-0.2D	240	45	1000	1.98	900	28.88	66.28	72.11	LB-DB	70.42	0.92	0.94
FTF240-t1.98-L1000-S900-0.4D	240	45	1000	1.98	900	28.7	68.59	71.51	LB-DB	69.51	0.96	0.99
FTF240-t1.98-L1000-S900-0.6D	240	45	1000	1.98	900	28.51	66.41	70.31	LB-DB	68.22	0.94	0.97
Mean											0.94	
COV											0.0004	
Slender												
FTF240-t1.98-L1500-S350-0.4D	240	45	1500	1.98	350	12.19	69.96	71.45	LB-DB-GB	65.16	0.98	1.07
Mean											0.98	1.00
COV												
FTF240-t1.98-L1500-S1400-0.2D	240	45	1500	1.98	1400	44.52	65.27	71.346	LB-DB-GB	60.32	0.91	1.18
FTF240-t1.98-L1500-S1400-0.4D	240	45	1500	1.98	1400	44.31	66.42	70.43	LB-DB-GB	60.12	0.94	1.10
FTF240-t1.98-L1500-S1400-.6D	240	45	1500	1.98	1400	44.1	63.4	67.15	LB-DB-GB	59.18	0.94	1.07
Mean											0.93	

Table 4-7: Compression of experimental, finite element and DSM results for FTF section with multiple holes in the web

Specimen	Web	Flang	Length	Thickness	screws Spacing	Modi. Seln	Expe. result	FEA result		Failure Mode	DSM	Comparison	
	A' (mm)	B' (mm0	L (mm)	t (mm)	(mm)	(KL/t)m	P_{EXP} (KN)	P_{FEA} (KN)	P_{EXP}/P_{FEA}		(KN)	P_{EXP}/P_{FEA}	P_{EXP}/P_{DSM}
SELENDERS													
FTF240-t2-L1500-S100-0.4D-3- hole	240	45	1500	2	100	6.12	83.41	83.71	1.00	LB-DB-GB	67.8	1.00	1.23
FTF240-t2-L1500-S100-0.4D-5- hole	240	45	1500	2	100	6.09	73.6	76.21	0.97	LB-DB-GB	63.2	0.97	1.16
FTF240-t2-L1500-S100-0.4D-7- hole	240	45	1500	2	100	6.01	73.2	75.45	0.97	LB-DB-GB	62.1	0.97	1.18
FTF240-t2-L1500-S100-0.4D-9- hole	240	45	1500	2	100	5.9	72.04	74.73	0.96	LB-DB-GB	60.3	0.96	1.19
Mean												0.98	1.1921
COV												0.00018	0.00119
FTF240-t2-L1500-S200-0.4D-3- hole	240	45	1500	2	200	8.17	75.4	78.8	0.96	LB-DB-GB	66.5	0.96	1.13
FTF240-t2-L1500-S200-0.4D-7- hole	240	45	1500	2	200	8.14	73.2	74.23	0.99	LB-DB-GB	65.9	0.99	1.11
FTF240-t2-L1500-S200-0.4D-9- hole	240	45	1500	2	200	8.11	70.71	70.79	1.00	LB-DB-GB	64.1	1.00	1.10
Mean												0.98	1.12
COV												0.00031	0.00018

	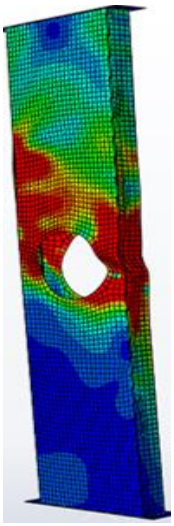		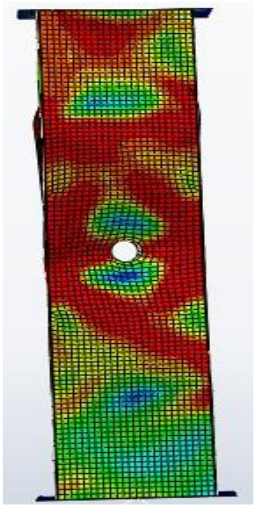
TEST	FEA	TEST	FEA
FTF240-t1.98-L1000-S900-0.6D		FTF240-t1.98-L1000-S225-0.2D	
	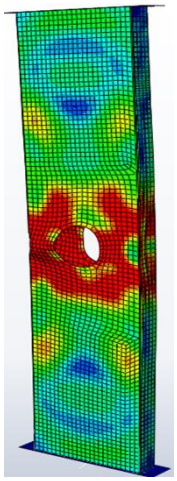		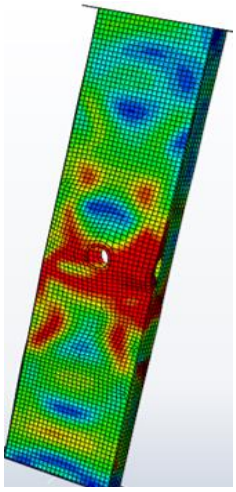
TEST	FEA	TEST	FEA
FTF240-t1.98-L1000-S900-0.2D		FTF240-t1.98-L1000-S900-0.4D	

<table>
<tr><td>  </td><td> 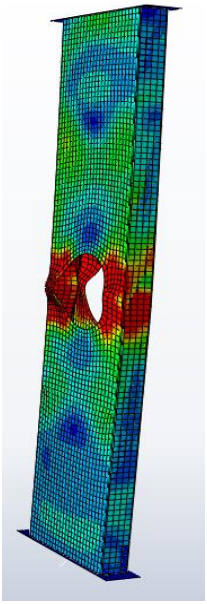 </td><td>  </td><td> 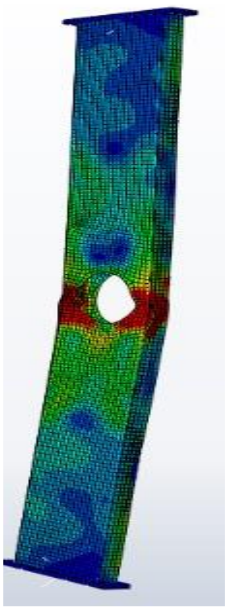 </td></tr>
<tr><td>TEST</td><td>FEA</td><td>TEST</td><td>FEA</td></tr>
<tr><td colspan="2">FTF240-t1.98-L1500-S1400-0.2D</td><td colspan="2">FTF240-t1.98-L1500-S350-0.4D</td></tr>
<tr><td colspan="2">  </td><td colspan="2"> 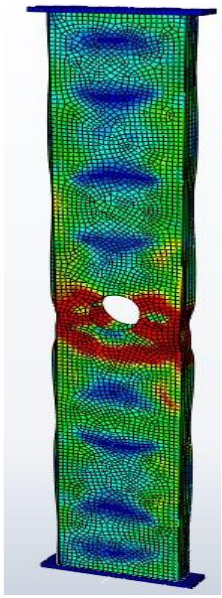 </td></tr>
<tr><td colspan="2">TEST</td><td colspan="2">FEA</td></tr>
<tr><td colspan="4">FTF240-t1.98-L1500-S1400-0.4D</td></tr>
</table>

Figure 4-9 :Deformed shapes at failure from experiments and FEA for one hole at web with FTF Channel

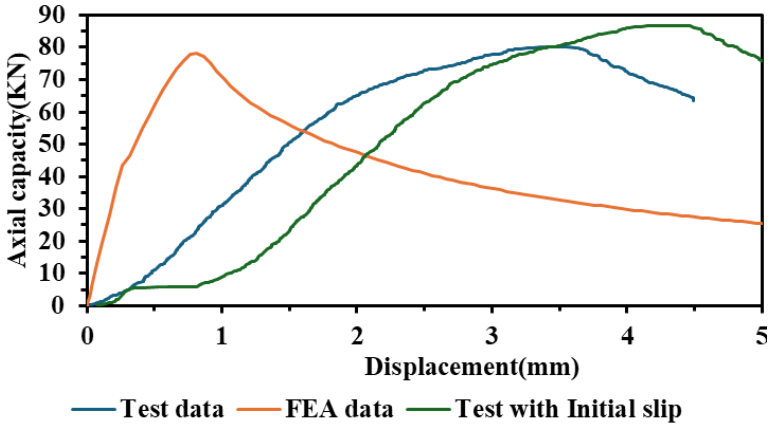

FTF240-t1.98-L500-S100-0.2D

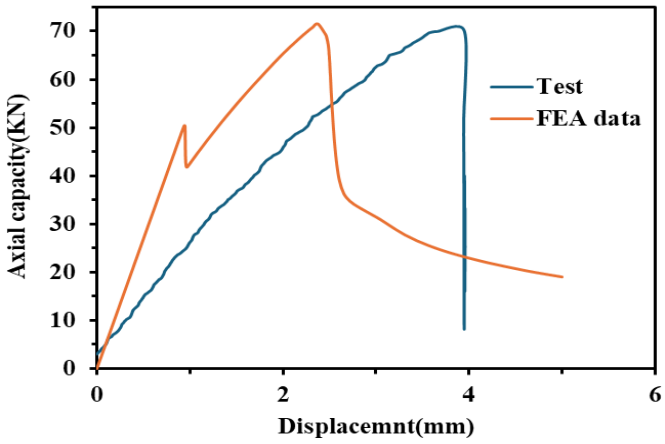

FTF240-t1.98-L1500-S1400-0.2D

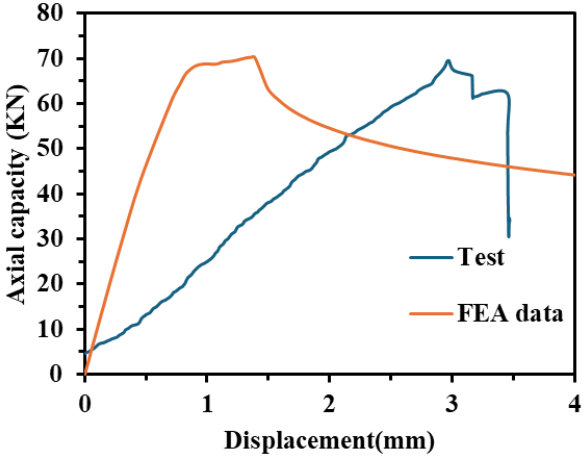

FTF240-t1.98-L1000-S900-0.6D

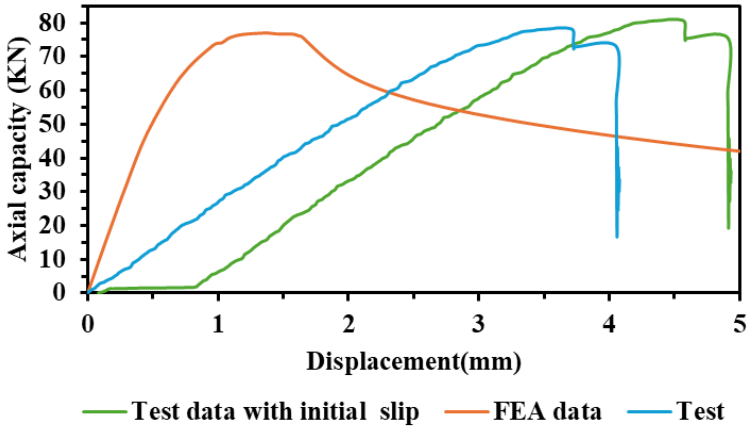

FTF240-t1.98-L1000-S225-0.2D

Figure 4-10: Axial capacity (KN) versus lateral displacement (mm) curves versus loading for one hole in web

	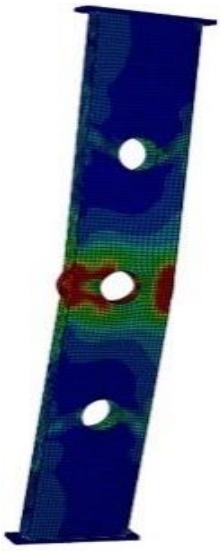		
TEST	FEA	TEST	FEA
FTF240-1.98-L1500-S100-0.4D-3H		FTF240-t1.98-L500-S100-0.4D-5H	
	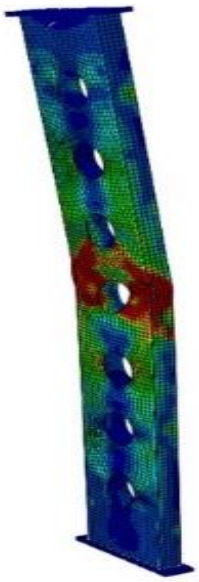		
TEST	FEA	TEST	FEA
FTF240-t1.98-L1500-S100-0.4D-7H		FTF240-t1.98-L1500-S100-0.4D-9H	

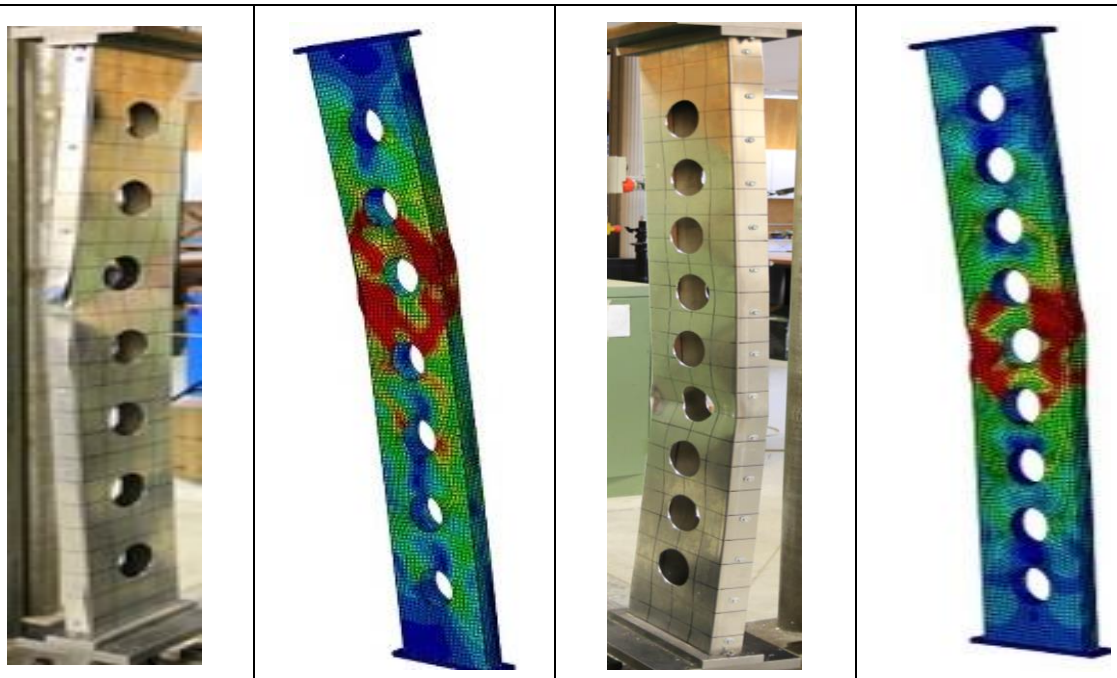

TEST	FEA	TEST	FEA
FTF240-t1.98-L1500-S200-0.4D-7H		FTF240-t1.98-L1500-S200-0.4D-9H	

Figure 4-11: Deformed shapes at failure from experiments and FEA for many holes at web with FTF Channel

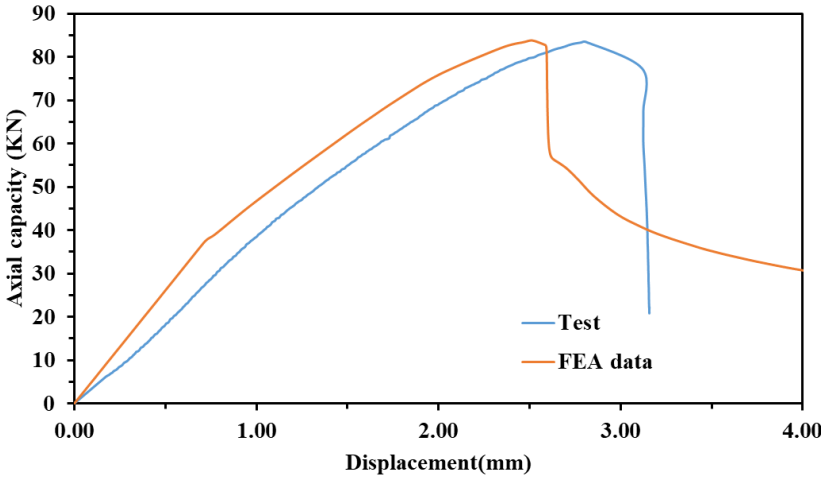

FTF240-t1.98-L1500-S100-0.4D-3H

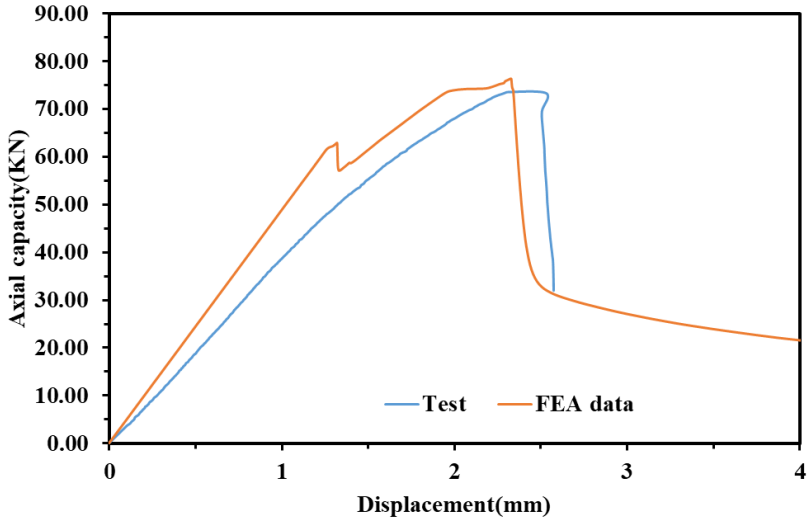

FTF240-t1.98-L1500-S100-0.4D-5H

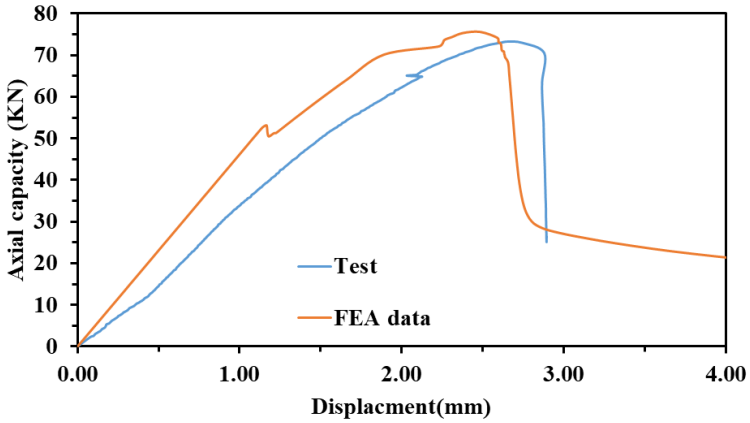

FTF240-t1.98-L1500-S100-0.4D-7H

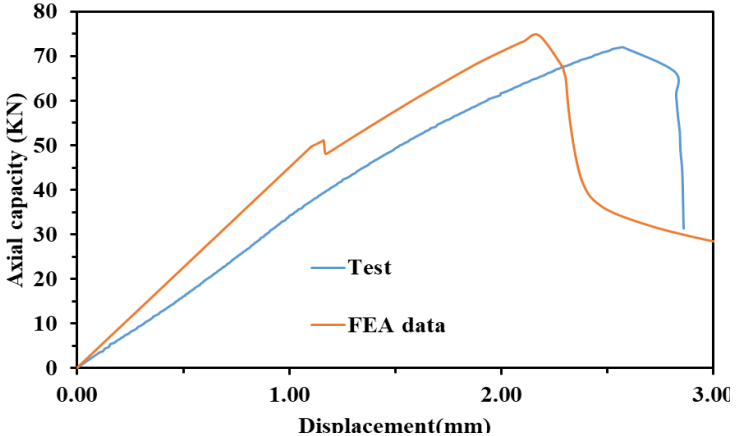

FTF240-t1.98-L1500-S100-0.4D-9H

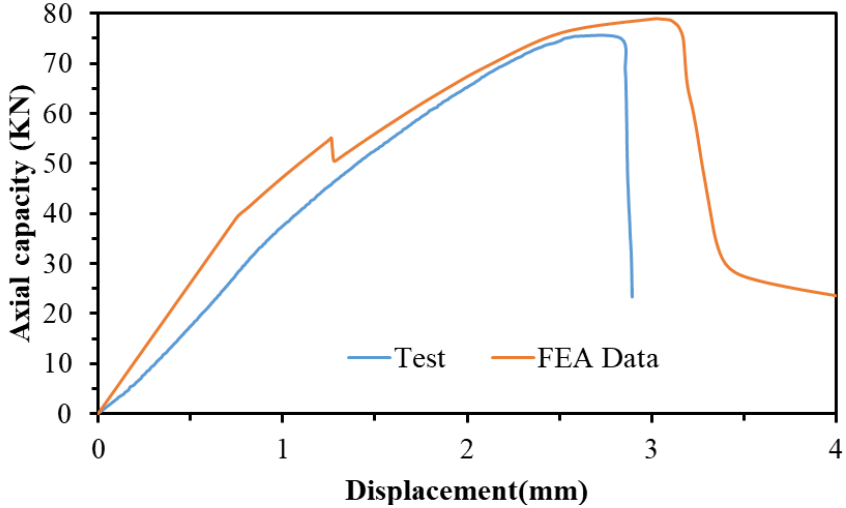

FTF240-t1.98-L1500-S200-0.4D-3H

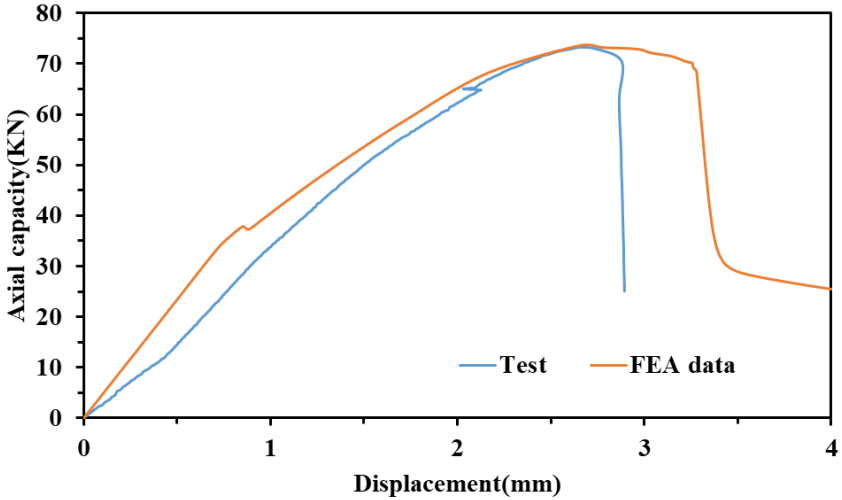

FTF240-t1.98-L1500-S200-0.4D-7H

Figure 4-12: Axial capacity (KN) versus lateral displacement (mm) curves versus loading for many holes in web

Chapter 5 – Parametric study

5.1 General

A comprehensive parametric study was conducted using validated finite element (FE) models. This study examined the FTF 240x45x500, FTF 240x45x1000, FTF 240x45x1500, and FTF 240x45x3000 channel sections across three different grades of yield strength: 5052-HS32, 5032-HS34, and 5032-HS36. The investigation included both plain sections and sections with a web hole at the centre for all three grades, resulting in a total of 495 models under consideration. Out of the 495 models, 120 are considered plain channel sections, while the remaining models feature a web hole at the centre and many holes.

For sections with web holes, the following designations were used: FTF 240x45x500-0.2D, FTF 240x45x500-0.4D, and FTF 240x45x500-0.6D, where the diameter was determined as a proportion of the web width (240 mm). Specifically, 0.2D corresponds to a diameter of 48 mm, 0.4D corresponds to 96 mm, and 0.6D corresponds to 144 mm. For many holes it is consider three, five seven and nine holes with 96mm diameter and, length are 1500mm and 3000mm channel section. The many holes are placed at symmetrically both side of the centre of the section. The modelling techniques employed for the parametric study were consistent with those used in the validation process. The key parameters considered in this study were material properties, screw spacing, and the thickness of the channel sections. For example, the label "FTF240-S100-T1.98-L500-0.2D-H-3" is elaborated below. FTF240- Web width, S100-Spacing of Screws, T1.98 -Thickness of plate, L500-length of channel, and 0.2D – Diameter of hole .H-Number of holes.

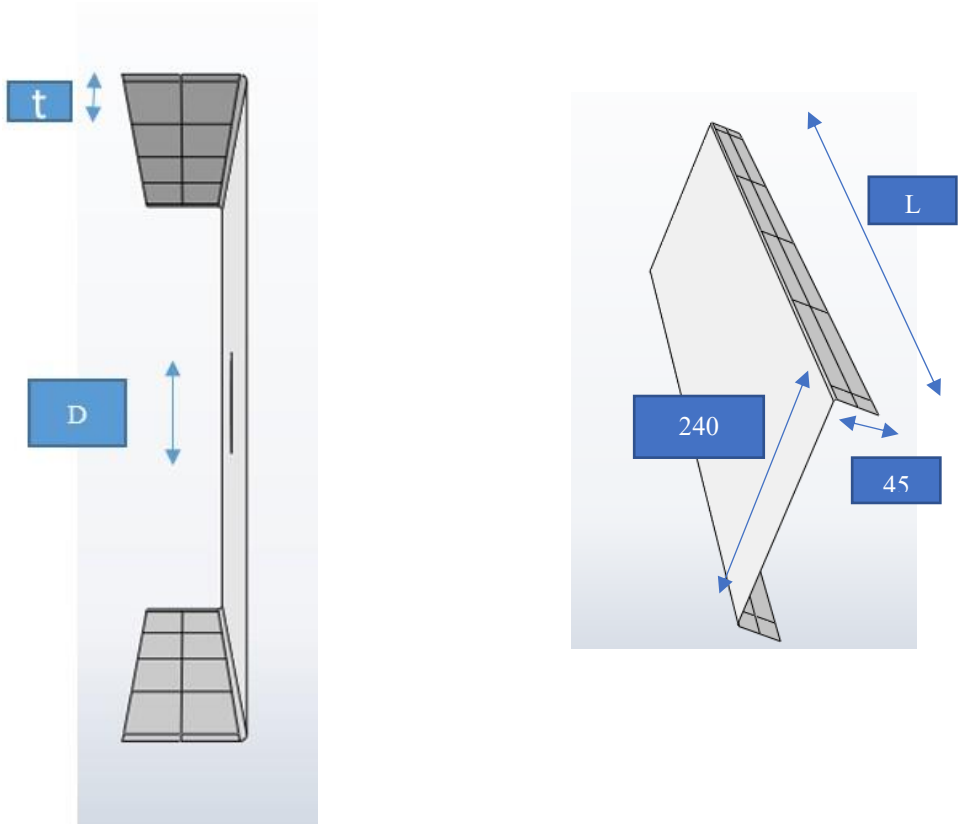

Figure 5-1: Cross-sectional details of channel for plain and web hole at centre (All dimensions are in mm)

5.2 Parametric Range

The parametric study is conducted by varying the parameters of each channel section as shown in the following Table 5-1, and Figure 5-1

Table 5-1: The Parametric study parameters and details of variation

Parameter	Variation Details (mm)
Channel web width (W)	Range: 500 ,1000 ,1500, 3000
Thickness (t)	Range: 1.3, 1.98,3,4,6
Hole Size(D)	Range: 48,96,144, = D = 0.2XwW, 0.4XW 0.6XW
Number of holes	3 ,5, 7 ,9
Grade	5052 HS32,5052 HS34 ,5052 HS36

Each of these parameters is systematically adjusted to analyse their impact on the performance of the channel sections under compression. This format clearly presents the parameters and their variations, making it easier to understand the scope of the parametric study. The results of Parametric model for the plain channel sections are documented in Table 5-2,Table 5-3 ,Table 5-4, while the results of parametric model for channel sections with a one

web hole and many holes in web are detailed in Table 5-5 ,Table 5-6, Table 5.-7 and Table-5-8 ,Table 5-9 respectively.

Table 5-2: The Parametric study parameters used to plain channel section with grade 5052 HS -32

Specimen	Thickness t(mm) (mm)	screw spacing(S) (mm) screws no's -2 (mm)	screws no's -3 (mm)	screws no's -5 (mm)	Failure Modes	P_{FEA} (KN) screws no's -2	screws no's -3	screws no's -5
Short								
FTF240-L500	1.3	400	200	100		38.12	39.21	42.24
	3					158.63	162.25	173.69
	4					276.12	288.99	319.46
	6					502.11	505.21	515.25
Intermediate								
FTF240-L1000	1.3	900	450	225		37.2	37.35	40.68
	3					153.89	159.2	170.25
	4					273.33	275.05	302.15
	6					495.33	500.1	510.12
Slender								
FTF240--L1500	1.3	1400	700	350		36.01	36.507	38.81
	3					152.69	156.62	165.25
	4					250.83	265.23	277.19
	6					491.57	497.35	503.25
FTF240-L3000	1.3	2400	1200	600		28.32	30.2	35.62
	3					107.54	143.5	160.65
	4					170.35	230.12	249.52
	6					255.65	371.23	496.2

(Aluminium grade HS 32 - Material -properties -yield stress = 155 and Ultimate tensile Stress = 205)

Table 5-3: The Parametric study parameters used to plain channel section with grade 5052 HS-34

Specimen	Thickness	screw spacing(S) (mm)			Failure Modes	$P_{FEA\ (KN)}$		
	t(mm)	screws no's -2	screws no's -3	screws no's -5		screws no's -2	screws no's -3	screws no's -5
	(mm)	(mm)	(mm)	(mm)				
Short								
FTF240-t1.98-L500	1.3	400	200	100		41.82	44.38	45.86
	3					171.83	181.96	192.26
	4					290.12	293.21	321.26
	6					568.67	575.12	587.12
Intermediate								
FTF240-t1.98-L1000	1.3	900	450	225		37.202	43.01	44.89
	3					165.23	177.28	189.52
	4					279.45	290.52	309.22
	6					558.5	565.12	585.22
Slender								
FTF240-t1.98-L1500	1.3	1400	700	350		36.32	41.27	43.75
	3					162.56	173.15	183.45
	4					264.61	286.85	305.25
	6					537.65	563.23	578.58
FTF240-t1.98-L3000	1.3	2400	1200	600		28.62	30.12	36.31
	3						144.54	173.25
	4						231.02	272.85
	6						370.94	539.54

Table 5-4: The Parametric study parameters used to plain channel section with grade 5052 HS-36

Specimen	Thickness	screw spacing(S) (mm)			Failure Modes	P_{FEA} (KN)		
	t(mm)	screws no's -2	screws no's -3	screws no's -5		screws no's -2	screws no's -3	screws no's -5
	(mm)	(mm)	(mm)	(mm)				
Short								
BU240-t1.98-L500	0.8	400	200	100		18.17	18.91	20.46
	4					307.2	309.1	330.96
Intermediate								
BU240-t1.98-L1000	0.8	900	450	225		15.2	17.11	18.25
	4					296.32	301.5	325.12
Slender								
BU240-t1.98-L1500	0.8	1400	700	350		14.59	16.1	17.94
	4					272.59	285.61	319.67
BU240-t1.98-L3000	0.8	2400	1200	600		135.43	13.12	15.21
	4					221.43	231.02	274.19

Table 5-5 The Parametric study parameters used to with one web hole section with grade 5052 HS-32

Specimen	Thickness	screw spacings(S) (mm)			Failure Modes	P_{FEA} -0.2XD (KN)			P_{FEA} -0.4XD (KN)			P_{FEA} -0.6XD (KN)		
	t(mm)	Screws no's -2	screws no' s -3	screws no' s -5		screws no' s -2	screws no' s -3	screws no' s -5	screws no' s -2	screws no' s -3	screws no' s -5	screws no' s -2	screws no' s -3	screws no' s -5
	mm	mm	mm	mm										
Short														
BU240-L500	1.98	400	200	100	LB &DB	70.8	74.4	80.4	69.1	72.4	79.5	67.1	71.2	77.1
	1.3				LB &DB	36.1	37.8	42.1	36.7	38.3	41.7	34.5	36.1	39.9
	3				LB &DB	165.78	167.58	202.85	157.2	162.54	195.45	152.4	157.25	190.45
	4				LB &DB	261.74	281.14	304.45	258; 74	268.4	290.41	220.54	228.4	257.21
	6				LB &DB	492.16	504.2	514.2	415.2	428.15	445.35	315.24	333.78	340.89
Intermediate														
BU240-L1000	1.98	900	450	225	LB &DB	68.4	72.1	77.9	64.9	68.2	74.1	63.2	66.14	71.4
	1.3				LB &DB	34.06	34.7	38.9	33.7	34.2	38.1	33.14	33.8	37.75
	3				LB &DB	160.5	171.52	172.5	153.2	163.1	167.2	145.2	157.01	159.4
	4				LB &DB	223.4	247.35	275.2	222.4	241.3	256.3	215.5	225.4	250.4
	6				LB &DB	421.25	423.22	435.12	412.3	418.6	430.85	312.5	330.1	339.2
Slender														
BU240--L1500	1.98	1400	700	350	LB &DB	71.346	72.25	73.25	70.46	70.87	71.45	67.15	71.65	70.66
	1.3				LB ,GB &DB	34.21	35.1	38.14	33.14	34.12	37.01	32.45	33.32	36.45
	3				LB,GB &DB	147.25	152.4	163.4	141.3	149.5	162.4	138.3	144.2	158.62
	4				LB,GB &DB	224.5	239.45	255.33	220.5	234.3	248.1	203.1	215.3	228.3
	6				LB,GB &DB	391.5	405.3	415.3	398.2	400.1	409.5	310.2	334.12	365.4
BU240-L3000	1.3	2400	1200	600	LB,GB &DB	27.5	29.4	35.33	24.3	28.4	34.33	21.3	24.2	30.5
	3				LB,GB &DB	100.3	135.4	154.3	90.5	124.5	141.2	85.4	115.3	134.3

Table 5-6: The Parametric study parameters used to channel with one web hole section with grade 5052 HS-34

Specimen	Thickness	screw spacings(S) (mm)			Failure Modes	P_{FEA} -0.2XD (KN)			P_{FEA} -0.4XD (KN)			P_{FEA} -0.6XD (KN)		
	t(mm)	screws no's -2	screws no's -3	screws no's -5		screws no's -2	screws no's -3	screws no's -5	screws no's -2	screws no's -3	screws no's -5	screws no's -2	screws no's -3	screws no's -5
Short	1.3	400	200	100	LB &DB	41.65	42.02	43.1	37.71	37.93	41.25	38.9	39.5	40.65
BU240-t1.98-L500	3	400	200	100	LB &DB	170.4	172.3	266.6	168.6	170.4	201.1	165.2	167.2	177.56
	4				LB &DB	270.8	298.3	330.1	268.4	288.6	310.5	259.5	260.2	264.8
	6				LB &DB	537.3	542.5	608.2	500.3	501.2	504.5	394.5	397.4	400.6
Intermediate	1.3	900	450	225	LB &DB	37.15	37.82	39.25	37.1	37.4	38.5	36.8	37.01	38.01
BU240-t1.98-L1000	3	900	450	225	LB &DB	168.52	170.2	175.6	167.2	169.4	175.2	163.2	166.2	174.2
	4				LB &DB	268.54	278.5	280.25	265.4	276.1	307.1	258.4	260.0	263.5
	6				LB &DB	486.9	490.1	490.5	484.3	488.3	502.4	390.5	395.2	400.1
Slender	1.3	1400	700	350	LB ,GB &DB	36.51	37.05	38.5	35.2	37.01	38.1	34.1	36.4	37.8
BU240-t1.98-L1500	3	1400	700	350	LB,GB &DB	165.4	168.2	173.25	164.1	166.5	172.4	163.2	165.5	170.5
	4				LB,GB &DB	266.5	270.1	274.2	265.8	269.8	273.8	256.3	258.1	262.5
	6				LB,GB &DB	480.5	482.3	485.1	480.1	481.3	485.0	388.5	390.2	392.5

Table 5-7: The Parametric study parameters used to channel with one web hole section with grade 5052 HS-36.

Specimen	Thickness	screw spacings(S) (mm)			Failure Modes	P_{FEA} -0.2XD (KN)			P_{FEA} -0.4XD (KN)			P_{FEA} -0.6XD (KN)		
	t(mm)	screws no's -2	screws no's -3	screws no's -5		screws no's -2	screws no's -3	screws no's -5	screws no's -2	screws no's -3	screws no's -5	screws no's -2	screws no's -3	screws no's -5
	(mm)	(mm)	(mm)											
Short														
FTF240-t1.98-L500	0.8	400	200	100	LB &DB	18.1	18.7	19.3	17.9	18.1	18.6	17.2	17.9	18.4
	4				LB &DB	285.1	312.0	331.5	289.6	300.4	330.2	288.1	300.0	320.1
Intermediate														
FTF240-t1.98-L1000	0.8	900	450	225	LB &DB	16.16	16.87	17.15	15.7	16.5	16.92	15.1	16.01	16.5
	4				LB &DB	283.9	291.8	300.3	280.4	290.5	297.5	277.5	288.1	295.6
Slender														

FTF240-t1.98-L1500	0.8	1400	700	350	LB,GB &DB	16.01	16.41	16.88	15.3	16.35	16.6	13.2	14.91	16.1
	4				LB,GB &DB	280.4	290.4	298.5	278.5	281.2	296.2	275.5	280.2	283.0

Material -properties - yields stress = 199 and Ultimate tensile Stress = 304)

Table 5-8: The Parametric study parameters used to channel with multiple holes in web section with grade 5052 HS-32

Specimen	**Thickness**	**Hole spacings (mm)**			**Failure Modes**	**P_{FEA} (kN)**					
	t	**Hole spacing - 150**	**Hole spacing- 200**	**Hole spacing- 300**		**No of Screws = 5**			**No of Screws = 3**		
	mm	**mm**	**mm**	**mm**		**Hole spacing - 150**	**Hole spacing - 200**	**Hole spacing - 300**	**Hole spacing - 150**	**Hole spacing - 200**	**Hole spacing - 300**
Slender											
BU240-L1500	3	150	200	300	LB-DB-GB	160.2	165.2	170.8	158.2	160.2	168.5
	4				LB-DB-GB	256.7	268.4	273.1	254.9	265.1	271.6
BU240-L3000	3	150	200	300	LB-DB-GB	118.0	130.9	**137.5**	116.5	125.4	132.4
	4				LB-DB-GB	195.5	197.8	205.1	189.0	194.1	198.4

Table 5-9: The Parametric study parameters used to channel with many holes in web section with grade 5052 HS-34

Specimen	**Thickness**	**Hole spacings (mm)**			**Failure Modes**	**P_{FEA} (kN)**					
	t	**Hole spacing - 150**	**Hole spacing- 200**	**Hole spacing- 300**		**No of Screws = 5**			**No of Screws = 3**		
	mm	**mm**	**mm**	**mm**		**Hole spacing - 150**	**Hole spacing - 200**	**Hole spacing - 300**	**Hole spacing - 150**	**Hole spacing - 200**	**Hole spacing - 300**
Slender											
BU240-L1500	3	150	200	300	LB-DB-GB	170.0	172.7	176.1	175.	176.0	185
	4				LB-DB-GB	282.4	278.6	292.0	281	282.2	294
BU240-L3000	3	150	200	300	LB-DB-GB	118.8	127.5	130.5	117	116.0	121
	4				LB-DB-GB	198.5	202.2	207.1	194	197.1	199

5.3 Influence of parameters to the axial capacity in aluminium alloy FTF plain section.

5.3.1 Influence of different grades of aluminium FTF channel sections with axial capacity

Figure 5-3 illustrates the effects of three different grades of aluminium alloy on the average axial capacity of face-to-face (FTF) channel sections. As shown in Table 5-10 and Figure 5-2, the compressive force varies with different aluminium alloy grades for a specific column length. The results indicate a clear trend: as the grade of aluminium alloy increases, corresponding to yield stresses of 155 MPa, 179 MPa, and 199 MPa, the compressive force also increases. This demonstrates that higher-grade aluminium alloys, with increased yield stress, result in greater compressive capacity. As shown in Table 5-11 and Figure 5-3, the average axial capacity increased by 0.56% to 3.02% for length 500 mm with upgrading strength from 152 to 179 and from 179 to 199, when it upgrades from material grade of the aluminium alloy FTF channel was upgraded from 5052-HS32 to 5052-HS34 and then to 5052-HS36 with keeping constant thickness of plate.

Table 5-10: Different grade of aluminium alloy compressive force with different column Length

	Compressive force (KN) for varied column length (mm)			
Yield stress (Pa)	**500 mm**	**1000 mm**	**1500 mm**	**3000mm**
152	319.46	302.15	277.19	249.52
179	321.26	309.22	305.25	272.85
199	330.96	325.12	319.67	274.19

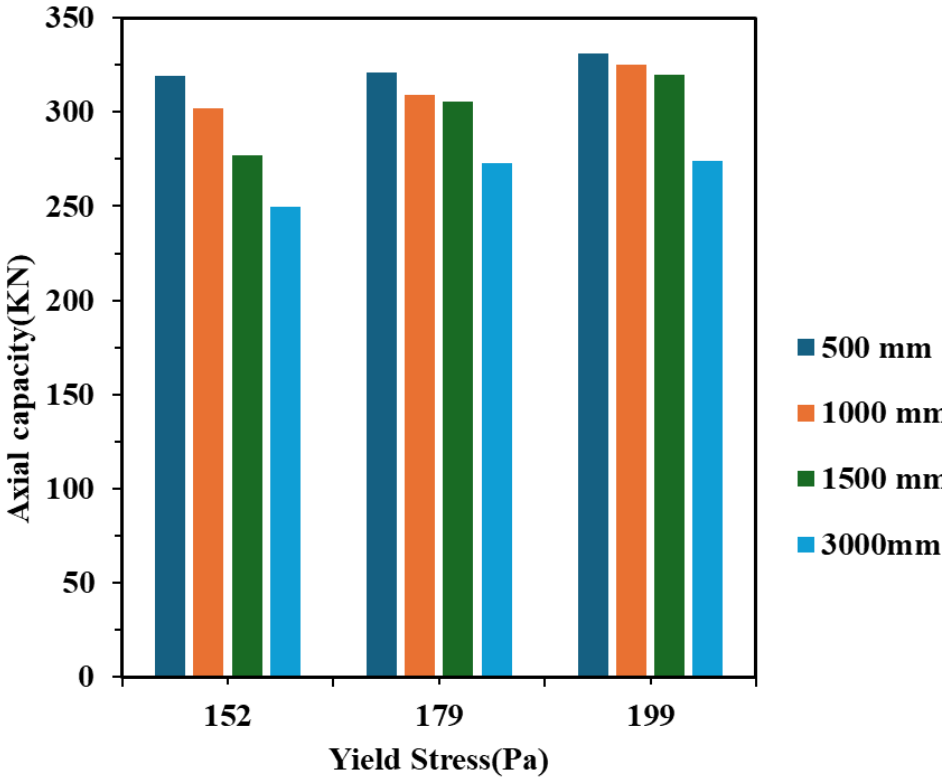

Figure 5-2: Different grade of aluminium alloy with axial capacity for different column length

Table 5-11: Upgrade in grade of aluminium alloy and % increment in axial capacity

Material yield stress (Pa)	**increment in axial capacity with upgrading yield stress for different column length (%)**			
Upgrading	**500**	**1000**	**1500**	**3000**
152-179(from HS 32 to HS 34)	0.56	2.34	10.12	9.35
179-199(From HS34 to HS 36)	3.02	5.14	4.72	9.89

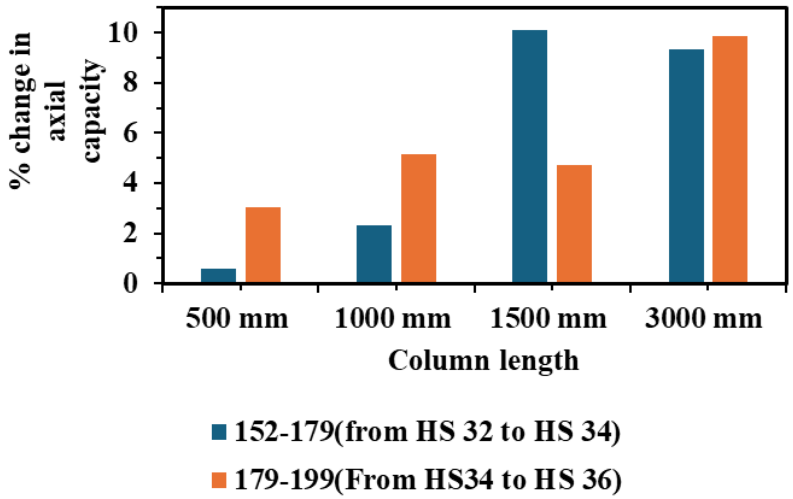

Figure 5-3: Different grade of aluminium alloy compressive force with different column length

Additionally, as shown in Table 5-12 and Figure 5-4, increasing the material grade by raising the yield stress from 152 MPa to 179 MPa results in the maximum axial capacity being reached within a column length range of 1400 mm to 1800 mm. Beyond this range, the compressive axial capacity tends to decrease, likely due to the increased impact of torsional or global buckling. This pattern is consistent when the material grade is further increased by raising the yield stress from 152 MPa to 199 MPa.

Therefore, to optimize the carrying capacity of the column, it is most favourable to select a section length within the range of 1400 mm to 1800 mm, particularly when upgrading the section to a higher-grade material. This selection ensures the best performance in terms of axial capacity.

Table 5-12: Upgrade in grade of aluminium alloy and % increment in axial capacity

	% increment of axial capacity (KN) for varied column length (mm)			
grade (Yield Stress)	**500**	**1000**	**1500**	**3000**
152-179	0.56	2.34	10.12	9.35
152-179	3.60	7.60	15.33	9.89

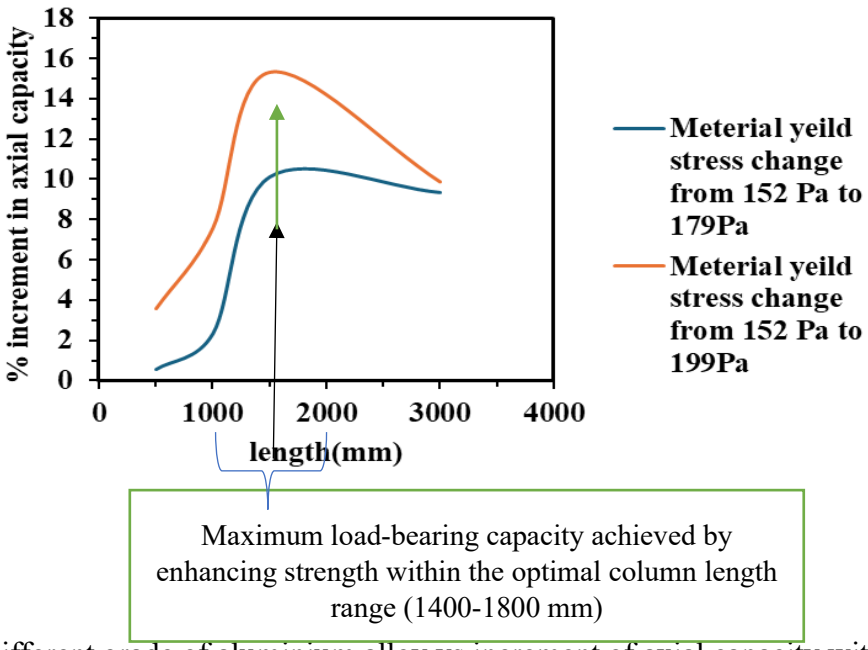

Figure 5-4: Different grade of aluminium alloy vs increment of axial capacity with optimum column length

5.3.2 Influence of screw spacing vs axial capacity for aluminium FTF plain channel sections

In this study, screw spacing was carefully designed to maintain consistency across different column types—short, intermediate, and slender. For each column, screws were placed 50 mm from the top and bottom for the first and last screws. For columns with five screws, the remaining length was divided into four equal parts; for columns with three screws, it was divided into two equal parts. In cases with two screws, no further division was needed. This approach ensured uniform screw spacing across all column types, enabling easy comparison of the results.

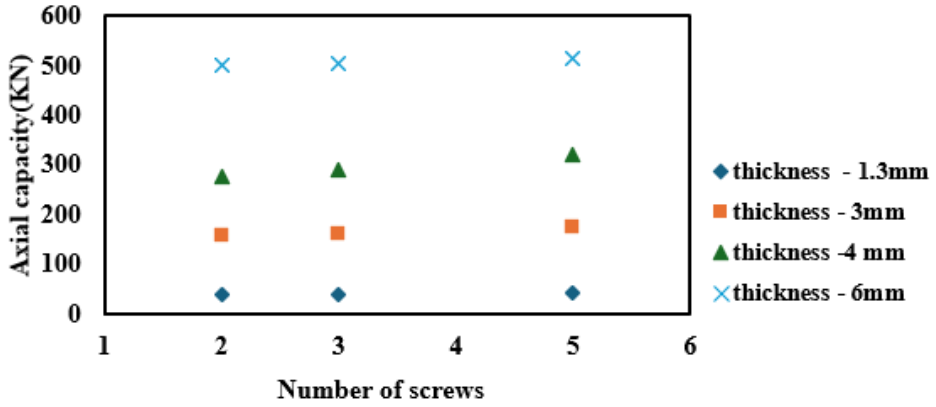

Figure 5-5: axial force changes against screw spacing in short column L -500mm varied thickness for grade 5052-HS32.

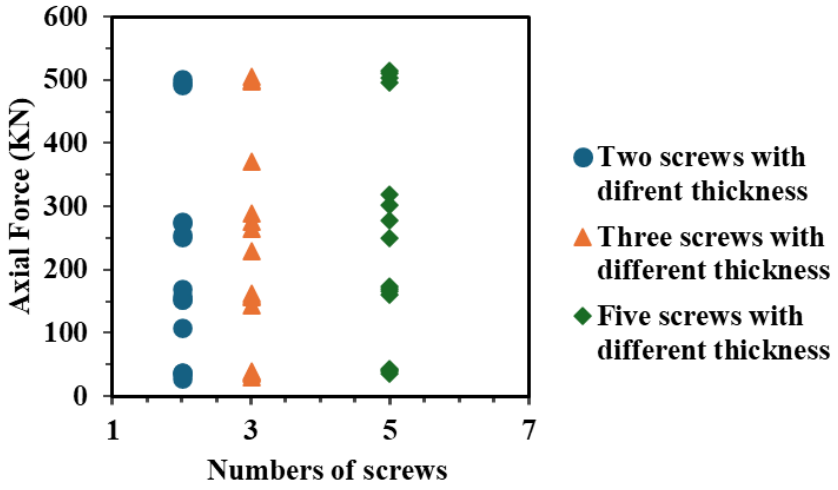

Figure 5-6: Influence of screw numbers(s) vs axial force for plain web section with varied thickness and different length for-5052 - HS 32

Figure 5-5 & Figure 5-6 demonstrates the impact of screw quantity on the structural performance of face-to-face (FTF) built-up channel sections made from grade 5052-HS32 aluminium alloy. For short columns with a length of 500mm, increasing the number of screws from two to five results in a rise in average axial capacity from 248.9 KN to 262.66 KN, an increase of 5.5%. In the case of intermediate columns with a length of 1000mm, the average axial capacity improves from 242.9 KN to 255.8 KN, representing a 5.3% increase as the screw count increases from two to five. For slender columns, with lengths of 1500mm and 3000mm, increasing the screw number from two to five leads to a 7.33% increase in average axial capacity, from 216.3 KN to 232.2 KN. These results suggest that for grade 5052-HS32

aluminium alloy, increasing the number of screws, thereby reducing the screw spacing, consistently enhances the axial capacity across various column lengths.

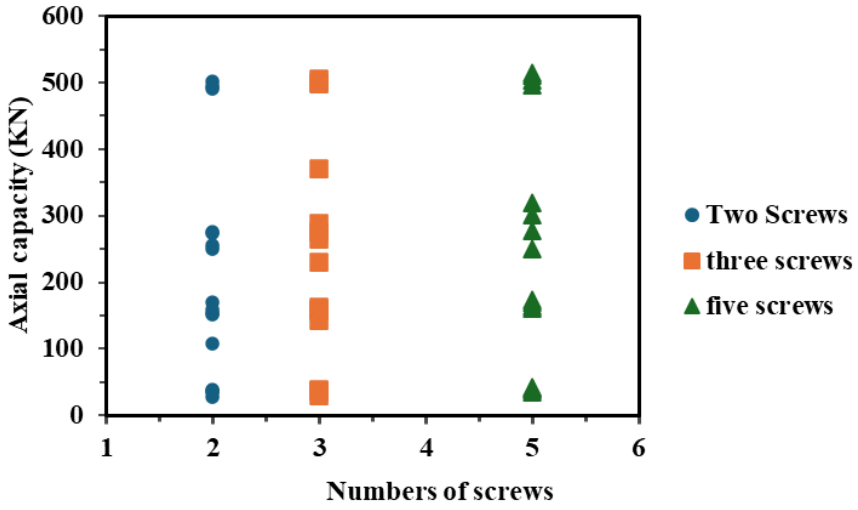

Figure 5-7: Influence of screw numbers(s) vs axial force for plain web section with varied thickness and length-5052 - HS 34

Figure 5-7 illustrates the effect of screw quantity on the structural performance of face-to-face (FTF) built-up channel sections made from grade 5052-HS 34 aluminium alloy. For short columns with a length of 500mm, increasing the number of screws from two to five raises the average axial capacity from 273.6 KN to 286.6 KN, marking a 4.73% increase. In the case of intermediate columns with a length of 1000mm, the average axial capacity increases from 268.9 KN to 282.21 KN, reflecting a 4.92% improvement as the screw count increases from two to five. For slender columns with lengths of 1500mm and 3000mm, increasing the number of screws from two to five results in a 4.37% rise in average axial capacity, from 266.12 KN to 277.75 KN.

These findings highlight that, for grade 5052-HS 34 aluminium alloy, increasing the number of screws—thus reducing the screw spacing—leads to a modest but consistent enhancement in axial capacity across different column lengths.

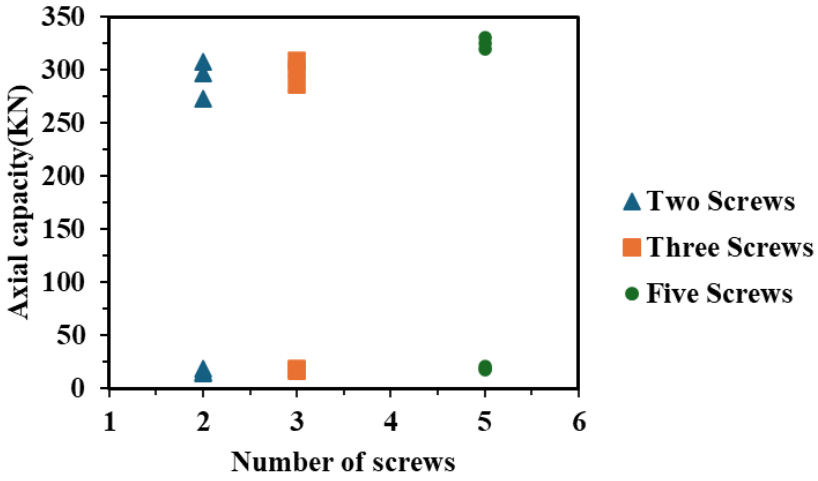

Figure 5-8: Influence of screw numbers(s) vs axial force for plain web section with varied thickness and length-5052 - HS 36

Figure 5-8 illustrates the impact of screw quantity on the structural performance of grade 5052-HS 36 aluminium alloy face-to-face (FTF) built-up channel sections. For short columns with a length of 500mm, increasing the number of screws from two to five raises the average axial capacity from 164.05 KN to 175.71 KN, representing a 7.13% increase. Similarly, for intermediate columns measuring 1000mm in length, the average axial capacity increases from 159.3 KN to 171.6 KN, a 7.3% improvement, when the screw count rises from two to five. In the case of slender columns with lengths of 1500mm and 3000mm, increasing the number of screws from two to five results in a 7.38% increase in average axial capacity, from 150.88 KN to 162.2 KN. These results indicate that for higher-grade aluminium alloys, reducing screw spacing—by increasing the number of screws—leads to a notable improvement in axial capacity. Overall, across different grades of aluminium alloy, the axial capacity of FTF built-up channel sections increases by an average of 6% with the addition of more screws.

5.3.3 Influence of column length (L) on axial capacity

Figure 5-9 illustrates the effect of length (L) on the axial force of the FTF built-up channel section. As the length increases from 500 mm to 3000 mm, the mean axial strength decreases across all thicknesses and material grades. Specifically, the axial strength drops from

259 KN to 189 KN, representing a 24% reduction at the longer length. This demonstrates that the axial strength of the FTF built-up channel section diminishes as the length increases.

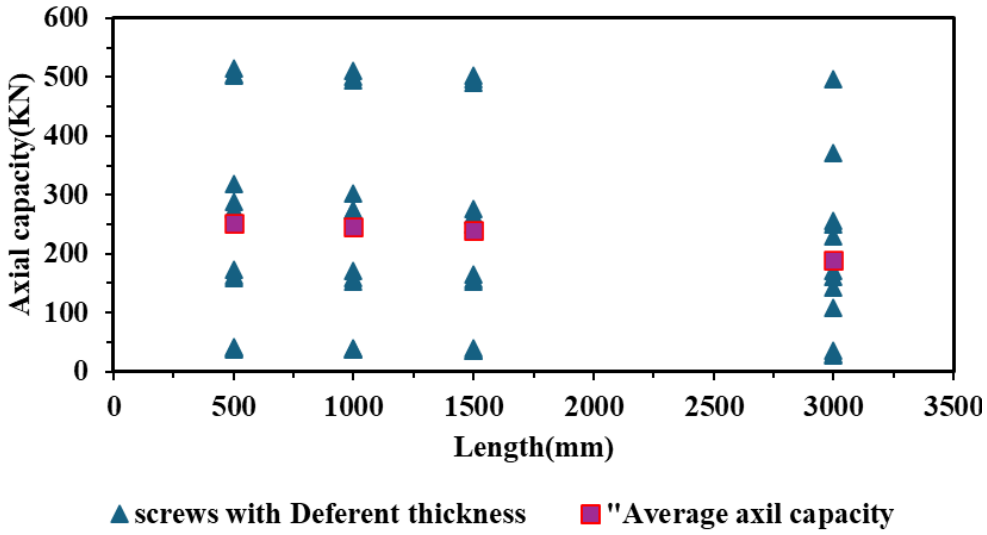

Figure 5-9: Influence of length(s) vs axial force for plain web section with varied thickness and grades

5.3.4 Effect of section thickness aluminium alloy FTF channel sections

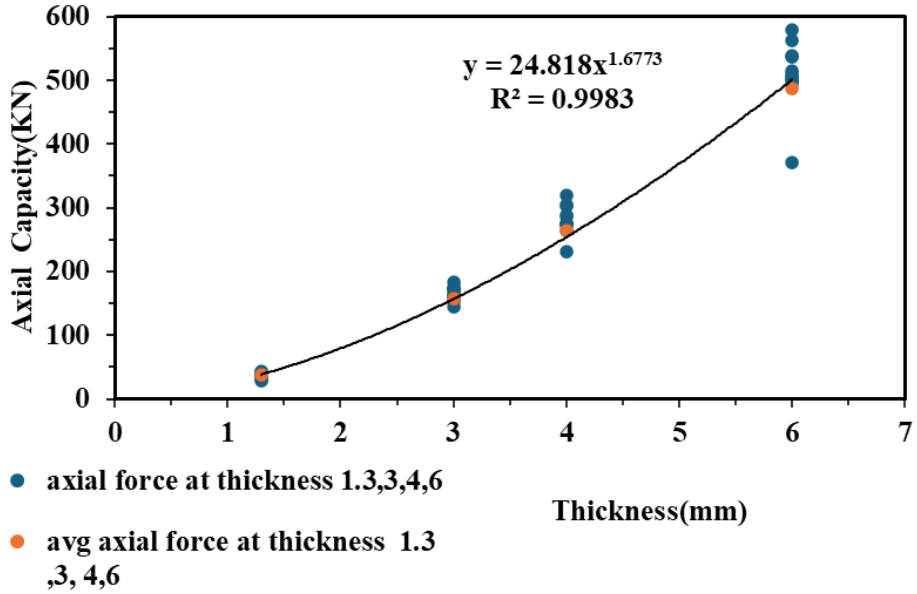

Figure 5-10: Influence of section thickness (t) vs axial force for plain web section with varied screws spacing

Figure 5-10 illustrates the impact of thickness (t) on the axial force of the FTF built-up channel section, considering variations in screw spacing. For channel sections made from grades 5052-HS 32 and 5052-HS 34, as the thickness increases from 1.3 mm to 6 mm, the mean axial

capacity significantly increases from 38 KN to 486 KN, reflecting an impressive 1117% improvement in axial capacity. Increasing the thickness significantly enhances the axial strength of FTF built-up channel sections. The equation for the graph, which corresponds to the critical strength capacity of FTF plain built-up sections, can be derived by substituting the plate thickness into the parameter X. This equation provides a close fit to the average critical force values for varying thicknesses, as indicated by its R^2 value of 0.998. This high R^2 value demonstrates the equation's reliability and applicability for accurately calculating the axial strength of the section.

$\mathbf{Y} = 24.41X^{1.678}$ Y =Asil steght

X – thickness of FTF built up channel (mm)

Y – axial strength (KN)

5.4 Influence of parameters to the axial capacity in aluminium alloy FTF with one web hole and many web holes section.

In this study, screw spacing was carefully designed to maintain consistency across different column types—short, intermediate, and slender. For each column, screws were placed 50 mm from the top and bottom for the first and last screws. For columns with five screws, the remaining length was divided into four equal parts; for columns with three screws, it was divided into two equal parts. In cases with two screws, no further division was needed. The process of creating holes in the web starts by drilling a single hole at the centre of the section. The diameter of this central hole varies, set at 0.2, 0.4, and 0.6 times the web width, allowing for the study of the effect of holes diameter on the axial capacity of the section. For sections with multiple holes, the diameter remains constant at 96 mm.

In the case of three-hole sections, two additional holes are created symmetrically by dividing the remaining length on either side of the central hole into two equal segments. The centres of these holes are positioned at the midpoints of each segment. This same method is used to create

configurations with five, seven, and nine holes, ensuring uniform spacing and distribution across all column types. This method facilitates consistent screw spacing, holes spacing and allows for straight forward comparison of results.

5.4.1 Influence of screw spacing vs axial capacity for aluminium FTF with one web hole section and many holes section

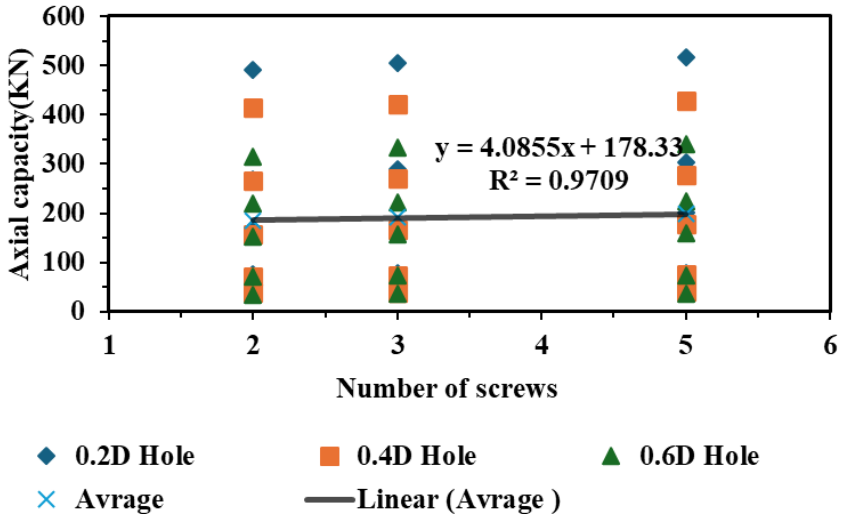

Figure 5-11: Influence of section screw spacing vs axial force for one web hole section.

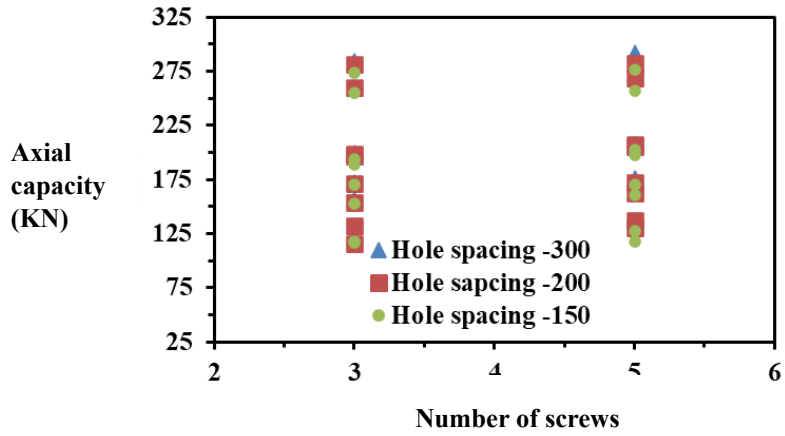

Figure 5-12: Influence of number of screws vs axial capacity for many webs hole section

Figure 5-11, Figure 5-12 illustrates the impact of screw spacing on the axial force of the FTF built-up channel section with one web hole and many web hole section respectively. For channel sections made from grades 5052-HS 32 and 5052-HS 34, as the screw spacing change from 2 ,3and 5, the mean axial capacity increases 4% from 185KN to 198 KN, reflecting not much impact to improvement in axial capacity for one web hole section. For channel

sections made from grades 5052-HS 32 and 5052-HS 34, as the screw spacing change from ,3 to 5, the mean axial capacity increases 3% from 211KN to 217 KN, reflecting not much impact to improvement in axial capacity for many web hole section This highlights the substantial effect that increasing screw spacing has on enhancing the axial strength by 4 %t of the FTF built-up channel sections with web holes. The equation in Figure 5-11 is used to determine the axial strength of channel with single perforated web with changing it screws keeping all other parameters are constant. Notation of the equation represent by

X – Screws numbers

Y – axial Strength for FTF built up section with single hole in web. (KN)

$Y = 4.0855X+178.33$

5.4.2 Influence of column length vs axial force for FTF section with one web hole and many web holes.

Figure 5-13, Figure 5-14 illustrates the behaviour of column length on consideration of changing on the axial force of the FTF built-up channel section with one web hole. For channel sections made from grades 5052-HS 32 and 5052-HS 34, as the screw spacing change from 2 ,3and 5, and same time the column length change from 500 mm to 3000 mm, the mean axial capacity decreases 8% from 178 to 165 KN, reflecting significant impact to in axial capacity for one web hole section. For channel sections made from grades 5052-HS 32 and 5052-HS 34, as the screw spacing change from 3 to 5, and same time the column length change from 1500 mm to 3000 mm, the mean axial capacity decreases 4.5% from 165 to 158 KN, reflecting significant impact to in axial capacity for many holes sections.

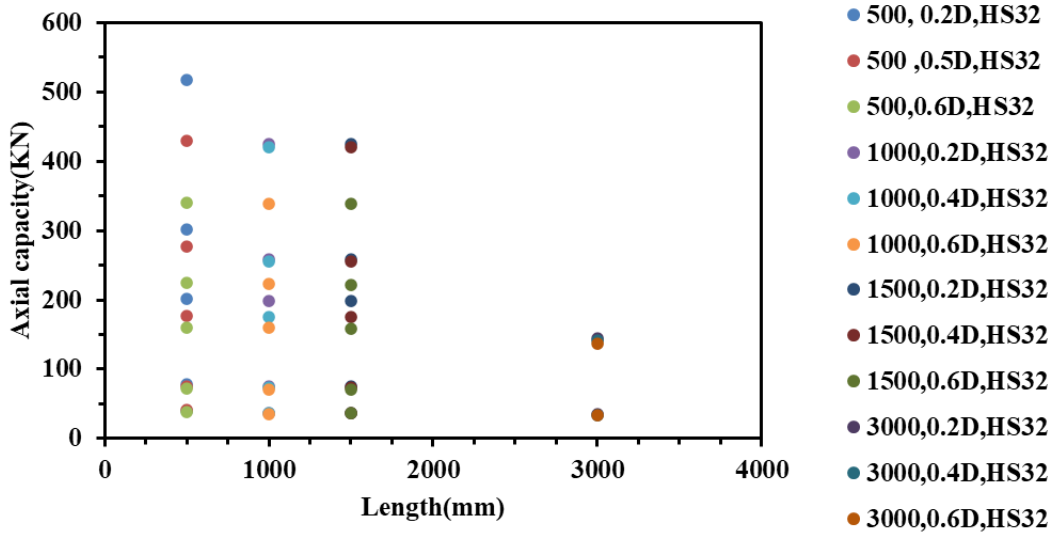

Grade - 5032-HS32 with 5 screws

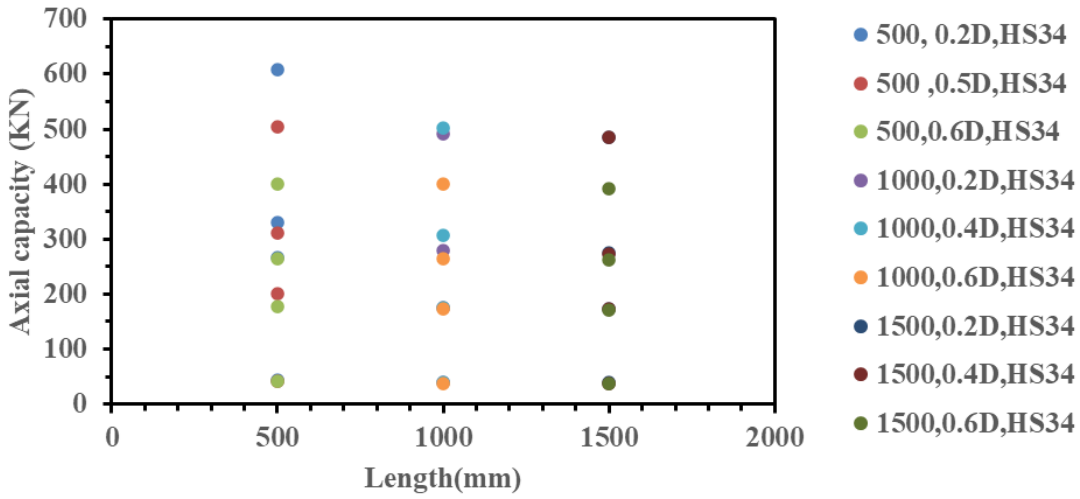

Grade - 5032-HS34 with 5 screws

Figure 5-13: Length to axial capacity variation for one web holes section with various thickness

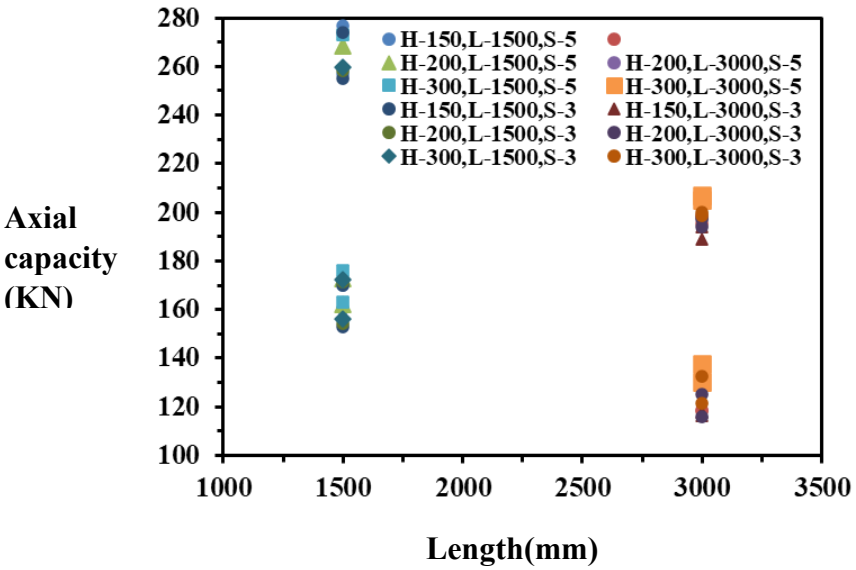

grade - 5032-HS 32 & 34 with 5&3 screws

Figure 5-14: Length (mm) to axial capacity (KN) variation for multiple web holes section with various thickness and grades (H -hole spacing, L-length, S-screws numbers)

5.4.3 Influence of diameter of hole vs axial force for FTF section with one web hole section

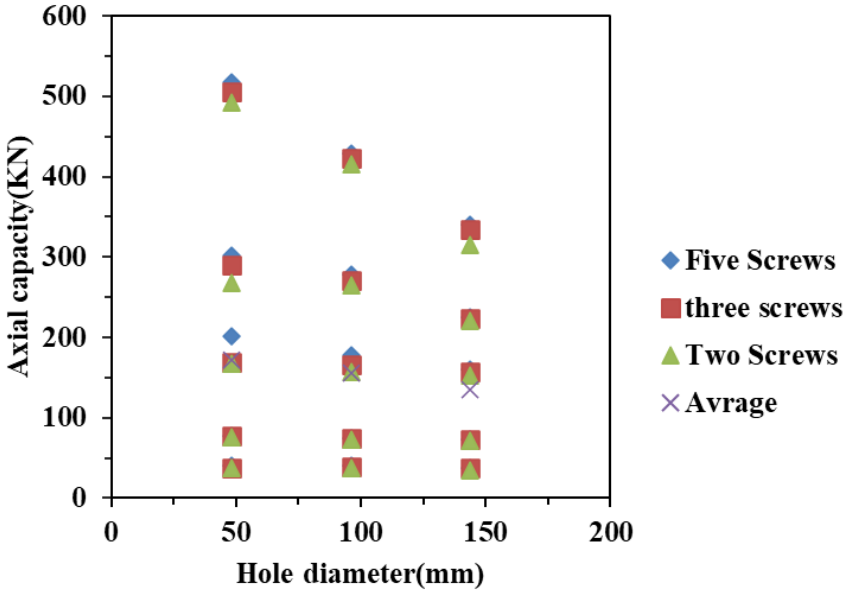

Figure 5-15: Influence of hole diameter vs axial capacity for one web hole column with various column length, thickness, & grades

Figure 5-15 illustrates the impact of hole diameter on the axial force of the FTF built-up channel section with one web holes. For channel sections made from grades 5052-HS 32 and 5052-HS 34, as the diameter change from 48mm ,96 mm ,144 mm. The mean axial capacity decreased 21% from 171KN to 134 KN, reflecting not much impact to improvement in axial

capacity. This highlights the substantial effect on axial capacity due to increasing holes diameter that reducing the axial strength by 21% of the FTF built-up channel sections with centre web hole.

5.4.4 Influence of a/h ratio vs axial force for aluminium FTF with one web hole section

The ratio of hole diameter (a) to web width (h) and its effect on axial compression capacity is presented in Tables 5-6 and 5-7. The relationship between these parameters is illustrated in Figure 5-16. From Figure 5-16, it is evident that as the ratio of a/h increases, the axial strength of the aluminium face-to-face (FTF) channels generally decreases. Specifically, as the a/h ratio increases from 0 to 0.6, the average axial strength of the aluminium FTF channels decreases by 8.1% and 16.4% for each 0.02 increment in the a/h ratio, respectively.

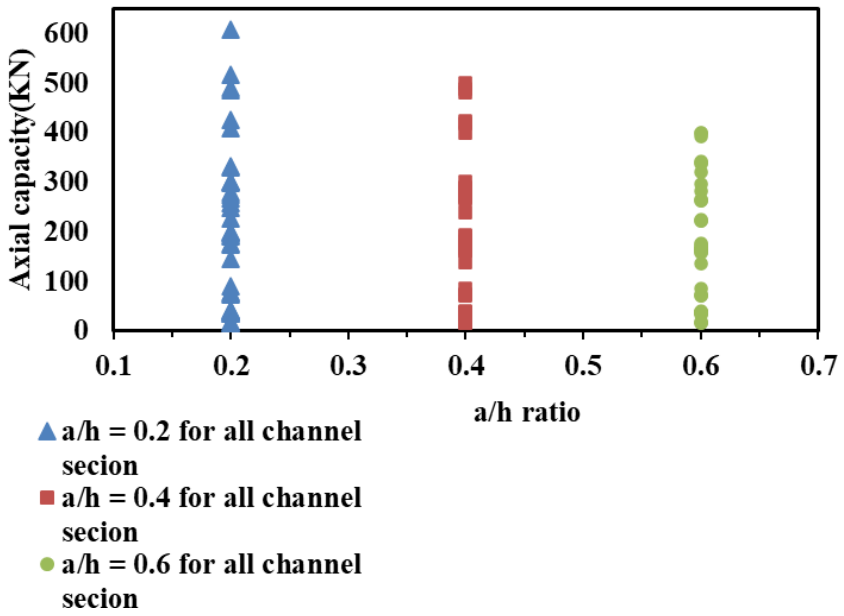

Figure 5-16 a/h ratio vs axial strength for all channel sections.

5.5 Parametric study on the strength reduction factor (R)

The strength reduction factor (R) can be calculated as follow: $R = P_{hole}/P_{A0}$

Where P_{hole} is the axial strength of section with centred web hole.

P_{A0} is the axial strength of plain section

5.5.1 Influence of slenderness ratio to strength reduction factor (R) for aluminium FTF section with one web hole.

As shown in Figure 5-17, the modified slenderness ratio varies with axial capacity in a somewhat random pattern. However, distinct changes in the slenderness value are observed at the purple region, which stands out from other axial strength values. This separation in slenderness values is utilized in the analysis of limitations for the reduction factor study. The limiting slenderness values are approximately 4 for the lower band and 17.5 for the upper band. Columns with lengths between these values are typically 3000 mm, while columns with lengths below the lower band range from 500 to 1500 mm.

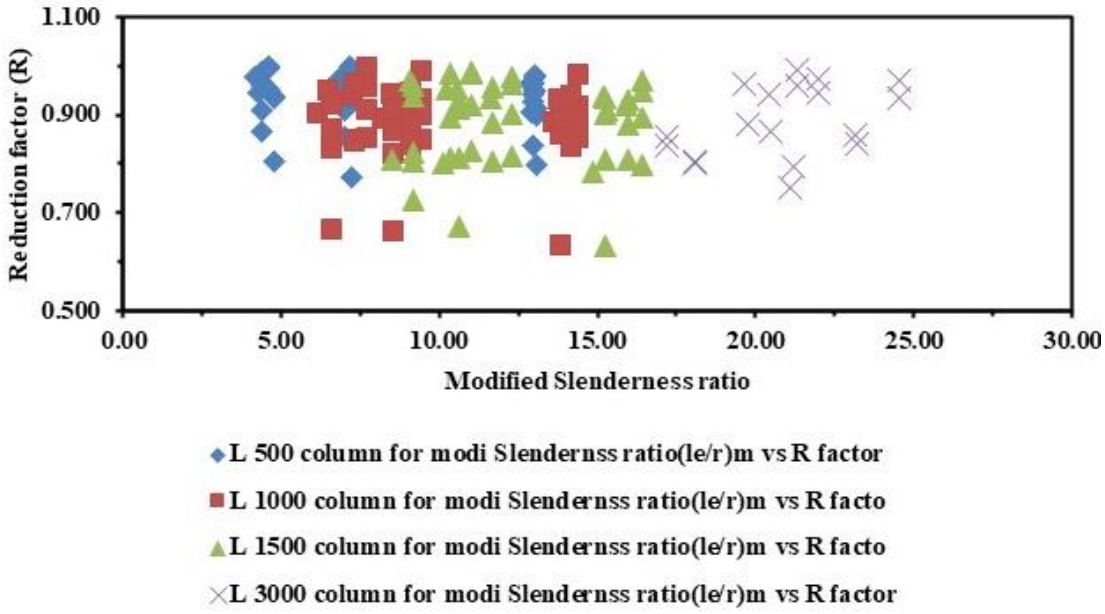

Figure 5-17: Modified slenderness ratio vs strength reduction factor (R) for all channel sections

5.5.2 Effect of a/h ratio on the strength reduction factor (R)

Figure 5-18 illustrates a downward trend in the axial strength reduction factor as the a/h ratio increases from 0.2 to 0.6. According to the data presented in Table 5-5, 5-6, 5-7, the reduction factors for sections with varying column lengths and numbers of screws are relatively consistent. Specifically, the average reduction factors are 0.96 for sections with a/h ratio of 0.2,

0.94 for a ratio of 0.4, and 0.88 for a ratio of 0.6. These values are consistent across different categories of slenderness ratios, as shown in Figure 5-17.

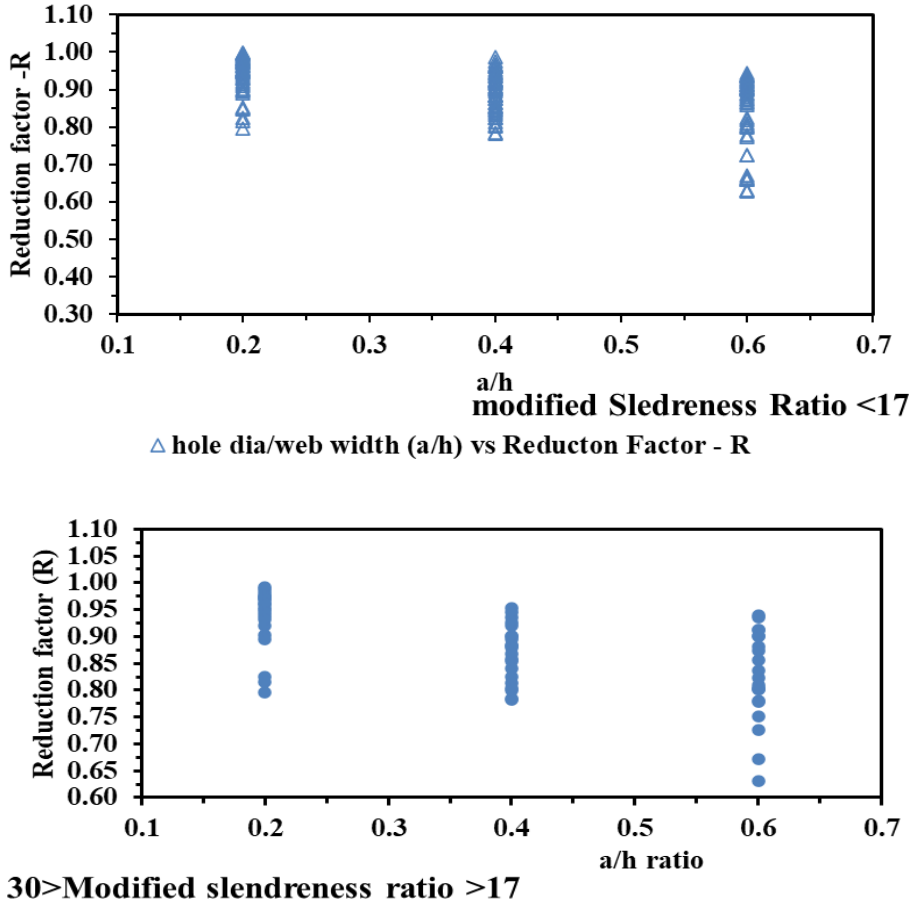

Figure 5-18: The a/h ratio vs reduction factor (R) for all channel length

5.5.3 Effect of number of screws on the strength reduction factor (R)

Figure 5-19 illustrates the effect of the number of screws (n) on the strength reduction factor (R). The average strength reduction factor remains relatively constant across sections with varying screw numbers, with a value of 0.92. This minimal variation indicates that the number of screws has a negligible impact on the strength reduction factor, suggesting that the effect of screw number on R is not significant.

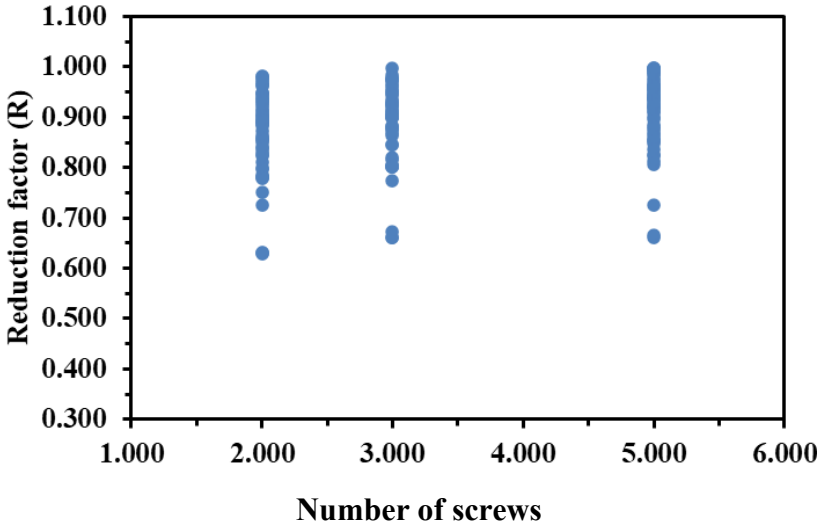

Figure 5-19: The number of screws vs axial capacity reduction factor (R) for all channel length.

5.5.4 Effect of column length (L) and modified slenderness ((KL/r)m) on the strength reduction factor (R) for one web hole section

Table 5-13 illustrates that the strength reduction factor (R) decreases from 0.99 to 0.88 as the number of web holes in the section increases from 3 to 9, for a fixed length of 1500 mm. This decrease in R is also influenced by the screw spacing, which varies from 100 mm to 200 mm. Additionally, the slenderness ratio of the sections decreases as the number of web holes increases, while maintaining a constant length of 1500 mm.Table 5-14 shows that the strength reduction factor (R) decreases from 0.98 to 0.82 as the column length (L) increases from 500 mm to 1000 mm. For sections with column lengths exceeding 1500 mm (i.e., modified slenderness ratios greater than 17.5), the coefficient of variation (COV) of the R values is lower than for shorter columns. However, the strength reduction factor (R) for these longer columns varies between 0.92 and 0.752.

Table 5-13:

Table 5-13: The strength reduction factor changing with length, slenderness ratio for many web hole section

Specimen	thickness(t) (mm)	screws spacing(s) (mm)	hole dia(d)(mm)	modified slenderness ratio(le/r)m	FEA(KN)	a/h	R_{EXP}
FTF240-t2-L1500-S100-0.4D-3- hole	2	100	96	8.5	83.71	0.4	0.99
FTF240-t2-L1500-S100-0.4D-5- hole	2	100	96	8.01	76.21	0.4	0.88
FTF240-t2-L1500-S100-0.4D-7- hole	2	100	96	7.6	75.45	0.4	0.87
FTF240-t2-L1500-S100-0.4D-9- hole	2	100	96	7.2	74.73	0.4	0.86
FTF240-t2-L1500-S200-0.4D-3- hole	2	200	96	10.21	78.8	0.4	0.94
FTF240-t2-L1500-S200-0.4D-7- hole	2	200	96	9.5	74.23	0.4	0.91
FTF240-t2-L1500-S200-0.4D-9- hole	2	200	96	8.11	70.79	0.4	0.88

Table 5-14: the strength reduction factor changing with length, slenderness ratio for one web hole section

Specimen	thickness(t) (mm)	screws spacing(s) (mm)	hole dia(d) (mm)	modified slenderness ratio(le/r)m	FEA (KN)	a/h	R exp
FTF240-L500	2	100	48	4.27	80.40	0.20	0.98
FTF240-L500	2	200	48	6.92	74.45	0.40	0.97
FTF240-L500	2	400	48	12.90	70.85	0.60	0.96
FTF240-L500	2	100	96	4.18	79.50	0.20	0.97
FTF240-L500	2	200	96	6.86	72.41	0.40	0.95
FTF240-L500	2	400	96	12.87	69.12	0.60	0.94
FTF240-L500	2	100	144	4.40	77.12	0.20	0.94
FTF240-L500	2	200	144	7.00	71.21	0.40	0.93
FTF240-L500	2	400	144	12.94	67.12	0.60	0.91
FTF240-L1000	2	100	48	6.52	77.90	0.20	0.95
FTF240-L1000	2	200	48	8.49	72.10	0.40	0.94
FTF240-L1000	2	400	48	13.81	68.40	0.60	0.93
FTF240-L1000	2	100	96	6.19	74.10	0.20	0.90
FTF240-L1000	2	200	96	8.25	68.20	0.40	0.89
FTF240-L1000	2	400	96	13.66	64.90	0.60	0.88
FTF240-L1000	2	100	144	6.62	71.40	0.20	0.87
FTF240-L1000	2	200	144	8.57	66.14	0.40	0.86

FTF240-L1000	2	400	144	13.86	63.20	0.60	0.86
FTF240-L3000	1.3	100	48	21.30	35.33	0.2	0.992
FTF240-L3000	1.3	200	48	21.98	29.4	0.4	0.974
FTF240-L3000	1.3	400	48	24.53	27.5	0.6	0.971
FTF240-L3000	1.3	100	96	19.67	34.33	0.2	0.964
FTF240-L3000	1.3	200	96	20.41	28.4	0.4	0.940
FTF240-L3000	1.3	400	96	23.13	24.3	0.6	0.858
FTF240-L3000	1.3	100	144	17.22	30.5	0.2	0.856
FTF240-L3000	1.3	200	144	18.06	24.2	0.4	0.801
FTF240-L3000	1.3	400	144	21.09	21.3	0.6	0.752

Chapter 6 – Current design guidelines

The design guidelines provided by the *Aluminium Design Manual* (ADM, 2020), *Australian/New Zealand Standards* (AS/NZS, 2018), *Eurocode 9* (EC9) (CEN, 2007), *Eurocode 3* (EC3) (CEN, 2005), and *American Iron and Steel Institute* (AISI, 2016) standards can be utilized for determining axial capacity. In this thesis, the AS/NZS 4600:2018 design standards are followed to provide guidance on determining the un-factored axial capacity of AAFTF channel sections with plain webs and web holes. Both the effective width method (EWM) and the Direct Strength Method (DSM) are viable options for assessing the design capacity of these AAFTF sections according to the specified standards. However, these standards were originally developed for cold-formed steel sections, not for cold-formed aluminium sections.

The study by Fang et al. (2020) explains the behaviour of back-to-back aluminium alloy channel sections and highlights that applying a strength reduction factor is a more conservative design approach than the existing AS/NZS 4600 standard. However, this study specifically addresses back-to-back aluminium alloy built-up sections. There remains a noticeable absence of design guidelines for evaluating the axial capacity of cold-formed AAFTF sections, both with and without web holes, as evident in the current literature and standards. The subsequent sub-sections introduce relevant design equations, aiming to enhance understanding and facilitate the calculation of axial capacity for these structural configurations.

6.1 EWM for CFSS channel sections with plain webs

The design standards outlined in *AS/NZS 4600:2018* (Standards Australia/New Zealand, 2018) provide design equations for computing the nominal axial capacity (P_0) of cold-formed stainless steel (CFSS) channel sections with plain webs. The axial capacity (P*) is required to satisfy the following equations:

$$P_* \leq \phi_C P_S = \phi_C A_e f_y \text{ ------ (1)}$$

$$P_* \leq \phi_C P_C = A_C f_y \text{ ------(2)}$$

Where, Ps is the nominal section capacity of columns; Pc is nominal member capacity of columns; ϕc is the capacity reduction factor; Pn is the critical stress; Ae is the effective area and fy is the yield stress.

The design equations to determine the critical stress P_n are given in Eqs. (3–5)

$$For\ \lambda_c \leq 1.5; P_n = (0.658\lambda_c^2) \times f_y \text{_____(3)}$$

$$For\ \lambda_c > 1.5; P_n = 0.877\lambda_c^2 f_y \text{_____(4)}$$

$$\lambda_c = \sqrt{(f_y / f_{oc})} \text{_____(5)}$$

Where, λ_c is non-dimensional slenderness; f_{oc} is the flexural–torsional buckling stress calculated in accordance with Appendix D of AS/NZS 4600:2018 with modified slenderness ration use to calculate f_{ox}, f_{oy}, $f_{oz.}$ The minimum value of these three is used to find $f_{oe\text{- global}}$ buckling stress of the section.

6.2 DSM for CFSS channel sections with plain webs

For CFSS channel sections with plain webs, the design capacity (AS/NZS) is established by determining the minimum value among the local buckling capacity (P_{nl}), distortional buckling capacity P_{nd}, and global buckling capacity P_{ne}.

Design capacity (AS/NZ) = min (P_{nl}, P_{nd}, P_{ne}) --(6)

The design equations to obtain the local buckling capacity (Pnl) are given in Eqs. (7–9):

$$For\quad \lambda_l \leq 0.776; P_{nl} = P_{ne} \text{----------(7)}$$

$$For\ \lambda_l = 0.776; P_n = \{[1 - 0.15(P_{cr} / P_{nl})^{0.4}] \times P_{ne} \text{----------(8)}$$

$$\lambda_l = \sqrt{\frac{P_{ne}}{P_{cr}}} \text{ ----------(9)}$$

The design equations to obtain the distortional buckling capacity (P_{nd}) are given in Eqs. (10–12):

$$For\ \lambda \leqslant 0.561\ ;\ P_{nd}=P_y \text{ --(10)}$$

$$For\ \lambda_d = 0.776; P_{nd} = \{[1-0.25(P_{crd}/P_y)^{0.6}]\times(P_{crd}\times P_y)^{0.6}\times P_y \text{ -----(11)}$$

$$\lambda_d = \sqrt{\frac{P_y}{P_{crd}}} \text{ ----------(12)}$$

The design equations to obtain the global buckling capacity (Pne) are given in Eqs. (13–15):

$$For\ \lambda_c \leq 1.5; P_{ne} = P_y(0.658\lambda_c^2)P_y \text{ -------(13)}$$

$$For\ \lambda_c > 1.5; P_{ne} = P_y(0.877\lambda_c^2)P_y \text{ ----------(14)}$$

$$\lambda_c = \sqrt{\frac{P_y}{P_{cre}}} \text{ ----------(15)}$$

Where P_{crl}, P_{crd}, P_{cre} are the elastic local, distortional and global buckling load, respectively, which were determined by the finite strip analysis method using constrained and unconstrained finite strip method (CUFSM) software Roy et al. (2021).

6.3 DSM for CFSS channel sections with single or multiple web holes

The The design standards outlined in *AS/NZS 4600:2018* (Standards Australia/New Zealand, 2018) for cold-formed stainless steel (CFSS) provide design equations for calculating the axial capacity of AAFTF channel sections with unstiffened web holes. These equations are derived from the design equations proposed by Moen and Schafer (2011).

Moen and Schafer (2011) introduced a "weighted average" method for assessing the global buckling capacity (P_{ne}) of CFSS channel sections with web hole. The classical equation used

to compute the elastic global buckling load (P_{creh}) for such columns is presented in Equation 16 below:

$$P_{creh} = \pi 2EI_{avg} A_g (KL)^2 \text{----------(16)}$$

To determine the local buckling capacity (P_{nl}) of CFS sections with unstiffened web holes, the design equations are given in Eqs. (17–18):

$$For \quad \lambda_l \leq 0.776; P_{nl} = P_{ne} \leq P_{ynet} \text{ -----(17)}$$

$$For \ \lambda_l > 0.776; P_{nl} = \{[1-0.15(P_{crlh}/P_y)^{0.6}] \times (P_{crd} \times P_y)^{0.6} \times P_y \text{ --------(18)}$$

$$\lambda_l = \sqrt{\frac{P_{ne}}{P_{crlh}}} \text{ ---------- (19)}$$

To determine the distortional buckling capacity (P_{nd}) of AAFTF sections with unstiffened single or multiple web holes, the design equations are given in Eqs. (20–25):

$$For \ \lambda_d \leqslant \lambda_{d1}; P_{nd} = P_{yne} \text{ -- (20)} \qquad \lambda_d \leq \lambda_{dl}; P_{nd} = P_{ynet} \text{ --------(20)}$$

$$For \ \lambda_{d1} < \lambda_d < \lambda_{d2}; P_{nd} = P_{ynet} - (P_{ynet} - P_{d2}\lambda_{d2} - \lambda_{d2})(\lambda_d - \lambda_{d1}) \text{ ---------(21)}$$

$$For \ \lambda_d > \lambda_{d2}; P_{nd} = \{[1-0.25(P_{ynet}P_y)^{0.6}] \times (P_{ynet}/P_y)^{0.6} \times P_y \text{ ----------(22)}$$

$$\lambda_d = \sqrt{\frac{P_y}{P_{crdh}}} \text{ ----------(23)}$$

$$\lambda_{d1} = 0.561(\frac{P_{ynet}}{P_y}) \text{ ---------(24)}$$

$$\lambda_{d2} = 0.561[14(P_y P_{ynet})^{0.4} - 13] \text{----------(25)}$$

Where P_y and P_{ynet} are the member yield capacity of the gross section and net section, respectively. Moreover, P_{crlh}, P_{crdh}, P_{creh} are the elastic local, distortional, and global buckling load, respectively, for the CFS channel sections with unstiffened web holes.

6.3.1 Comparison of design strength with the FEA results for plain web sections, single web hole sections and multiple web holes sections.

The axial capacity of the FTF channel section with plain webs, determined through parametric study, was compared to the axial capacities calculated using the Design Strength Method (DSM) equations 6 to 15. As shown in Table 4-5 and Figure 6-1, the mean and coefficient of variation (COV) for the ratio of experimental axial capacity to DSM axial capacity (P_{Exp}/P_{DSM}) are 1.004 and 0.003, respectively, for the 5032 HS-32 material with 2 mm thick plate. Additionally, the ratio of experimental axial capacity to finite element analysis (FEA) capacity (P_{Exp}/P_{FEA}) yielded a mean of 1.02 and a COV of 0.0003.

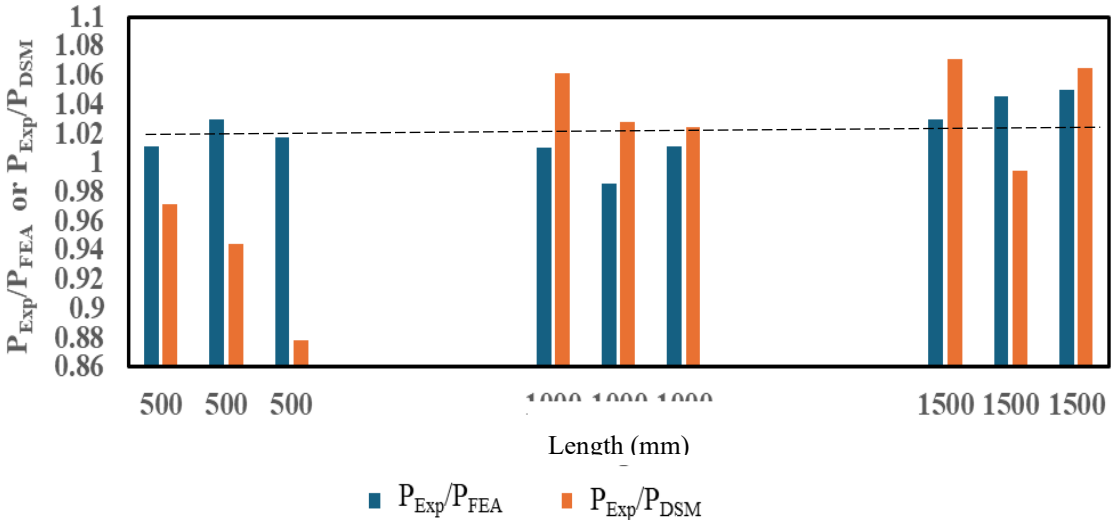

Figure 6-1: Comparing the outcomes of the P_{Exp}/P_{DSM} and P_{Exp}/P_{FEA} results for FTF channel sections with plain web.

The design strengths predicted by DSM equations 6 to 15 show an average axial capacity that is 98% consistent with the results obtained from finite element analysis (FEA) and

experimental testing. The deviation between the DSM predictions and the Y = 1 line is minimal, remaining within ±0.3. However, for a 500 mm long column with screw spacing exceeding 100 mm, the predicted axial capacity deviates from the DSM by 5% when compared to both the FEA and experimental results, as illustrated in Figure 6-1.

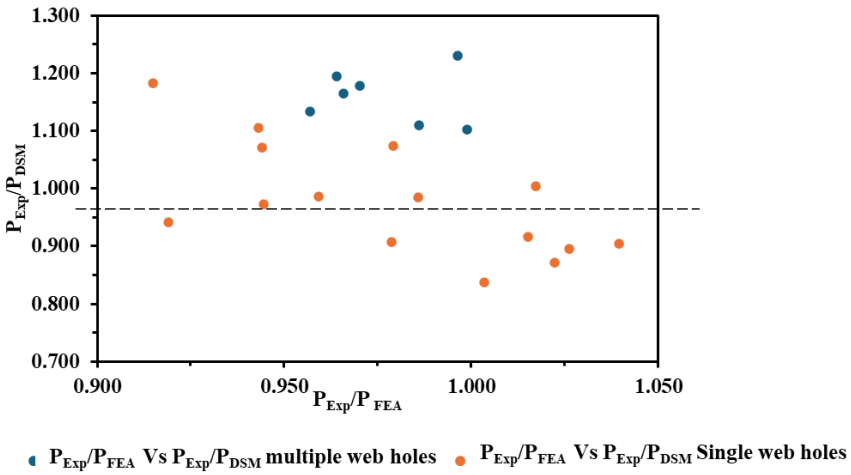

Figure 6-2: Comparing the results of the DSM, FEA results, and experimental results for single and multiple hole in the web

The axial capacity of the FTF built up channel section, with both single and multiple web holes, was analysed through a parametric study and compared with the axial capacities calculated using DSM equations 6 to 25. Figure 6-2 illustrates that the P_{Exp}/P_{DSM} results range between 0.85 and 1.15 in relation to the Y = 1 line. In contrast, the P_{Exp}/P_{FEA} results show relatively lower deviations, ranging from 0.85 to 1.05. The P_{Exp}/P_{FEA} and P_{Exp}/P_{DSM} versus the Modified Slenderness Ratio are presented in Figures 6-3 and 6-4. As shown in Figures 6-3 and 6-4, the P_{Exp}/P_{DSM} values exhibit significant variation in relation to the Y=1 line. This indicates that the DSM predictions tend to overestimate the axial capacity by an average of 15% for sections with a single web hole, while underestimating the capacity by approximately 12% for sections with multiple web holes. therefore, an alternative equation is needed to more accurately determine the axial capacity, as the predictions of the DSM method are not sufficiently precise.

To address this, a reduction factor (R) for strength capacity is introduced, which relates the strength of sections with holes to that of plain sections. This factor can be used to calculate the strength of a section with holes, provided the strength of the plain section is known. Figures 6-3 and 6-4 include two additional lines representing the deviation bands for the $\mathbf{P_{Exp}/P_{DSM}}$ results: a lower band at -15% and an upper band at +12%.

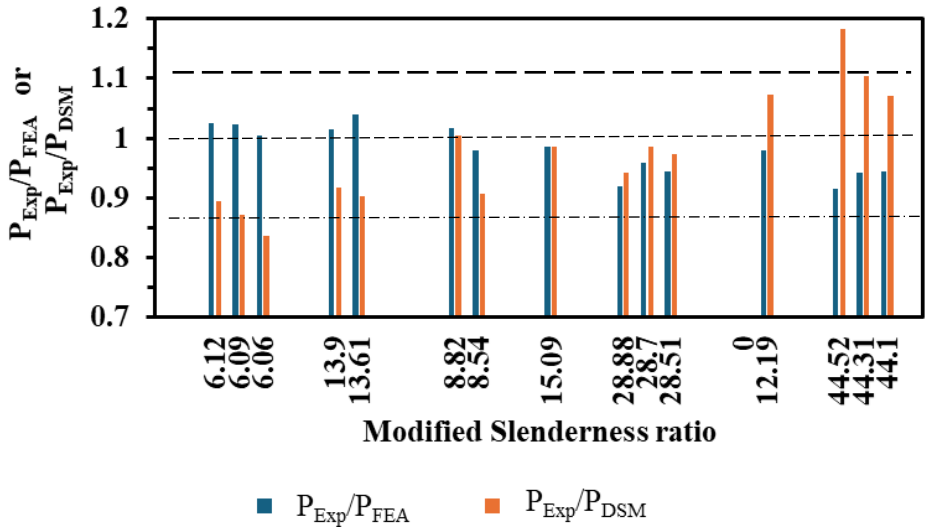

Figure 6-3: Comparing the outcomes of the P_{Exp}/P_{DSM} and P_{Exp}/P_{FEA} results for FTF channel sections for one web holes.

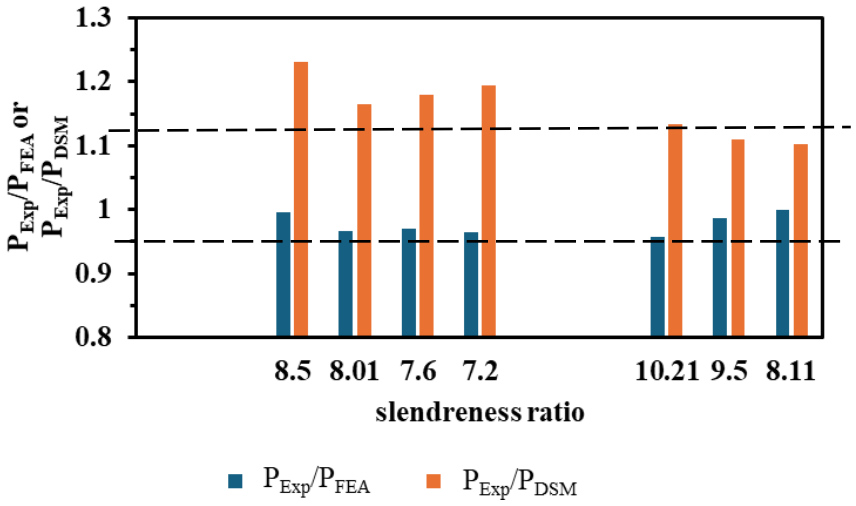

Figure 6-4: Comparing the outcomes of the P_{Exp}/P_{DSM} and P_{Exp}/P_{FEA} results for FTF channel sections for many web holes.

In Figure 6-5, equation 26 to determine the DSM value corresponding to the relevant FEA results can be established. This holds true for aluminum alloy face-to-face built-up sections

with a thickness of 2 mm, regardless of length or screw arrangement, provided with one web holes.

$Y = 0.0091X^2 - 0.2989X + 12.746$--------- 26

Y - -- P_{FEA} / P_{DSM}

X --- P_{FEA} - Result obtained from FEA model of the 2 mm thickness grade 5032 HS32

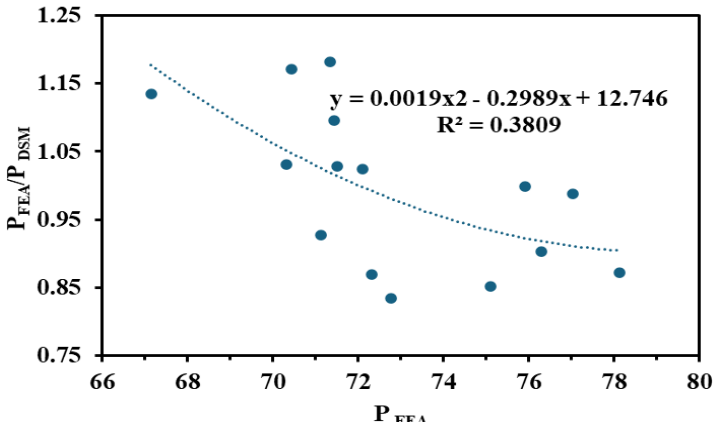

Figure 6-5: Finite Element Analysis (FEA) axial capacity (KN) Vs P_{FEA} / P_{DSM} for 5032 – HS32 grade aluminium with 2 mm thickness for one web hole

6.4 Proposed design reduction factor equation for one or more web hole FTF channel section

The design equations for the axial strength reduction factors of aluminium Face-to-Face (FTF) channels with a centre web hole were developed based on validated finite element (FE) models. These models offer more accurate predictions of reduced axial strength compared to existing design standards. Non-linear regression analysis was used to derive the design equations. The proposed equations are valid for sections that meet the following limits: h/t ≤190 and a/h ≤0.6. Specifically, the equations for axial strength reduction factors (R_{prop}) in relation to the a/h ratio were developed for FTF aluminium channels with a single circular web hole and multiple holes. The reduction factor calculation based on proposed design equations for these sections are presented below Table 6-2 and Table 6-3 for one hole and many holes respectively.

Strength reduction factors (R_{prop}). is calculate as below equation (27), which is the proposed design equations for sections with one circular web hole as well as multiple holes:

$$R_{prop} = \left(\frac{KL}{r}\right)^{(-0.031)} - \left(\frac{a}{h}\right)^{4.394}; 0 < R \leq 1 \text{---------(27)}$$

For FTF Section having Modified slenderness ratio for web hole column – KL/r is within (4 < (KL/r) ≤30)

The average strength reduction factor for various a/h ratio are as follows, is derived from equation 27.

The strength reduction factor for sections with multiple holes is also applied in Equation (27) because the effect of multiple holes is considered during the modified slenderness calculation, as outlined in Appendix D of AS/NZS 4600:2018. Therefore, it is not necessary to account for the strength reduction factor separately when calculating the capacity of single- and multiple-hole sections. If the axial capacity of the plain section is known and modified slenderness ratio for web hole section knew, , the axial capacity of the holed section can be easily determined by multiplying the plain section's axial capacity by the strength reduction factor. This approach improves the accuracy of determining the strength capacity of holed sections compared to the methods used in the P_{DSM} equations.

Based on proposed equation no (27) the general Reduction factor for a/h ratio from 0.2 0.4, 0.6 are given in Table 6-1, but the accurate axial capacity reduction value for each channel section can be determined using equation (27) for single hole web section or multiple hole with web..

Table 6-1 Average axial capacity reduction factor based on proposed equation for one hole section

a/h	0.2	0.4	0.6
R(slen<17)	0.92	0.89	0.82
R(30>slen>17)	0.90	0.88	0.80

Table 6-2: Axial capacity reduction factor based on proposed equation for one web hole section and reliability

Specimen	Modi Seln (KL/t)m	Expe Res P_{EXP} KN	FEA result PFEA KN	DSM KN	Comparison P_{EXP}/P_{FEA}	P_{EXP}/P_{DSM}	P_{FEA}/P_{DSM}	R_{exp}	R_{pros}	R_{DSM}	Remarks
Short											
FTF240-t1.98-L500-S100-0.2D	6.12	80.18	78.14	89.6	1.03	0.89	0.87	0.96	0.94	1.05	
FTF240-t1.98-L500-S100-0.4D	6.09	76.79	75.11	88.16	1.02	0.87	0.85	0.92	0.93	1.03	over estimation by DSM, experimental and Proposed eq results are closely match
FTF240-t1.98-L500-S100-0.6D	6.06	73.01	72.76	87.2	1.00	0.84	0.83	0.88	0.84	1.02	
Mean			75.34	88.32	1.02	0.87	0.85	0.92	0.90	1.03	
COV					0.0001	0.0008	0.0004	0.0019	0.0032	0.0002	
FTF240-t1.98-L500-S400-0.2D	13.9	77.44	76.29	84.5	1.02	0.92	0.90	1.07	0.92	1.02	
FTF240-t1.98-L500-S400-0.4D	13.61	75.19	72.328	83.2	1.04	0.90	0.87	1.03	0.90	1.01	over estimation by DSM, & the experimental error exists in R_{exp} results
Mean			74.309	83.85	1.03	0.91	0.89	1.05	0.91	1.01	
COV					0.0003	0.0001	0.0006	0.0005	0.0001	0.0001	
Intermediate											
FTF240-t1.98-L1000-S225-0.2*D	8.82	78.36	77.029	77.98	1.02	1.00	0.99	0.98	0.93	1.03	
FTF240-t1.98-L1000-S225-0.6*D	8.54	69.6	71.12	76.66	0.98	0.91	0.93	0.87	0.83	1.01	over estimation by DSM, experimental and Proposed eq results are closely match
Mean			73.92	77.32	1.00	0.96	0.96	0.92	0.88	1.02	
COV											
FTF240-t1.98-L1000-S450-0.2D	15.09	74.85	75.92	76.01	0.99	0.98	1.00	1.00	0.92	1.04	
Mean			75.92	76.01	0.99	0.98	1.00	1.00	0.92	1.04	
COV			0								
FTF240-t1.98-L1000-S900-0.2D	28.88	66.28	72.11	70.42	0.92	0.94	1.02	0.92	0.90	1.00	
FTF240-t1.98-L1000-S900-0.4D	28.7	68.59	71.51	69.51	0.96	0.99	1.03	0.95	0.88	0.98	over estimation by DSM, experimental and Proposed eq results are closely match
FTF240-t1.98-L1000-S900-0.6D	28.51	66.41	70.31	68.22	0.94	0.97	1.03	0.92	0.80	0.96	
Mean			71.31	69.38	0.94	0.97	1.03	0.93	0.86	0.98	
COV					0.0004	0.0005	0.000012	0.000321	0.003165	0.000244	
Slender											
FTF240-t1.98-L1500-S350-0.4D	12.19	69.96	71.45	65.16	0.98	1.07	1.10	1.01	0.91	1.01	

Mean					0.98	1.07	1.10	1.01	0.91	1.01	over estimation by DSM,&the experimental error exist in R_{exp} results
COV											
FTF240-t1.98-L1500-S1400-0.2D	44.52	65.27	71.346	60.32	0.91	1.18	1.18	1.07	0.89	1.05	over estimation by DSM,&the experimental error exist in R_{exp} results
FTF240-t1.98-L1500-S1400-0.4D	44.31	66.42	70.43	60.12	0.94	1.10	1.17	0.99	0.87	1.05	
FTF240-t1.98-L1500-S1400-.6D	44.1	63.4	67.15	59.18	0.94	1.07	1.13	1.04	0.78	1.03	
Mean			69.6	59.9	0.93	1.12	1.16	1.03	0.85	1.04	
COV					0.00028	0.00327	0.00063	0.00182	0.00317	0.00011	

Table 6-3: Axial capacity reduction factor based on proposed equation for many web holes section and reliability

Specimen	Modi	Expe	FEA	DSM	Comparison			R_{exp}	R_{pros}	R_{DSM}	Remarks
	Slenderness ratio	Res	result								
	(KL/t)m	P_{EXP}	PFEA		P_{EXP}/P_{FEA}	P_{EXP}/P_{DSM}	P_{FEA}/P_{DSM}				
		KN	KN	KN							
FTF240-t2-L1500--S100-0.4D-3- hole	8.5	83.41	83.71	67.8	0.996	1.230	1.235	0.99	0.918	0.90	The DSM results tend to overestimate, whereas the experimental results closely align with the proposed equation. However, the results for the plain FTF section with 100 mm and 200 mm screw spacing, required for calculating **R_{exp}**, are not available. Consequently, FEA results were used for this calculation. As a result, the experimental **R_{exp}** does not closely match either **R_{pro}** or **R_{DSM}**, highlighting the need for additional experimental data to accurately validate the proposed equation.
FTF240-t2-L1500-S100-0.4D-5- hole	8.01	73.6	76.21	63.2	0.966	1.165	1.206	0.88	0.920	0.84	
FTF240-t2-L1500-S100-0.4D-7- hole	7.6	73.2	75.45	62.1	0.970	1.179	1.215	0.87	0.921	0.82	
FTF240-t2-L1500-S100-0.4D-9- hole	7.2	72.04	74.73	60.3	0.964	1.195	1.239	0.86	0.923	0.80	
FTF240-t2-L1500-S200-0.4D-3- hole	10.21	75.4	78.8	66.5	0.957	1.134	1.185	0.94	0.913	0.88	
FTF240-t2-L1500-S200-0.4D-7- hole	9.5	73.2	74.23	65.98	0.986	1.109	1.125	0.91	0.915	0.87	
FTF240-t2-L1500-S200-0.4D-9- hole	8.11	70.71	70.79	64.1	0.999	1.103	1.104	0.88	0.919	0.85	

W

It should be noted that the regression analysis calculation for proposed reduction factor equation (27) ,get the coefficients of determination (R^2) is 0.329. While these values are relatively less than 0.5, the proposed equations still provide a noticeably better prediction of the experimental results, as shown in Table 6-2, Table 6-3 when compared to the predictions from the Direct Strength Method (DSM). The discrepancies in the R^2 values can be attributed to the limitations outlined above and the practical challenges encountered during experimental testing. Despite these factors, Table 6-2, Table 6-3 demonstrates that the proposed axial strength reduction factors (Rp_{rop}) closely align with the experimental results, confirming the accuracy and reliability of the proposed design equations.

Chapter 7 – Conclusion and Future studies

7.1 Key finding

A non-linear finite element (FE) model, which accounted for both material non-linarites and initial geometric imperfections, was developed and validated against experimental test results. Additionally, a comprehensive parametric study involving 495 FE models was conducted to examine the effects of various parameters, including hole size, screw spacing, section thickness, column length, and modified slenderness, on the axial strength of aluminum Face-to-Face (FTF) channels with a centered web hole.

The results of the parametric study revealed that section thickness (t) has a significant impact on the axial strength of aluminum built-up columns. As the section thickness increased from 1.3 mm to 6 mm, the average axial strength of plain aluminum FTF channels increased from 42 kN to 550 kN, while the axial strength for channels with a web hole increased from 39 kN to 340 kN for short columns.

However, as shown in Figure 5-17, the relationship between modified slenderness ratio and axial capacity follows a somewhat random pattern. Notably, distinct changes in slenderness are observed in the purple region, which stands out from other axial strength values. This separation in slenderness values is crucial for identifying the limitations of the reduction factor study. The limiting slenderness values are approximately 17.5 for the lower bound and 30 for the upper bound. Columns with lengths between these values typically range from 3000 mm to 1500 mm, while columns with lengths below the lower bound typically range from 500 mm to 1000 mm.

The effect of the holes diameter-to-web width ratio (a/h) on axial compression is presented in Tables 5-5, Table 5-6, and Table 5-7, with the relationship between these parameters illustrated in Figure 5-16. As the a/h ratio increases, the axial strength of the aluminum face-to-face (FTF) channels tends to decrease. Specifically, as the a/h ratio increases from 0 to 0.6, the average

axial strength of the aluminum FTF channels decreases by 8% for each 0.02 increment in the a/h ratio, and by 16% for the total.

The axial strength of channels decreases by 8% and 16% for each 0.02 increment in the a/h ratio, respectively. Besides, it can be found that the ratio of a/h affected the strength reduction factor significantly.

7.1.2The experimental results and FEA results in terms of failure mode

The design strengths calculated according to the Australian/New Zealand Standard (AS/NZS) and the American Iron and Steel Institute (AISI) standard were compared with experimental and finite element analysis (FEA) results. For short and intermediate columns, failure predominantly occurred due to local and distortion buckling. In slender columns, failure was mainly caused by distortion and global buckling modes. However, in cases where screw spacing was larger, such as with two screws, slender columns occasionally failed due to torsional buckling. In most columns, failure resulted from a combination of global and distortion buckling modes.

The The Direct Strength Method (DSM), as outlined in *AS/NZS 4600:2018* (Standards Australia/New Zealand, 2018), considers three types of buckling loads. It was observed that local and distortional buckling were the primary modes responsible for failure, consistent with the findings of the AS/NZS standard.Additionally, the comparison results in Table 6-2 ,Table 6-3 and Figure 6-3 ,Figure 6-4 show that the AS/NZS design strengths were conservative by 15% for one web hole columns, while 12% under estimation for multiple web holes, which primarily failed due to distortional and global buckling modes but it is impossible to separate it as critical failure mode. It will occur in combination of all three buckling modes, as well as lateral torsional buckling also imposed in some case with two screws of channel sections with length more than 1500mm.

7.2 Limitations and future study

Finally, design recommendations in the form of axial strength reduction factors were proposed for aluminium Face-to-Face (FTF) channels with a one web hole. As demonstrated in Table 6-1, the accuracy of the newly proposed strength reduction factors has been validated against the Direct Strength Method (DSM). The equations (27), provide more accurate predictions of the axial compressive capacity of aluminium FTF built-up channels with a single web hole and multiple web holes in the web, yielding results that align more closely with experimental values.

This study identified several limitations regarding the applicability of the proposed design equations.

Scope of application: The equations are specifically developed for FTF built-up sections with either a single web hole or multiple web holes. To determine the strength capacity of such sections, the plain section capacity must first be calculated, along with the modified slenderness ratio for sections with web holes. The reduction factor is then determined using the proposed equation. The strength capacity of the section with web holes is obtained by multiplying the plain section capacity by the reduction factor.

Static load assumption: The study is limited to static loading conditions and does not account for the effects of moving or dynamic loads.

Geometric limitations: The applicability of the equations is restricted to specific height-to-thickness (h/t) ratios and slenderness ratios, as discussed in Chapter Six.

Failure Modes: The analysis is confined to weak axis buckling failure, with no consideration of other potential failure modes.

These limitations should be addressed in future studies to enhance the generalizability and robustness of the proposed equations.

Several limitations were identified in this study regarding the applicability of the proposed design equations. First, the equations are specifically intended for sections with a one web hole as well as more web holes.to determine the capacity, it must be calculating plain section capacity and modified slenderness ratio for web holes section. Then determine the reduction factor using above equation. Multiply strength capacity of plain section and reduction factor will provide hole section Strength capacity. Second, the study is limited to consider static force does not consider moving loads and it limit to given h/t and Slenderness ration in chapter six. Finally, the failure modes considered in this study are confined to weak axis buckling failure.

These limitations highlight the need for future research in the following areas:

1) Investigating the effective use of AAFTF of cross-section in bridge beams or trusses,

2) Exploring the application of different AAFTF cross-sectional designs for vehicular bridges, particularly with varying plate thicknesses.

3) Studying the use of Aluminium Alloy Face to Face (AAFTF) tube combined with timber in composite section design for low-cost bridge construction, with a focus on optimizing the bridge's life cycle cost.

References

A. Crisan, V. Ungureanu, D. Dubina, Calibration of design formula for buckling strength of built-up back-to-back cold-formed steel members in compression, Procedings of the ICTWS 2014 7th International Conference on Thin-Walled Structures, ICTWS, Busan, Korea, 2014, 28th September to 2nd October 2014.

American Iron and Steel Institute (AISI). North American Specification for the Design of Cold-formed Steel Structural Members AISI D100-17E; 2017.

American Iron and Steel Institute (AISI). North American standard for Specification for the Design of Cold-formed Steel Structural Members AISI S100-12; 2012.

Ananthi. G, Ashvini. B, Experimental theoretical and numerical studies on cold-formed steel stub channel columns with stiffeners, Asian J. Civ. Eng. 20 (2019) 171-185.

AS 1391:2020 Metallic materials - Tensile testing - Method of test at room temperature

ASCE, Specification for the Design of Cold-Formed Stainless Steel Structural Members, SEI/ASCE 8-02, American Society of Civil Engineers, New York, 2002 (Standard No. 02-008).

Atlas Steels. (2021). Aluminium alloy 5052 data sheet (24-06-21). Retrieved from https://atlassteels.com.au/wp-content/uploads/2021/08/Aluminium-Alloy-5052-Data-Sheet-24-06-21.pdf.

Australia/New Zealand Standard (AS/NZS). Cold-Formed Steel Structures, AS/NZS 4600:2018. Standards Australia/ Standards New Zealand; 2018.

Australia/New Zealand Standard (AS/NZS). Cold-Formed Steel Structures, AS/NZS 4673-2001. Standards Australia/ Standards New Zealand; 2001.

Australian/New Zealand Standard (AS/NZS), Aluminium Structures Part 2: Allowable Stress Design, AS/NZS 1664.2: 1997, Sydney, Australia, 1997.

Australian/New Zealand Standard (AS/NZS). Aluminium Structures Part 1: Limit State Design. AS/NZS 1664.1: 1997, Sydney, Australia, 1997.

B. Young, W. Hartono, Compression tests of stainless steel tubular members, J. Struct. Eng. 128(6) (2002) 754-761.

C. Faella, F.M. Mazzolani, V. Piluso, G. Rizzano, Local buckling of aluminium members: testing and classification, J. Struct. Eng. 126 (3) (2000) 353-360.

Chen B, Roy K, Uzzaman A, Raftery GM, Nash D, Clifton GC, Lim JB. Effects of edge-stiffened web openings on the behaviour of cold-formed steel channel sections under compression. Thin-Walled Structures 2019; 144, 106307.

Chen, W., Li, G., & Young, B. (2020). Compression resistance of cold-formed steel channel sections with edge-stiffened and unstiffened web openings. *Thin-Walled Structures, 152*, 106786.

D.C. Fratamico, S. Torabian, X. Zhao, K.J.R. Rasmusen, B.W. Schafer, Experiments on the global and collapse of built-up cold-formed steel columns. J. Constr. Steel Res. 144 (2018) 65-80.

Das SK, Kaufman JG. Aluminum alloys for bridges and bridge decks. The Minerals, Metals & Materials Society. 2007:61-72.

Eurocode 9 (EC9), Design of Aluminium Structures - Part 1-1: General Structural Rules, European Committee for Standardization, EN 1999-1-1:2007, CEN, Brussels, Belgium, 2007.

F.M. Mazzolani, V. Piluso, G. Rizzano, Local buckling of aluminium alloy angles under uniform compression, J. Struct. Eng. 137(2) (2011) 173-184.

Fang, Z., Roy, K., & Lim, J. B. P. (2023). Structural design for Roll-Formed aluminium alloy perforated channels subjected to Interior-Two-Flange web crippling: experimental tests, numerical simulation, and neural network. International Journal of Steel Structures, 23(3), 692–708. https://doi.org/10.1007/s13296-023-00722-6

Fang, Z., Roy, K., Chen, B., Xie, Z., & Lim, J. B. (2021). Local and distortional buckling behaviour of aluminium alloy back-to-back channels with web holes under axial compression. Journal of Building Engineering, 47, 103837. https://doi.org/10.1016/j.jobe.2021.103837

Fang, Z., Roy, K., Chen, B., Xie, Z., Ingham, J., & Lim, J. B. (2022). Effect of the web hole size on the axial capacity of back-to-back aluminium alloy channel section columns. Engineering Structures, 260, 114238.

Fang, Z., Roy, K., Chen, B., Xie, Z., Ingham, J., & Lim, J. B. (2022b). Effect of the web hole size on the axial capacity of back-to-back aluminium alloy channel section columns. Engineering Structures, 260, 114238. https://doi.org/10.1016/j.engstruct.2022.114238

Fang, Z., Roy, K., Dai, Y., & Lim, J. B. (2022c). Effect of web perforations on end-two-flange web crippling behaviour of roll-formed aluminium alloy unlipped channels through experimental test, numerical simulation and deep learning. Thin-Walled Structures, 179, 109489. https://doi.org/10.1016/j.tws.2022.109489

Fang, Z., Roy, K., Ingham, J. M., & Lim, J. B. (2022a). Assessment of end-two-flange web crippling strength of roll-formed aluminium alloy perforated channels by experimental testing, numerical simulation, and deep learning. Engineering Structures, 268, 114753. https://doi.org/10.1016/j.engstruct.2022.114753

Fang, Z., Roy, K., Xu, J., Dai, Y., Paul, B., & Lim, J. B. (2022d). A novel machine learning method to investigate the web crippling behaviour of perforated roll-formed aluminium alloy unlipped channels under interior-two flange loading. Journal of Building Engineering, 51, 104261. https://doi.org/10.1016/j.jobe.2022.104261

Gardner L. The continuous strength method. Proceedings of the Institution of Civil Engineers-Structures and Buildings. 2008 Jun;161(3):127-33.

H.X. Yuan, Y.Q. Wang, Y.J. Shi, L. Gardner, Stub column tests on stainless steel built-up sections, Thin-Walled Struct. 83 (2014) 103-114.

Hancock, G.J., 2003. Cold-formed steel structures. Journal of constructional steel research, 59(4), pp.473-487.

International Conference on Engineering Research and Practice for Steel Construction 2018 (ICSC2018). September 5-7 (2018) Hong Kong, China.

J. Dobrić, M. Zlatko, B. Dragan, S. Milan, F. Nenad, Resistance of cold-formed built-up stainless-steel columns-Part I: Experiment, J. Constr. Steel Res. 145 (2018) 552-572.

J. Dobrić, P. Marko, M. Zlatko, B. Dragan, S. Milan, Resistance of cold-formed built-up stainless-steel columns - Part II: Numerical simulation, J. Constr. Steel Res. 145 (2018) 247-260.

J. Rondal, M. Niazi, Stability of built-up beams and columns with thin -walled members, J. Constr. Steel Res. 16 (1990) 329-335.

Jacob S, Aneeshkumar SL, Ajeesh SS. Investigation on Axial Capacity of Cold-Formed Aluminium Alloy Built-Up Columns. Journal of The Institution of Engineers (India): Series A. 2024 Apr 6:1-2.

K. Roy, B.S. Chen, Z.Y. Fang, A. Uzzaman, X. Chen, J.B.P. Lim, Local and distortional buckling behaviour of back-to-back built-up aluminium alloy cha

K. Roy, C. Mohammadjani, J.B.P. Lim, Experimental and numerical investigation into the behaviour of face-to-face built-up cold-formed steel channel sections under compression. Thin Walled Struct. 134 (2019) 291-309., Thin Walled Struct. 163(1) (2021).

K. Roy, H.H. Lau, A.M.M. Ahmed, J.B.P. Lim, Nonlinear behavior of cold-formed stainless steel built-up box sections under axial compression, Struct. 30 (2021) 390-408.

K. Roy, H.H. Lau, B.S. Chen, T.C.H. Ting, J.B.P. Lim, Effect of screw spacing on axial strength of cold-formed steel built-up box sections-numerical investigation and parametric study.(2019) World Congress on Advances in Structural Engineering and Mechanics. September 17-21 (2019) Jeju, South Korea.

K. Roy, H.H. Lau, J.B.P. Lim, Finite element modelling of back-to-back built-up cold-formed stainless-steel lipped channels under axial compression, Steel Compos. Struct. 33 (2019) 37-66.

K. Roy, H.H. Lau, J.B.P. Lim, Numerical investigations on the axial capacity of back-to-back gapped built-up cold-formed stainless-steel channels, Adv. Struct. Eng. 22 (10) (2019) 2289-2310.

K. Roy, J.B.P. Lim, Numerical investigation into the buckling behaviour of face-to-face built-up cold-formed stainless steel channel sections under axial compression, Struct. 20 (2019) 42-73.

K. Roy, T.C.H. Ting, H.H. Lau, J.B.P. Lim, Effect of screw spacing into the behaviour of back-to-back cold-formed duplex stainless steel built-up channel sections under compression.

K. Roy, T.C.H. Ting, H.H. Lau, J.B.P. Lim, Effect of thickness on the behaviour of axially loaded back-to-back cold-formed steel built-up channel sections-Experimental and numerical investigation, Struct. 16 (2018) 327-346.

K. Roy, T.C.H. Ting, H.H. Lau, J.B.P. Lim, Experimental investigation into the behaviour of back-to-back gapped built-up cold-formed steel channel sections under compression, in: Proceedings of the 'Wei-Wen Yu International Specialty Conference on Cold-Formed Steel Structures. November 7-8 (2018) St. Louis, Missouri, USA, accepted.

K. Roy, T.C.H. Ting, H.H. Lau, J.B.P. Lim, Nonlinear behavior of back-to-back gapped built-up cold-formed steel channel sections under compression, J. Constr. Steel Res. 147 (2018) 257-276.

L.A.T. Huynh, C.H. Pham, K.J.R. Rasmussen, Mechanical properties of cold-rolled aluminium alloy 5052 channel sections. Proceedings of 8th International Conference on Steel and Aluminium Structures, Hong Kong, China 670-684 (2016).

L.A.T. Huynh, C.H. Pham, K.J.R. Rasmussen, Stub column tests and finite element modelling of cold-rolled aluminium alloy 5052 channel sections, in: Proceedings of the Eighth International Conference on Steel and Aluminium Structures, Hong Kong, China 1–14 (2016).

M. Dabaon, E. Ellobody, K. Ramzy, Experimental investigation of built-up cold-formed steel section battened columns, Thin-Walled Struct. 92 (2015) 137-145.

M. Dabaon, E. Ellobody, K. Ramzy, Nonlinear behaviour of built-up cold-formed steel section battened columns, J. Constr. Steel Res. 110(2015) 16-28.

M.N. Su, B. Young, L. Gardner, Assessment of Eurocode 9 slenderness limits for elements in compression. Tubular Structures-Proceedings of the 15th International Symposium on Tubular Structures. May 569-574 (2016) Rio de Janeiro, Brazil.

M.N. Su, B. Young, L. Gardner, Testing and design of aluminium alloy cross sections in compression. J. Struct. Eng. 140 (9) (2014) 04014047.

Moen, C. D., & Schafer, B. W. (2009). Elastic buckling of cold-formed steel columns and beams with holes. Engineering Structures, 31(12), 2812-2824.

Paul, B., Roy, K., Ji, Y., Fang, Z., Sivaji, V., & Lim, J. B. (2024). Moment capacity of perforated cold-formed aluminium channels–Tests, analysis, and design. Thin-Walled Structures, 204, 112261. https://doi.org/10.1016/j.tws.2024.112261

R. Feng, B. Young, Experimental Investigation of Aluminium Alloy Stub Columns with Circular Openings, J. Struct. Eng. 141(11) (2015) 04015031.

R. Feng, W. Sun, C. Shen, J. Zhu, Experimental investigation of aluminium square and rectangular beams with circular perforations, Eng. Struct. 151 (2017) 613-632.

R. Feng, X. Mou, A. Chen, Y. Ma, Tests of aluminium alloy CHS columns with circular openings, Thin-Walled Struct. 109 (2016) 113-131.

Roy K, Mohammadjani C, Lim JB. Experimental and numerical investigation into the behaviour of face-to-face built-up cold-formed steel channel sections under compression. Thin-Walled Structures. 2019 Jan 1;134:291-309.

Roy, K., Chen, B., Fang, Z., Uzzaman, A., & Lim, J. B. (2022). Axial capacity of back-to-back built-up aluminum alloy channel section columns. Journal of Structural Engineering, 148(2), 04021265.

Roy, K., Chen, B., Fang, Z., Uzzaman, A., Chen, X., & Lim, J. B. (2021). Local and distortional buckling behaviour of back-to-back built-up aluminium alloy channel section columns. Thin-Walled Structures, 163, 107713. https://doi.org/10.1016/j.tws.2021.107713.

S. Kechidi, D.C. Fratamico, B.W. Schafer, C.J. Miguel, Simulation of screw connected built-up cold formed steel back-to-back lipped channels under axial compression. Eng. Struct. 206 (2020) 110109.

S. Kechidi, D.C. Fratamico, N. Bourahla, J.M. Castro, B.W. Schafer, Numerical study of screw fasteners in built-up CFS chord studs. Ce/papers. 1 (2-3) (2017) 1543-1552.

S. Kesawan, M.Mahendran, Y. Dias, W.B. Zhao, Compression tests of built-up cold-formed steel hollow flange sections, Thin-Walled Struct. 116 (2017) 180-193.

Siwowski T. Aluminium bridges–past, present and future. Structural engineering international. 2006 Nov 1;16(4):286-93.

The Aluminum Association, Aluminum Design Manual (ADM). The Aluminum Association, Washington, D.C., USA, 2015.

W.S. Miller, L.Z. Zhuang, J. Bottema, A.J. Wittebrood, D.S. Peter, A. Haszler, A. Vieregge, Recent development in aluminium alloys for the automotive industry. Mater. Sci. Eng. 280 (1) (2000) 37–49.

Walker A.C. (Ed.), Design and Analysis of Cold-Formed Sections, John Wiley & Sons (1975)

Y. Chen, R. Feng, J. Xu, Flexural behaviour of CFRP strengthened concrete-filled aluminium alloy CHS tubes, Contra Build Mater. 142 (2017) 295-319.

Y. Chen, R. Feng, W. Gong, Flexural behaviour of concrete-filled aluminium alloy circular hollow section tubes, Constr Build Mater. 165 (2018) 173-186.

Zhu JH, Young B. Aluminum alloy tubular columns—Part I: Finite element modeling and test verification. Thin-Walled Structures. 2006 Sep 1;44(9):961-8.

Zhu, J. H., & Young, B. (2008). Behavior and design of aluminum alloy structural members. Advanced Steel Construction.

Appendix "A" – Coupon testing for material properties

To determine the material properties of the samples provided coupon testing was conducted, and the results were used to carry out the parametric study as mentioned in the chapter three. The details of the Instron machine are provided in the Figure A-1. The deformed shape of the coupon samples is shown in the Figure A-2.

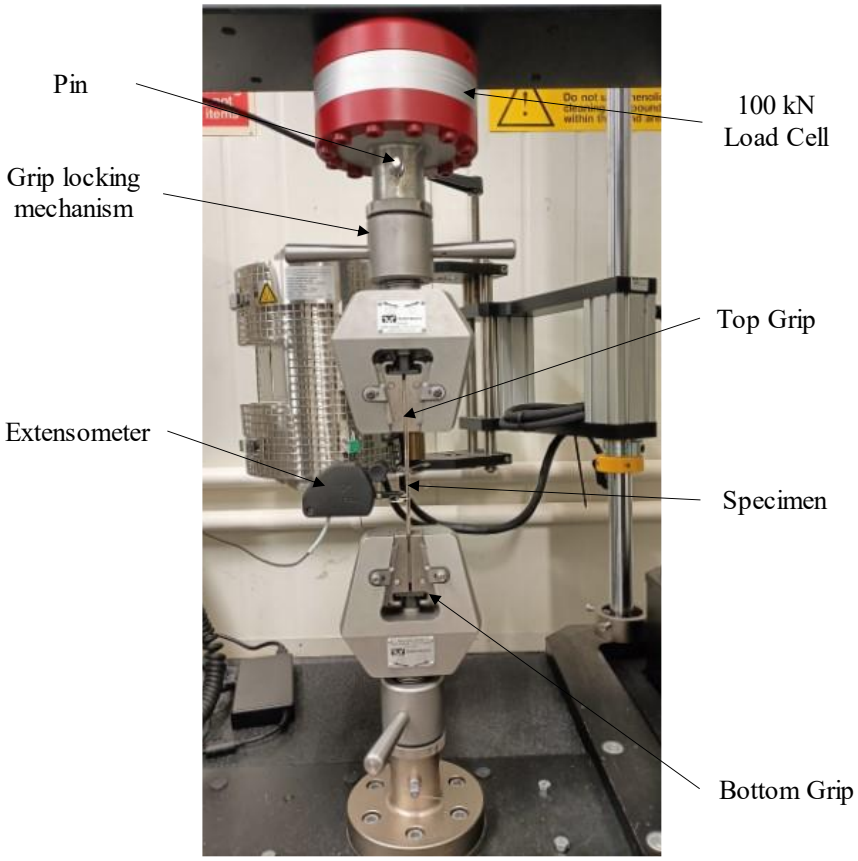

Figure A-1: Instron testing machine

Figure A-2: Deformed shape of the coupons

Material properties obtained from the coupon testing can be seen in the Figure A-3.

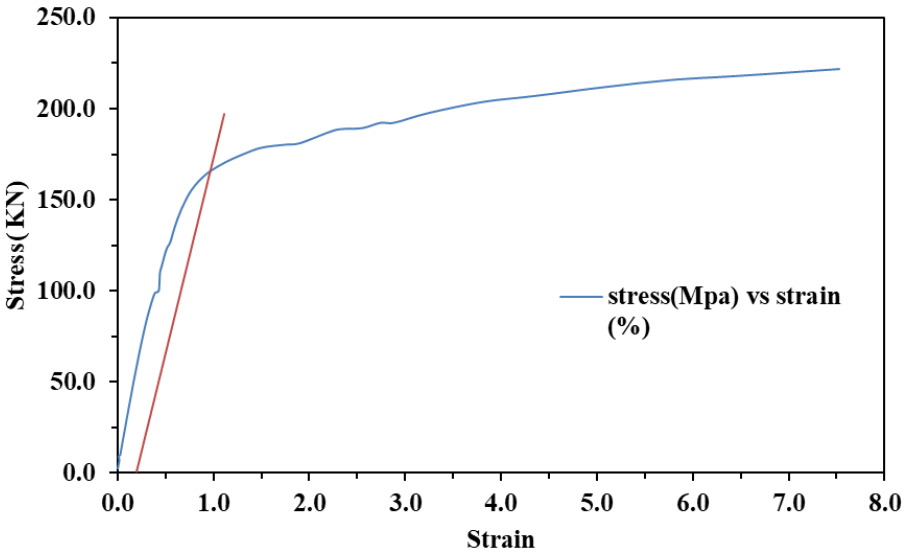

Figure A-3: Stress-strain curve from the coupon testing

Appendix “B” – Python Programme used to build multiple holes model in parameter study.

This Python program was created by Alexis Peyret, an international internship student from France at the University of Waikato. Alexis developed this program as part of his internship while working with our team. The program significantly reduced the time required for modelling section with multiple hole in the web, contributing both to his degree studies and the efficiency of this thesis research. I have included this program here with his consent.

```
# -*- coding: utf-8 -*-
"""
This script models a face-to-face column with holes and fasteners in Abaqus.
"""

# Standard library imports
import os
import math
import shutil
import re
import inspect
import itertools

# Abaqus-specific imports
from abaqus import mdb
from abaqusConstants import *
from odbAccess import *
import regionToolset
import mesh


# ============================================================
# Functions
# ============================================================


def create_material_and_section(model, E, nu, sigma_yield, folded_sigma_yield,
thickness):
    """Create material and section properties."""

    def create_material(name, E_modulus, poisson_ratio, yield_stress):
        """Helper function to create a material with elastic and plastic
properties."""
        material = model.Material(name=name)
        material.Elastic(table=((E_modulus, poisson_ratio),))
```

```
        material.Plastic(table=((yield_stress, 0.0),))
        return material

    # Create base material
    create_material('ALUMINIUM-ALLOY', E, nu, sigma_yield)

    # Create sections using the base material
    model.HomogeneousShellSection(
        name='COLUMN-SECTION',
        material='ALUMINIUM-ALLOY',
        thickness=thickness,
        numIntPts=5,
        integrationRule=SIMPSON
    )
    model.HomogeneousSolidSection(
        name='END-PLATE-SECTION',
        material='ALUMINIUM-ALLOY',
        thickness=None
    )

    # Create folded material by copying and modifying the plastic properties
    folded_material_name = 'FOLDED-ALUMINIUM-ALLOY'
    model.Material(
        name=folded_material_name,
        objectToCopy=model.materials['ALUMINIUM-ALLOY']
        )
    model.materials['FOLDED-ALUMINIUM-ALLOY'].plastic.setValues(
        table=((folded_sigma_yield, 0.0),)
    )

    # Create folded section using the folded material
    model.HomogeneousShellSection(
        name='FOLDED-SECTION',
        material='FOLDED-ALUMINIUM-ALLOY',
        thickness=thickness,
        numIntPts=5,
        integrationRule=SIMPSON
    )


def create_end_plate(model, length, width, thickness, mesh_size):
    """Create the END-PLATE part and configure its mesh and section
assignment."""

    # Create a rectangle sketch for the end plate
    sketch = model.ConstrainedSketch(name='__profile__', sheetSize=500.0)
    sketch.rectangle(point1=(0.0, 0.0), point2=(width, length))

    # Create the part by extruding the sketch
```

```
    p_end_plate = model.Part(
        name='END-PLATE',
        dimensionality=THREE_D,
        type=DEFORMABLE_BODY
    )
    p_end_plate.BaseSolidExtrude(sketch=sketch, depth=thickness)

    # Clean up the sketch
    del model.sketches['__profile__']

    # Create a reference point in the center of the rectangle
    p_end_plate.ReferencePoint(point=(width / 2.0, length / 2.0, 0.0))

    # Configure the mesh for the part.
    p_end_plate.seedPart(size=mesh_size, deviationFactor=0.1,
minSizeFactor=0.1)
    elem_type_end_plate = mesh.ElemType(elemCode=C3D8R, elemLibrary=STANDARD)
    cells_end_plate = p_end_plate.cells
    region_cells = regionToolset.Region(cells=cells_end_plate)
    p_end_plate.setElementType(regions=(cells_end_plate,),
elemTypes=(elem_type_end_plate,))
    p_end_plate.generateMesh()

    # Assign section properties to the part
    p_end_plate.SectionAssignment(
        region=region_cells,
        sectionName='END-PLATE-SECTION',
        offsetType=MIDDLE_SURFACE,
        thicknessAssignment=FROM_SECTION
    )

    return p_end_plate


def create_half_column(model, length, height, width):
    """Create the HALF-COLUMN part with holes and partitions."""

    # Create a sketch for the half-column
    sketch = model.ConstrainedSketch(name='__profile__', sheetSize=500.0)

    # Draw the edges of the half-column
    sketch.Line(point1=(width, 0.0), point2=(0.0, 0.0))
    sketch.Line(point1=(0.0, 0.0), point2=(0.0, height))
    sketch.Line(point1=(0.0, height), point2=(width, height))

    # Create the half-column part
    part = model.Part(
        name='HALF-COLUMN',
        dimensionality=THREE_D,
```

```
        type=DEFORMABLE_BODY
    )
    part.BaseShellExtrude(sketch=sketch, depth=length)

    # Clean up the sketch
    del model.sketches['__profile__']

    return part


def partition_side_face(model, part, length, height, partition_height,
partition_width, num_holes,
                        hole_radius, hole_spacing):
    """Partition the side face for hole creation."""

    def draw_vertical_line(sketch, x_position):
        """Draw a vertical line at the specified x_position."""
        sketch.Line(
            point1=(x_position, -height / 2.0),
            point2=(x_position, height / 2.0)
        )

    def draw_horizontal_line(sketch, y_position):
        """Draw a horizontal line at the specified y_position."""
        sketch.Line(
            point1=(-partition_width / 2.0, y_position),
            point2=(partition_width / 2.0, y_position)
        )

    # Get the face and edge for sketch transformation
    faces = part.faces
    edges = part.edges
    partition_face = faces.findAt(coordinates=(0.0, height  / 2.0, length  /
2.0), normal=(0.0, 0.0, 1.0))
    partition_edge = edges.findAt(coordinates=(0.0, height  / 2.0, length ))

    # Create sketch transform
    transform  = part.MakeSketchTransform(
        sketchPlane=partition_face,
        sketchUpEdge=partition_edge,
        sketchPlaneSide=SIDE1,
        origin=(0.0, height / 2.0, length / 2.0))

    # Create a new sketch
    sketch = model.ConstrainedSketch(
        name='__profile__',
        sheetSize=5000.0,
        gridSpacing=100.0,
        transform=transform
```

```
    )

    # Draw partition lines
    draw_vertical_line(sketch, -partition_width / 2.0)
    draw_vertical_line(sketch, 0.0)
    draw_vertical_line(sketch, partition_width / 2.0)

    draw_horizontal_line(sketch, partition_height / 2.0)
    draw_horizontal_line(sketch, 0.0)
    draw_horizontal_line(sketch, -partition_height / 2.0)

    # Draw the central hole
    sketch.CircleByCenterPerimeter(center=(0.0, 0.0), point1=(hole_radius,
0.0))

    # Copy the hole geometry for additional holes
    geometry = sketch.geometry.values()
    hole_positions = []
    start_position = -((num_holes - 1) / 2.0) * hole_spacing

    for i in range(num_holes):
        z_offset = start_position + i * hole_spacing
        if z_offset != 0.0:
            sketch.copyMove(objectList=geometry, vector=(z_offset, 0.0))
        hole_positions.append(z_offset)

    # Partition the face using the sketch
    part.PartitionFaceBySketch(faces=partition_face, sketch=sketch)

    # Clean up the sketch
    del model.sketches['__profile__']

    return hole_positions


def cut_holes(model, part, length, height, hole_positions, hole_diameter):
    """Cut holes in the HALF-COLUMN part at specified positions."""

    all_faces = part.faces
    all_edges = part.edges

    for z_offset in hole_positions:

        # Calculate the center point for the hole
        y_center = height / 2.0
        z_center = length / 2.0 - z_offset
        face_point = (0.0, y_center, z_center)

        # Find the face and edge at the specified position
```

```
        hole_face = all_faces.findAt(coordinates=face_point, normal=(0.0, 0.0,
1.0))
        hole_edge  = all_edges.findAt(coordinates=face_point)

        # Create a sketch transform for the hole
        transform = part.MakeSketchTransform(
            sketchPlane=hole_face,
            sketchUpEdge=hole_edge,
            sketchPlaneSide=SIDE1,
            origin=face_point
        )

        # Create the sketch for the hole
        sketch = model.ConstrainedSketch(
            name='__profile__',
            sheetSize=5000.0,
            gridSpacing=100.0,
            transform=transform
        )

        # Draw the circle representing the hole
        sketch.CircleByCenterPerimeter(
            center=(0.0, 0.0),
            point1=(0.0, hole_diameter / 2.0)
        )

        # Cut the hole using the sketch
        part.CutExtrude(
            sketchPlane=hole_face,
            sketchUpEdge=hole_edge,
            sketchPlaneSide=SIDE1,
            sketchOrientation=RIGHT,
            sketch=sketch
        )

        # Clean up the sketch
        del model.sketches['__profile__']


def partition_top_bottom_faces(model, part, length, height, width,
fillet_radius, num_fasteners,
                               first_fastener_pos, fasteners_spacing):
    """Partition the top and bottom faces for fasteners regions."""

    all_faces = part.faces
    all_edges = part.edges

     # Calculate the x-position centered along the width, adjusted for the
fillet
```

```
    x_position = (width / 2.0) + (fillet_radius / 2.0)

    # Positions for bottom and top faces
    y_positions = [0.0, height]

    # Effective half-width excluding the fillet radius
    y_fastener = width

    # Iterate over both bottom and top faces
    for y_position in y_positions:
        # Define points for locating the face and edge
        face_point = (x_position, y_position, length / 2.0)
        edge_point = (x_position, y_position, length)

        # Find the face and edge at the specified coordinates
        face = all_faces.findAt(coordinates=face_point, normal=(0.0, 0.0,
1.0))
        edge = all_edges.findAt(coordinates=edge_point)

        # Create a sketch transform for the face
        transform = part.MakeSketchTransform(
            sketchPlane=face,
            sketchUpEdge=edge,
            sketchPlaneSide=SIDE1,
            origin=(x_position, y_position, 0.0)
        )

        # Create the sketch for partitioning
        sketch = model.ConstrainedSketch(
            name='__profile__',
            sheetSize=5000.0,
            gridSpacing=100.0,
            transform=transform
        )

        # Draw a horizontal line along the length of the half-column
        sketch.Line(point1=(0.0, 0.0), point2=(length, 0.0))

        # Draw vertical lines at fasteners positions
        for i in range(num_fasteners):
            x_fastener = first_fastener_pos  + i * fasteners_spacing
            # Draw a vertical line at x_fastener
            sketch.Line(
                point1=(x_fastener, -y_fastener),
                point2=(x_fastener, y_fastener)
            )

        # Partition the face using the sketch
```

```
        part.PartitionFaceBySketch(faces=face, sketch=sketch)

        # Clean up the sketch
        del model.sketches['__profile__']


def add_fillet(part, height, fillet_radius):
    """Apply a fillet to the part at the specified edges."""

    # Get edges
    all_edges = part.edges
    edges_1 = all_edges.getByBoundingBox(
        xMin=0.0, xMax=0.0,
        yMin=0.0, yMax=0.0
    )
    edges_2 = all_edges.getByBoundingBox(
        xMin=0.0, xMax=0.0,
        yMin=height, yMax=height
    )

    # Apply the fillet
    part.Round(radius=fillet_radius, edgeList=(edges_1[0], edges_2[0]))


def assign_section(part, height, fillet_radius):
    """Assign sections to the HALF-COLUMN part."""

    # Assign 'COLUMN-SECTION' to all faces
    all_faces = part.faces
    entire_region = regionToolset.Region(faces=all_faces)
    part.SectionAssignment(
        region=entire_region,
        sectionName='COLUMN-SECTION',
        offsetType=BOTTOM_SURFACE,
        thicknessAssignment=FROM_SECTION
    )

    # Define the regions for folded sections (top and bottom fillets)
    fillet_regions = [
        (0.0, fillet_radius),                  # Bottom fillet region
        (height - fillet_radius, height)       # Top fillet region
    ]

    # Collect folded faces from fillet regions
    folded_faces = []
    for y_min, y_max in fillet_regions:
        faces_in_region = all_faces.getByBoundingBox(
            xMin=0.0, xMax=fillet_radius,
            yMin=y_min, yMax=y_max
```

```
        )
        folded_faces.append(faces_in_region)

    # Assign 'FOLDED-SECTION' to folded faces
    folded_region = regionToolset.Region(faces=folded_faces[0] +
folded_faces[1])
    part.SectionAssignment(
        region=folded_region,
        sectionName='FOLDED-SECTION',
        offsetType=BOTTOM_SURFACE,
        thicknessAssignment=FROM_SECTION
    )


def mesh_half_column(part, length, height, fillet_radius, hole_diameter,
hole_positions, partition_height,
                     partition_width, partition_hole_radius, mesh_size,
refined_mesh_size):
    """Mesh the HALF-COLUMN part."""

    # Seed the entire part with the general mesh size
    part.seedPart(size=mesh_size, deviationFactor=0.1, minSizeFactor=0.1)

    # Set element type for all faces
    elem_type = mesh.ElemType(elemCode=S4R, elemLibrary=STANDARD)
    all_faces = part.faces
    all_edges = part.edges
    part.setElementType(regions=(all_faces,), elemTypes=(elem_type,))

    # Find faces near all holes for structured meshing
    faces_to_mesh = []
    y_center = height  / 2.0
    for z_offset in hole_positions:
        z_center = length  / 2.0 - z_offset
        x_half_width = partition_width / 2.0
        y_half_height = partition_height / 2.0
        z_half_width = partition_width / 2.0

        # Identify faces in the bounding box
        faces_near_hole = all_faces.getByBoundingBox(
            xMin=-x_half_width, xMax=x_half_width,
            yMin=y_center - y_half_height, yMax=y_center + y_half_height,
            zMin=z_center - z_half_width, zMax=z_center + z_half_width
        )
        faces_to_mesh.extend(faces_near_hole)

    # Apply structured meshing
    part.setMeshControls(
        regions=faces_to_mesh,
```

```
        elemShape=QUAD,
        technique=STRUCTURED
    )

    # Seed edges around each hole
    for z_offset in hole_positions:
        z_center = length / 2.0 - z_offset
        radius_offset = (partition_hole_radius + hole_diameter / 2.0) / 2.0

        # Find edges near the hole
        edge1 = all_edges.findAt((0.0, y_center + radius_offset, z_center), )
        edge2 = all_edges.findAt((0.0, y_center - radius_offset, z_center), )
        edge3 = all_edges.findAt((0.0, y_center, z_center + radius_offset), )
        edge4 = all_edges.findAt((0.0, y_center, z_center - radius_offset), )

        # Seed edges with refined mesh size
        part.seedEdgeByNumber(
            edges=(edge1, edge2, edge3, edge4),
            number=refined_mesh_size,
            constraint=FINER
        )

    # Seed edges of fillets
    edges = all_edges.getByBoundingBox(xMin=0.0, xMax=fillet_radius)
    selected_edges = []
    for edge in edges:
        x_coord = edge.pointOn[0][0]
        if 1e-03 <= x_coord <= fillet_radius - 1e-03:
            selected_edges.append(edge)

    # Seed edges with refined mesh size
    part.seedEdgeByNumber(
        edges=selected_edges,
        number=4,
        constraint=FINER
    )

    # Generate the mesh
    part.generateMesh()


def create_assembly(model, p_end_plate, p_half_column, length, height, width,
thickness, fillet_radius,
                    end_plate_length, end_plate_width):
    """Create the assembly with instances of the end plate and half column
parts."""

    def rotate_instance(instance_name, axis_point, axis_direction, angle):
        """Rotate an instance in the assembly."""
```

```
        assembly.rotate(
            instanceList=(instance_name,),
            axisPoint=axis_point,
            axisDirection=axis_direction,
            angle=angle
        )

    def translate_instance(instance_name, vector):
        """Translate an instance in the assembly."""
        assembly.translate(
            instanceList=(instance_name,),
            vector=vector
        )

    # Initialize the assembly
    assembly = model.rootAssembly
    assembly.DatumCsysByDefault(CARTESIAN)

    # Create part instances
    assembly.Instance(name='HALF-COLUMN-1', part=p_half_column, dependent=ON)
    assembly.Instance(name='HALF-COLUMN-2', part=p_half_column, dependent=ON)
    assembly.Instance(name='END-PLATE-1', part=p_end_plate, dependent=ON)
    assembly.Instance(name='END-PLATE-2', part=p_end_plate, dependent=ON)

    # Calculation of displacement
    x_disp = -end_plate_width / 2.0
    y_disp = -end_plate_length / 2.0
    delta_x_disp = (width + fillet_radius) / 2.0
    delta_y_disp = (-height + thickness) / 2.0

    # Position End Plate 1
    rotate_instance(
        instance_name='END-PLATE-1',
        axis_point=(end_plate_width / 2.0, 0.0, 0.0),
        axis_direction=(0.0, 1.0, 0.0),
        angle=180.0
    )
    translate_instance('END-PLATE-1', vector=(x_disp, y_disp, 0.0))

    # Position End Plate 2
    translate_instance('END-PLATE-2', vector=(x_disp, y_disp, length))

    # Position HALF-COLUMN-1
    translate_instance('HALF-COLUMN-1', vector=(-delta_x_disp, delta_y_disp,
0.0))

    # Position HALF-COLUMN-2
    rotate_instance(
```

```
        instance_name='HALF-COLUMN-2',
        axis_point=(0.0, 0.0, length / 2.0),
        axis_direction=(0.0, 1.0, 0.0),
        angle=180.0
    )
    translate_instance(
        'HALF-COLUMN-2',
        vector=(delta_x_disp, (-thickness - height) / 2.0, 0.0)
    )

    # Create reference point set on END-PLATE-2
    ref_point = (assembly.instances['END-PLATE-
2'].referencePoints.values()[0],)
    assembly.Set(referencePoints=ref_point, name='TOP-RF-SET')

    return assembly


def create_surfaces(assembly, length):
    """Create surfaces and sets for boundary conditions at specified
positions."""

    positions = [0.0, length]  # Positions for surfaces (bottom and top)
    surface_names = ['BOTTOM', 'TOP']  # Names for the surfaces
    instance_names = ['HALF-COLUMN-1', 'HALF-COLUMN-2']  # Instances to
include in the surfaces

    # Create a surface and corresponding set for a given position and name
    for position, name in zip(positions, surface_names):
        edges = [
            edge
            for instance in instance_names
            for edge in [assembly.instances[instance].edges.getByBoundingBox(
                zMin=position, zMax=position
                )]
        ]

        set_name = '{}-SET'.format(name)
        surface_name = '{}-SURFACE'.format(name)

        # Create the set and surface in the assembly
        assembly.Set(edges=edges, name=set_name)
        assembly.Surface(side1Edges=edges, name=surface_name)


def define_analysis_steps(model, imperfections):
    """Define analysis steps based on whether imperfections is considered."""

    # Choose the step type based on imperfections
```

```
    if imperfections:
        # Define the buckling analysis step
        model.BuckleStep(
            name='BUCKLING-STEP',
            previous='Initial',
            numEigen=3,
            vectors=100,
            maxIterations=300
        )
    else:
        # Delete existing buckling step if it exists
        if 'BUCKLING-STEP' in model.steps:
            del model.steps['BUCKLING-STEP']

        # Delete existing buckling step if it exists
        model.StaticStep(
            name='COMPRESSION-STEP',
            previous='Initial',
            timePeriod=1.0,
            maxNumInc=10000,
            initialInc=1e-02,
            minInc=1e-06,
            maxInc=1e-01,
            nlgeom=ON,
            stabilizationMagnitude=2e-06,
            stabilizationMethod=DISSIPATED_ENERGY_FRACTION
        )


def define_output_requests(model, assembly):
    """Define history output requests for the model."""

    # Delete an existing history output request if it exists
    if 'H-Output-1' in model.historyOutputRequests.keys():
        del model.historyOutputRequests['H-Output-1']

    # Define region for history output request
    region_def = assembly.sets['TOP-RF-SET']

    # Define primary history output request
    model.HistoryOutputRequest(
        name='H-Output-1',
        createStepName='COMPRESSION-STEP',
        variables=('RF3', 'U3'),
        timeInterval=0.01,
        region=region_def,
        sectionPoints=DEFAULT,
        rebar=EXCLUDE
    )
```

```
    # Define energy output request
    model.HistoryOutputRequest(
        name='EnergyOutput',
        createStepName='COMPRESSION-STEP',
        variables=('ALLIE', 'ALLWK', 'ALLKE', 'ALLPD', 'ALLSE', 'ALLSD'),
        frequency=1
    )


def define_contact_properties(model):
    """Define contact properties and interactions for a material in the
model."""

    # Create contact property
    model.ContactProperty('ALUMINIUM-ALLOY-PROPERTIES')

    # Define tangential behavior
    model.interactionProperties['ALUMINIUM-ALLOY-
PROPERTIES'].TangentialBehavior(
        formulation=PENALTY,
        table=((0.3,),),
        fraction=0.005
    )

    # Define normal behavior
    model.interactionProperties['ALUMINIUM-ALLOY-PROPERTIES'].NormalBehavior(
        pressureOverclosure=HARD,
        allowSeparation=ON,
        constraintEnforcementMethod=DEFAULT
    )


def create_surface_interactions(model, assembly, height, thickness):
    """Create surface-to-surface contact interactions between half-column
surfaces."""

    def create_surface(instance_faces, y_coordinate, surface_name):
        """Create a surface on the instance at the specified y-coordinate."""
        surface_faces = instance_faces.getByBoundingBox(yMin=y_coordinate,
yMax=y_coordinate)
        assembly.Surface(side1Faces=surface_faces, name=surface_name)

    # Access faces of the half-column instances
    half_column_1_faces = assembly.instances['HALF-COLUMN-1'].faces
    half_column_2_faces = assembly.instances['HALF-COLUMN-2'].faces

    # Define sides and corresponding y-coordinates
    sides = {'LEFT': -height / 2.0, 'RIGHT': height / 2.0}
```

```
    # Process each side
    for side, y_coord in sides.items():
        # Determine surface names based on side
        surface_inner_name = '{}-INNER-SURFACE'.format(side)
        surface_outer_name = '{}-OUTER-SURFACE'.format(side)
        interaction_name = '{}-INTERACTION'.format(side)

        # Create surfaces on both half-columns
        if side == 'LEFT':
            create_surface(half_column_1_faces, y_coord + thickness / 2.0,
surface_inner_name)
            create_surface(half_column_2_faces, y_coord - thickness / 2.0,
surface_outer_name)
        else:
            create_surface(half_column_2_faces, y_coord - thickness / 2.0,
surface_inner_name)
            create_surface(half_column_1_faces, y_coord + thickness / 2.0,
surface_outer_name)

        # Define master and slave regions
        master_surface = assembly.surfaces[surface_outer_name]
        slave_surface = assembly.surfaces[surface_inner_name]

        # Create surface-to-surface contact interaction
        model.SurfaceToSurfaceContactStd(
            name=interaction_name,
            createStepName='Initial',
            main=master_surface,
            secondary=slave_surface,
            sliding=FINITE,
            interactionProperty='ALUMINIUM-ALLOY-PROPERTIES',
            adjustMethod=NONE,
            initialClearance=OMIT
        )


def add_fasteners(assembly, height, thickness, num_fasteners,
first_fastener_pos,
                  fasteners_spacing):
    """Add fasteners between the HALF-COLUMN instances."""

    # References to instances for efficiency
    half_column_1 = assembly.instances['HALF-COLUMN-1']
    half_column_2 = assembly.instances['HALF-COLUMN-2']

    # Define sides and corresponding y-coordinates
    sides = {'LEFT': -height / 2.0, 'RIGHT': height / 2.0}
```

```
    # Process each side
    for side, y_coord in sides.items():
        # Define names for fasteners and surfaces
        fastener_name = '{}-FASTENERS'.format(side)
        fastener_set_name = '{}-FASTENERS-SET'.format(side)
        surface_name_inner = '{}-INNER-SURFACE'.format(side)
        surface_name_outer = '{}-OUTER-SURFACE'.format(side)

        # Calculate y-range for bounding box
        y_min = y_coord - thickness / 2.0
        y_max = y_coord + thickness / 2.0

        # Initialize list to hold pairs of vertices for fasteners
        wire_points = []

        # Compute z_positions for the fasteners
        z_positions = [
            first_fastener_pos + i * fasteners_spacing
            for i in range(num_fasteners)
        ]
        x_coord = 0.0  # x-coordinate is constant

        for z_pos in z_positions:
            # Find corresponding vertices on both HALF-COLUMN instances
            vertex1 = half_column_1.vertices.findAt(((x_coord, y_max,
z_pos),))
            vertex2 = half_column_2.vertices.findAt(((x_coord, y_min,
z_pos),))
            wire_points.append((vertex1[0], vertex2[0]))

        # Create wires (edges) connecting the vertices
        assembly.WirePolyLine(points=tuple(wire_points), mergeType=IMPRINT,
meshable=OFF)

        # Get edges from created wires and create a set for them
        edges = assembly.edges.getByBoundingBox(yMin=y_min, yMax=y_max)
        assembly.Set(edges=edges, name=fastener_set_name)

        # Get target surfaces for the fasteners
        target_surfaces = [
            assembly.surfaces[surface_name_outer],
            assembly.surfaces[surface_name_inner]
        ]

        # Assign the MPC section to the wires
        region = assembly.sets[fastener_set_name]
        # Create the point fastener feature
        assembly.engineeringFeatures.PointFastener(
```

```
            name=fastener_name,
            region=region,
            targetSurfaces=tuple(target_surfaces),
            physicalRadius=10.0,
            connectionType=BEAM_MPC,
            unsorted=OFF
        )


def define_constraints(model, assembly, length):
    """Define constraints between end plates and column nodes."""

    # Configuration for constraints
    constraint_configs = [{
            'position': 'BOTTOM',
            'z_coord': 0.0,
            'end_plate_name': 'END-PLATE-1',
            'surface_name': 'BOTTOM-SURFACE',
            'set_name': 'BOTTOM-SET'
        },
        {
            'position': 'TOP',
            'z_coord': length,
            'end_plate_name': 'END-PLATE-2',
            'surface_name': 'TOP-SURFACE',
            'set_name': 'TOP-SET'
        }]

    for constraint in constraint_configs:
        position = constraint['position']
        z_coord = constraint['z_coord']
        end_plate_name = constraint['end_plate_name']
        surface_name = constraint['surface_name']
        set_name = constraint['set_name']

        # Get the end plate instance
        end_plate_instance = assembly.instances[end_plate_name]

        # Find the face at the specified coordinates
        face_point = (0.0, 0.0, z_coord)
        face = end_plate_instance.faces.findAt((face_point,))
        region_master = regionToolset.Region(side1Faces=face)
        region_slave = assembly.surfaces[surface_name]

        # Apply the Tie constraint
        model.Tie(
            name="{}-CONSTRAINT".format(position),
            main=region_master,
```

```
            secondary=region_slave,
            positionToleranceMethod=COMPUTED,
            adjust=ON,
            tieRotations=ON,
            thickness=ON
        )

        # Define the reference points and rigid body constraints
        ref_point = end_plate_instance.referencePoints.values()[0]
        ref_point_region = (ref_point,)

        # Get the region set from the assembly
        tie_region = assembly.sets[set_name]

        # Define the Rigid Body constraint
        model.RigidBody(
            name="{}-RP".format(position),
            refPointRegion=ref_point_region,
            tieRegion=tie_region
        )


def apply_boundary_conditions(model, assembly, displacement, imperfections):
    """Apply boundary conditions and loads to the model."""

    def create_displacement_bc(name, step_name, region,
**displacement_values):
        """Helper function to create a displacement boundary condition."""
        model.DisplacementBC(
            name=name,
            createStepName=step_name,
            region=region,
            **displacement_values
        )

    # Get reference points for top and bottom regions
    ref_points_bottom = (assembly.instances['END-PLATE-
1'].referencePoints.values()[0],)
    ref_points_top = (assembly.instances['END-PLATE-
2'].referencePoints.values()[0],)

    # Apply boundary conditions at the bottom (fixed)
    create_displacement_bc(
        name='BOTTOM-BC',
        step_name='Initial',
        region=ref_points_bottom,
        u1=0.0, u2=0.0, u3=0.0, ur1=0.0, ur3=0.0
    )
```

```
    # Apply boundary conditions at the top based on the scenario
    create_displacement_bc(
        name='TOP-BC',
        step_name='Initial',
        region=ref_points_top,
        u1=0.0, u2=0.0, ur1=0.0, ur3=0.0
    )

    if imperfections:
        # Apply concentrated force for the buckling step (unit load)
        model.ConcentratedForce(
            name='TOP-LOAD',
            createStepName='BUCKLING-STEP',
            region=ref_points_top,
            cf3=-1.0
        )
    else:
        # Apply displacement for the compression step
        create_displacement_bc(
            name='TOP-COMPRESSION',
            step_name='COMPRESSION-STEP',
            region=ref_points_top,
            u3=displacement
        )


def create_job(model, job_name, description):
    """Create a job."""

    mdb.Job(
        name=job_name,
        model=model.name,
        description=description,
        numCpus=6,
        numDomains=6
    )


def save_model(folder_name):
    """Save the model in a new unique directory and set it as the working
directory."""

    # Get the directory of the current script
    script_path = inspect.getfile(inspect.currentframe())
    script_directory = os.path.dirname(os.path.abspath(script_path))
    base_folder_path = os.path.join(script_directory, folder_name)
    unique_folder_path = base_folder_path

    # Create a unique folder name if the folder already exists
```

```
    count = 1
    while os.path.exists(unique_folder_path):
        unique_folder_path = "{}-{}".format(base_folder_path, count)
        count += 1

    # Create the unique folder and save the model
    os.makedirs(unique_folder_path)
    mdb.saveAs(pathName=os.path.join(unique_folder_path, folder_name))
    os.chdir(unique_folder_path)

    return unique_folder_path


def run_buckling_datacheck(job_name):
    """Run a DataCheck for the specified buckling job to generate the .inp
file."""

    job = mdb.jobs[job_name]
    job.submit(datacheckJob=True)
    job.waitForCompletion()


def modify_buckling_inp(job_name, folder_path):
    """Modify the buckling .inp file to include NODE FIL U output."""

    # Define the paths for the input and output files
    inp_file_path = os.path.join(folder_path, '{}.inp'.format(job_name))
    modified_inp_file_path = os.path.join(folder_path, '{}-
IMPERFECTIONS.inp'.format(job_name))

    # Define the output lines to insert
    output_lines = [
        '*NODE FILE, GLOBAL=NO,\n',
        'MODE=1, LAST MODE=3\n',
        'U\n'
    ]

    # Open the input and output files
    with open(inp_file_path, 'r') as infile:
        inp_lines = infile.readlines()
    new_inp_lines = []
    for line in inp_lines:
        new_inp_lines.append(line)
        # Check if the line is '*END STEP'
        if line.strip().upper().startswith('*END STEP'):
            # Insert the output request lines before '*END STEP'
            new_inp_lines[-1:-1] = output_lines

    # Write the current line to the output file
```

```
    with open(modified_inp_file_path, 'w') as outfile:
        outfile.writelines(new_inp_lines)

    return modified_inp_file_path


def compute_cross_sectional_area(height, width, thickness, fillet_radius):
    """Compute the cross-sectional area of the U-shaped half-column."""

    # Compute individual component areas
    web_area = thickness * (height - 2 * fillet_radius)
    flange_area = 2 * thickness * (width - fillet_radius)
    fillet_area = 2 * (0.25 * math.pi * fillet_radius ** 2)

    # Compute half-column area and total area
    half_column_area  = web_area + flange_area + fillet_area
    total_area  = 2 * half_column_area

    return total_area


def extract_eigenvalues(job_name):
    """Opens the ODB file from the buckling analysis and extracts the
eigenvalues."""

    # Open the ODB and extract eigenvalues
    odb = openOdb(path='{}.odb'.format(job_name))

    eig_step  = odb.steps['BUCKLING-STEP']
    eigenvalues = []
    frame_count = 0

    for frame in eig_step.frames:
        frame_count += 1
        if frame_count == 1:
            continue  # Skip the first frame (mode 0)
        description = frame.description  # e.g., 'Eigenvalue = 1.2345e+02'
        eigenvalue_str = description.split('=')[1].strip()
        eigenvalue = float(eigenvalue_str)
        eigenvalues.append(eigenvalue)
    odb.close()

    return eigenvalues


def compute_imperfection_magnitudes(eigenvalues, thickness, sigma_yield,
area):
    """Computes the imperfection magnitudes for each buckling mode."""
```

```
    imperfection_modes = []
    applied_load = -1.0  # Applied load is -1.0 N

    for i, eigenvalue in enumerate(eigenvalues):
        mode_number = i + 1  # Modes start from 1
        Pcr = eigenvalue * applied_load  # Critical load for the mode (N)

        sigma_cr = abs(Pcr) / area  # Critical stress for the mode in MPa
(N/mm^2 = MPa)

        # Compute lambda_s (slenderness)
        lambda_s = math.sqrt(sigma_yield / sigma_cr)

        # Determine imperfection magnitude omega_d
        if thickness < 3.0:
            # For t < 3 mm, omega_d = 0.94 * t (distortional)
            omega_d = 0.94 * thickness
        else:
            # For t ≥ 3 mm, use Walker's equation
            omega_d = 0.3 * thickness * lambda_s

        imperfection_modes.append((mode_number, omega_d))

        # Print imperfection magnitude for debugging
        print("Omega_d: {:.6f} mm".format(omega_d))

    return imperfection_modes


def apply_imperfections(model, assembly, height, width, thickness,
fillet_radius,
                        displacement, sigma_yield, job_name_buckling,
job_name_compression, folder_path):
    """Apply imperfections to the compression model using the distortional
buckling mode."""

    # Run the buckling analysis
    run_buckling_datacheck(job_name_buckling)

    # Modify the buckling .inp file to include NODE FILE U output
    modified_buckling_inp = modify_buckling_inp(job_name_buckling,
folder_path)

    # Run the buckling job with the modified .inp file
    mdb.JobFromInputFile(
        name=job_name_buckling,
        inputFileName=modified_buckling_inp,
        numCpus=6,
        numDomains=6)
```

```
    mdb.jobs[job_name_buckling].submit()
    mdb.jobs[job_name_buckling].waitForCompletion()

    # Extract eigenvalues from the buckling ODB
    eigenvalues = extract_eigenvalues(job_name_buckling)

    # Compute cross-sectional area
    area = compute_cross_sectional_area(height, width, thickness,
fillet_radius)

    # Compute imperfection magnitudes
    imperfection_modes = compute_imperfection_magnitudes(eigenvalues,
thickness, sigma_yield, area)

    # Prepare the compression model
    define_analysis_steps(model, imperfections=False)
    apply_boundary_conditions(model, assembly, displacement,
imperfections=False)
    # Define output requests
    define_output_requests(model, assembly)

    # Create the compression job and run DataCheck
    create_job(model, job_name_compression, 'Compression test job')
    mdb.jobs[job_name_compression].submit(datacheckJob=True)
    mdb.jobs[job_name_compression].waitForCompletion()

    # Modify the compression .inp file to include imperfections
    # Define the paths for the input and output files
    inp_file_path = os.path.join(folder_path,
'{}.inp'.format(job_name_compression))
    modified_inp_file_path = os.path.join(folder_path, '{}-
IMPERFECTIONS.inp'.format(
        job_name_compression))

    # Define the output lines to insert
    imperfection_lines = ['*IMPERFECTION, FILE={},
STEP=1\n'.format(job_name_buckling)]
    for mode_num, omega in imperfection_modes:
        imperfection_lines.append('{}, {:.8f}\n'.format(mode_num, omega))

    new_inp_lines = []
    imperfection_inserted = False

    with open(inp_file_path, 'r') as infile:
        inp_lines = infile.readlines()
    for line in inp_lines:
        new_inp_lines.append(line)
        # Check if the line is '** STEP ...'
```

```
        if not imperfection_inserted and line.strip().upper().startswith('**
STEP: COMPRESSION-STEP'):
            # Insert the output request lines before '*END STEP'
            new_inp_lines[-2:-2] = imperfection_lines
            imperfection_inserted = True

    # Write the current line to the output file
    with open(modified_inp_file_path, 'w') as outfile:
        outfile.writelines(new_inp_lines)

    # Create and submit the compression job with imperfections
    del mdb.jobs[job_name_compression]
    mdb.JobFromInputFile(
        name=job_name_compression,
        inputFileName=modified_inp_file_path,
        numCpus=6,
        numDomains=6)


# ======================================================================
# Main script execution
# ======================================================================


def run_simulation(length, thickness, hole_spacing, fasteners_spacing,
sigma_yield):

    # Define constants
    # length = ...                # Length of the column (mm)
    # thickness = ...             # Thickness of the profile (mm)
    height = 240.0                # Height of the profile (mm)
    width = 45.0                  # Width of the profile (mm)
    fillet_radius = 2.5           # Fillet radius (mm)
    hole_diameter = 96.0          # Diameter of the holes (mm)
    # hole_spacing = ...          # Spacing between holes (mm)
    # fasteners_spacing = ...     # Spacing between fasteners (mm)
    # Material properties
    E = 68000.0           # Young's modulus (MPa)
    nu = 0.3              # Poisson's ratio
    # sigma_yield = ...   # Yield strength (MPa)
    folded_sigma_yield = sigma_yield + 3.0   # Folded field strength (MPa)
    # Mesh parameters
    end_plate_mesh_size = 10.0   # Element size for end plate (mm)
    column_mesh_size = 8.0       # Global element size for column (mm)
    refined_mesh_size = 3        # Number of elements on edges around holes
    # Compression parameter
    total_displacement = -5.0    # Total imposed displacement during
compression (mm)
    # Imperfection parameter
```

```
    imperfection = True          # Toggle imperfections

    # Calculated parameters
    # Number of holes
    number_of_holes = 2 * int(((length - hole_spacing) / 2.0) // hole_spacing)
+ 1
    # Partition dimensions based on hole spacing
    partition_width = min(hole_spacing, 200.0)
    partition_height = 200.0
    partition_hole_radius = hole_diameter / 2.0 + 15.0
    # Number of fasteners
    number_of_fasteners = int(length / fasteners_spacing)
    if length % fasteners_spacing != 0:
        number_of_fasteners += 1
    total_fasteners_length = (number_of_fasteners - 1) * fasteners_spacing
    first_fastener = (length - total_fasteners_length) / 2.0
    # End plate dimensions
    end_plate_length = height + 50.0  # Length of the end plate (mm)
    end_plate_width = width + 50.0    # Width of the end plate (mm)
    end_plate_thickness = 10.0        # Thickness of the end plate (mm)

    # Create a new model
    model_name = 'FACE-TO-FACE COLUMN'
    if imperfection:
        model_name += ' BUCKLING'
    if 'Model-1' in mdb.models:
        mdb.models.changeKey(fromName='Model-1', toName=model_name)
    model = mdb.models[model_name]
    # Create material and section
    create_material_and_section(model, E, nu, sigma_yield, folded_sigma_yield,
thickness)
    # Create parts
    p_end_plate = create_end_plate(model, end_plate_length, end_plate_width,
end_plate_thickness,
                                   end_plate_mesh_size)
    p_half_column = create_half_column(model, length, height, width)
    # Partition and cut holes
    hole_positions = partition_side_face(model, p_half_column, length, height,
partition_height,
                                         partition_width, number_of_holes,
partition_hole_radius,
                                         hole_spacing)
    cut_holes(model, p_half_column, length, height, hole_positions,
hole_diameter)
    # Partition for fasteners
    partition_top_bottom_faces(model, p_half_column, length, height, width,
fillet_radius,
```

```
                                number_of_fasteners, first_fastener,
fasteners_spacing)
    # Apply a fillet to the part
    add_fillet(p_half_column, height, fillet_radius)
    # Assign section
    assign_section(p_half_column, height, fillet_radius)
    # Mesh the half-column
    mesh_half_column(p_half_column, length, height, fillet_radius,
hole_diameter, hole_positions,
                     partition_height, partition_width, partition_hole_radius,
column_mesh_size,
                     refined_mesh_size)
    # Create assembly
    assembly = create_assembly(model, p_end_plate, p_half_column, length,
height, width, thickness,
                               fillet_radius, end_plate_length,
end_plate_width)
    # Create surfaces
    create_surfaces(assembly, length)
    # Define analysis steps
    define_analysis_steps(model, imperfection)
    # Define contact properties
    define_contact_properties(model)
    # Create surface interactions
    create_surface_interactions(model, assembly, height, thickness)
    # Add fasteners
    add_fasteners(assembly, height, thickness, number_of_fasteners,
first_fastener, fasteners_spacing)
    # Define constraints
    define_constraints(model, assembly, length)
    # Apply boundary conditions
    apply_boundary_conditions(model, assembly, total_displacement,
imperfection)
    # Create the jobs
    job_name_buckling = 'BUCKLING-JOB'
    job_name_compression = 'COMPRESSION-JOB'
    if imperfection:
        create_job(model, job_name_buckling, 'Buckling analysis job')
    else:
        # Define output requests
        define_output_requests(model, assembly)
        create_job(model, job_name_compression, 'Compression test job')
    # Save the model
    folder_name = 'FTFC-{}x{}x{}-L{}-H{}-F{}'.format(int(height), int(width),
int(math.ceil(thickness)),
                                                     int(length),
int(hole_spacing), int(fasteners_spacing))
    if imperfection:
```

```
        folder_name += '-IMPERFECTIONS'
    folder_path = save_model(folder_name)
    # Apply imperfections if required
    if imperfection:
        compression_model = mdb.Model(
            name='FACE-TO-FACE COLUMN COMPRESSION',
            objectToCopy=mdb.models[model_name]
            )
        apply_imperfections(compression_model, assembly, height, width,
thickness, fillet_radius,
                            total_displacement, sigma_yield,
job_name_buckling, job_name_compression,
                            folder_path)
    # Submit the job directly
    mdb.jobs[job_name_compression].submit(consistencyChecking=OFF)
    mdb.jobs[job_name_compression].waitForCompletion()

if __name__ == '__main__':
    # Define parameter lists
    length_values = [1500.0]   # Length in mm
    thickness_values = [1.98]  # Thickness in mm
    hole_spacing_values = [375.0]       # Hole spacing in mm
    fasteners_spacing_values = [350.0]  # Fastener spacing in mm
    sigma_yield_values = [152.0]        # Yield strength (MPa)
    # Create all combinations
    parameter_combinations = list(itertools.product(length_values,
thickness_values, hole_spacing_values,
        fasteners_spacing_values, sigma_yield_values))
    # For each combination
    for length, thickness, hole_spacing, fasteners_spacing, sigma_yield in
parameter_combinations:
        if hole_spacing == 187.5 and fasteners_spacing == 350.0:
            continue
        if hole_spacing == 250.0 and fasteners_spacing == 700.0:
            continue
        # Run the simulation with the parameters
        run_simulation(length, thickness, hole_spacing, fasteners_spacing,
sigma_yield)
        mdb.save()
        mdb = Mdb()
```

Appendix "C" – All Parametric result

Table c 1: The Parametric study parameters used to plain channel section with grade 5052 HS -32

Specimen	Thickness	screw spacing(S) (mm)			Failure Modes	P_{FEA}		
	t(mm) (mm)	screws no's -2 (mm)	screws no's -3 (mm)	screws no's -5 (mm)		screws no's -2	screws no's -3	screws no's -5
Short								
FTF240-L500	1.3	400	200	100		38.12	39.21	42.24
	3					158.63	162.25	173.69
	4					276.12	288.99	319.46
	6					502.11	505.21	515.25
Intermediate								
FTF240-L1000	1.3	900	450	225		37.2	37.35	40.68
	3					153.89	159.2	170.25
	4					273.33	275.05	302.15
	6					495.33	500.1	510.12
Slender								
FTF240--L1500	1.3	1400	700	350		36.01	36.507	38.81
	3					152.69	156.62	165.25
	4					250.83	265.23	277.19
	6					491.57	497.35	503.25
FTF240-L3000	1.3	2400	1200	600		28.32	30.2	35.62
	3					107.54	143.5	160.65
	4					170.35	230.12	249.52
	6					255.65	371.23	496.2

Table c 2: The Parametric study parameters used to plain channel section with grade 5052 HS -34

Specimen	Thickness	screw spacing(S) (mm)			Failure Modes	P_{FEA}		
	t(mm)	screws no's -2	screws no's -3	screws no's -5		screws no's -2	screws no's -3	screws no's -5
	(mm)	(mm)	(mm)	(mm)				
Short								
FTF240-t1.98-L500	1.3	400	200	100		41.82	44.38	45.86
	3					171.83	181.96	192.26
	4					290.12	293.21	321.26
	6					568.67	575.12	587.12
Intermediate								
FTF240-t1.98-L1000	1.3	900	450	225		37.202	43.01	44.89
	3					165.23	177.28	189.52
	4					279.45	290.52	309.22
	6					558.5	565.12	585.22
Slender								
FTF240-t1.98-L1500	1.3	1400	700	350		36.32	41.27	43.75
	3					162.56	173.15	183.45
	4					264.61	286.85	305.25
	6					537.65	563.23	578.58
FTF240-t1.98-L3000	1.3	2400	1200	600		28.62	30.12	36.31
	3						144.54	173.25
	4						231.02	272.85
	6						370.94	539.54

Table c 3: The Parametric study parameters used to plain channel section with grade 5052 HS -36

Specimen	Thickness	screw spacing(S) (mm)			Failure Modes	P_{FEA}		
	t(mm)	screws no's -2	screws no's -3	screws no's -5		screws no's - 2	screws no's - 3	screws no's - 5
	(mm)	(mm)	(mm)	(mm)				
Short								
BU240-t1.98-L500	0.8	400	200	100		18.17	18.91	20.46
	4					307.2	309.1	330.96
Intermediate								
BU240-t1.98-L1000	0.8	900	450	225		15.2	17.11	18.25
	4					296.32	301.5	325.12
Slender								
BU240-t1.98-L1500	0.8	1400	700	350		14.59	16.1	17.94
	4					272.59	285.61	319.67
BU240-t1.98-L3000	0.8	2400	1200	600		135.43	13.12	15.21
	4					221.43	231.02	274.19

Table c 4: The Parametric study parameters used to with single web hole section with grade 5052 HS-32

Specimen	Thickness	screw spacings(S) (mm)			Failure Modes	P_{FEA} -0.2XD			P_{FEA} -0.4XD			P_{FEA} -0.6XD		
	t(mm)	Screws no's -2	screws no's -3	screws no's -5		screws no's -2	screws no's -3	screws no's -5	screws no's -2	screws no's -3	screws no's -5	screws no's -2	screws no's -3	screws no's -5
	mm	mm	mm	mm										
Short														
BU240-L500	1.98	400	200	100	LB &DB	70.8	74.4	80.4	69.1	72.4	79.5	67.1	71.2	77.1
	1.3				LB &DB	36.1	37.8	42.1	36.7	38.3	41.7	34.5	36.1	39.9
	3				LB &DB	165.78	167.58	202.85	157.2	162.54	195.45	152.4	157.25	190.45
	4				LB &DB	261.74	281.14	304.45	258; 74	268.4	290.41	220.54	228.4	257.21
	6				LB &DB	492.16	504.2	514.2	415.2	428.15	445.35	315.24	333.78	340.89
Intermediate														
BU240-L1000	1.98	900	450	225	LB &DB	68.4	72.1	77.9	64.9	68.2	74.1	63.2	66.14	71.4
	1.3				LB &DB	34.06	34.7	38.9	33.7	34.2	38.1	33.14	33.8	37.75
	3				LB &DB	160.5	171.52	172.5	153.2	163.1	167.2	145.2	157.01	159.4
	4				LB &DB	223.4	247.35	275.2	222.4	241.3	256.3	215.5	225.4	250.4
	6				LB &DB	421.25	423.22	435.12	412.3	418.6	430.85	312.5	330.1	339.2
Slender														
BU240--L1500	1.98	1400	700	350	LB &DB	71.346	72.25	73.25	70.46	70.87	71.45	67.15	71.65	70.66
	1.3				LB ,GB &DB	34.21	35.1	38.14	33.14	34.12	37.01	32.45	33.32	36.45
	3				LB,GB &DB	147.25	152.4	163.44	141.3	149.5	162.4	138.3	144.2	158.62
	4				LB,GB &DB	224.5	239.45	255.33	220.5	234.3	248.1	203.1	215.3	228.3
	6				LB,GB &DB	391.5	405.3	415.3	398.2	400.1	409.5	310.2	334.12	365.4
BU240-L3000	1.3	2400	1200	600	LB,GB &DB	27.5	29.4	35.33	24.3	28.4	34.33	21.3	24.2	30.5
	3				LB,GB &DB	100.3	135.4	154.3	90.5	124.5	141.2	85.4	115.3	134.3

Table c 5: The Parametric study parameters used to with single web hole section with grade 5052 HS-34

Specimen	Thickness	screw spacings(S) (mm)			Failure Modes	P_{FEA} -0.2XD			P_{FEA} -0.4XD			P_{FEA} -0.6XD		
	t(mm)	screws no's -2	screws no's -3	screws no's -5		screws no's -2	screws no's -3	screws no's -5	screws no's -2	screws no's -3	screws no's -5	screws no's -2	screws no's -3	screws no's -5
Short	1.3	400	200	100	LB &DB	41.65	42.02	43.1	37.71	37.93	41.25	38.9	39.5	40.65
BU240-t1.98-L500	3	400	200	100	LB &DB	170.4	172.3	266.6	168.6	170.4	201.1	165.2	167.2	177.56
	4				LB &DB	270.8	298.3	330.1	268.4	288.6	310.5	259.5	260.2	264.8
	6				LB &DB	537.3	542.5	608.2	500.3	501.2	504.5	394.5	397.4	400.6
Intermediate	1.3	900	450	225	LB &DB	37.15	37.82	39.25	37.1	37.4	38.5	36.8	37.01	38.01
BU240-t1.98-L1000	3	900	450	225	LB &DB	168.52	170.2	175.6	167.2	169.4	175.2	163.2	166.2	174.2
	4				LB &DB	268.54	278.5	280.25	265.4	276.1	307.1	258.4	260.0	263.5
	6				LB &DB	486.9	490.1	490.5	484.3	488.3	502.4	390.5	395.2	400.1
Slender	1.3	1400	700	350	LB ,GB &DB	36.51	37.05	38.5	35.2	37.01	38.1	34.1	36.4	37.8
BU240-t1.98-L1500	3	1400	700	350	LB,GB &DB	165.4	168.2	173.25	164.1	166.5	172.4	163.2	165.5	170.5
	4				LB,GB &DB	266.5	270.1	274.2	265.8	269.8	273.8	256.3	258.1	262.5
	6				LB,GB &DB	480.5	482.3	485.1	480.1	481.3	485.0	388.5	390.2	392.5

Table c 6: The Parametric study parameters used to with single web hole section with grade 5052 HS-36

Specimen	Thickness	screw spacings(S) (mm)			Failure Modes	P_{FEA} -0.2XD			P_{FEA} -0.4XD			P_{FEA} -0.6XD		
	t(mm)	screws no's -2	screws no's -3	screws no's -5		screws no's -2	screws no's -3	screws no's -5	screws no's -2	screws no's -3	screws no's -5	screws no's -2	screws no's -3	screws no's -5
	(mm)	(mm)	(mm)	(mm)										
Short														
FTF240-t1.98-L500	0.8	400	200	100	LB &DB	18.1	18.7	19.3	17.9	18.1	18.6	17.2	17.9	18.4
	4				LB &DB	285.1	312.0	331.5	289.6	300.4	330.2	288.1	300.0	320.1
Intermediate														
FTF240-t1.98-L1000	0.8	900	450	225	LB &DB	16.16	16.87	17.15	15.7	16.5	16.92	15.1	16.01	16.5
	4				LB &DB	283.9	291.8	300.3	280.4	290.5	297.5	277.5	288.1	295.6
Slender														
FTF240-t1.98-L1500	0.8	1400	700	350	LB,GB &DB	16.01	16.41	16.88	15.3	16.35	16.6	13.2	14.91	16.1
	4				LB,GB &DB	280.4	290.4	298.5	278.5	281.2	296.2	275.5	280.2	283.0

Table c 7: The Parametric study parameters used to channel with multiple holes web section with grade 5052 HS-32

Specimen	Thickness	Hole spacings (mm)			Failure Modes	FEA (kN)					
	t	Hole spacing - 150	Hole spacing- 200	Hole spacing- 300		No of Screws = 5			No of Screws = 3		
	mm	mm	mm	mm		Hole spacing - 150	Hole spacing - 200	Hole spacing - 300	Hole spacing - 150	Hole spacing - 200	Hole spacing - 300
Slender											
BU240-L1500	3	150	200	300	LB-DB-GB	160.2	165.2	170.8	158.2	160.2	168.5
	4				LB-DB-GB	256.7	268.4	273.1	254.9	265.1	271.6
BU240-L3000	3	150	200	300	LB-DB-GB	118.0	130.9	**137.5**	116.5	125.4	132.4
	4				LB-DB-GB	195.5	197.8	205.1	189.0	194.1	198.4

Table c 8: The Parametric study parameters used to channel with multiple holes web with grade 5052 HS-34

Specimen	Thickness	Hole spacings (mm)			Failure Modes	FEA (kN)					
	t	Hole spacing - 150	Hole spacing- 200	Hole spacing- 300		No of Screws = 5			No of Screws = 3		
	mm	mm	mm	mm		Hole spacing - 150	Hole spacing - 200	Hole spacing - 300	Hole spacing - 150	Hole spacing - 200	Hole spacing - 300
Slender											
BU240-L1500	3	150	200	300	LB-DB-GB	170.0	172.7	176.1	175.	176.0	185
	4				LB-DB-GB	282.4	278.6	292.0	281	282.2	294
BU240-L3000	3	150	200	300	LB-DB-GB	118.8	127.5	130.5	117	116.0	121
	4				LB-DB-GB	198.5	202.2	207.1	194	197.1	199